Consortium

for

Small-Scale Modelling

CONSORTIUM FOR SMALL SCALE MODELING
COSMO

Newsletter

June 2015 ***No. 15***

Deutscher Wetterdienst

MeteoSwiss

Ufficio Generale Spazio Aereo e Meteorologia

ΕΘΝΙΚΗ ΜΕΤΕΩΡΟΛΟΓΙΚΗ ΥΠΗΡΕΣΙΑ

Instytucie Meteorogii i Gospodarki Wodnej

Administratia Nationala de Meteorologie

Agenzia Regionale per la Protezione Ambientale dell'Emilia Romagna Servizio Idro Meteo Clima

Federal Service for Hydrometeorology and Environmental Monitoring

Amt fur GeoInformationswesen der Bundeswehr

Centro Italiano Ricerche Aerospaziali

Agenzia Regionale per la Protezione Ambientale del Piemonte

www.cosmo-model.org

Editors: Mihaela Bogdan (NMA); Massimo Milelli (ARPA-Piedmont); Ulrich Schattler (DWD);

Table of Contents

The current issue of the COSMO Newsletter presents a selection of articles on the recent developments of the consortium. I would like to thank the authors for sharing their results on the hot and interesting topics and to encourage all of you to use the Newsletter for presentation of your results.

An extensive review and discussion of our recent progress and results took place during the COSMO General Meeting held from 8 to 11 September 2014 in Eretria, Greece. You can find the presentations at http://www.cosmo-model.org/content/consortium/generalMeetings/general2014/default.htm .

An important achievement of the current COSMO year was the release of new edition of the COSMO Science Plan. The document was approved by the COSMO Steering Committee in March 2015 and will guide the development of our consortium by the year 2020. You can find the document at http://cosmo-model.org/content/consortium/reports/sciencePlan_2015-2020.pdf The preparation of the document stimulated very interesting discussions and involved feedback from many of you and from scientists from outside of the consortium. I would like to thank and express my gratitude to all who participated in the work and influenced the final shape of the Plan.

Other important milestone was the release of new version 5.1 of the COSMO model, which begins practical implementation of our Strategy aimed at harmonization with ICON, that is an implementation COSMO-ICON physics library. The release of V5.1 was the first to be tested with newly prepared NWP test suite, in accordance with our code management standards. I would like to thank all the developers, involved, and wish many successes in further work on the COSMO model and its tools.

For the next General Meeting, we will meet in Wrocław, Poland, from 7 to 10 September 2015. I wish every success in your work!

Michał Ziemiański
COSMO Scientific Project Manager

Figure 1: Participants of the 16th COSMO General Meeting in Eretria

The parameterization of the interaction between the subgrid-scale orography scheme and the turbulence closure in COSMO model

Ines Cerenzia[1]
Maria Stefania Tesini[2]
Matthias Raschendorfer[3]

[1] *Universita' degli studi di Bologna, Italy*
[2] *Arpa-EMR, Bologna, Italy*
[3] *Deutscher Wetterdienst, Offenbach am Main, Germany*

Abstract

The COSMO model considers a direct impact on the employed prognostic equation of Turbulent Kinetic Energy (TKE) by accounting for the effect of the Subgrid Scale Orography (SSO) scheme on the momentum budget. The treatment of that interaction is already implemented in the COSMO code and can be optionally activated by the namelist parameter *ltkesso*. The impact on the simulated TKE and dynamical variables is investigated by the use of two case studies over North Italy area. Results indicates that the related increase of turbulent mixing at grid points above a pronounced SSO at different altitudes produces main changes in the temperature and wind fields in the same points and downflow to them. Further, within the Stably stratified Boundary Layer (SBL), some (small) impact is also visible above less pronounced SSO. Moreover, near surface variables are verified against observations, distinguishing between stations located at model grid points with a high or low amount of SSO. Scores are improved at high-SSO points and they do not change at the other ones, with the exception of temperature at 2m level, which worsens for SBL cases.

1. Introduction

In the present study, we are dealing with the effect of an extra source for TKE, which has been expressed as a function of the momentum sink term generated by the SSO scheme. This additional TKE source term is already present in M. Raschendorfer's scheme and can be activated by the namelist switch *ltkesso*. The feature is running operationally at DWD (COSMO-EU) since 2011 and has also been activated at Meteo-Swiss (COSMO-7), following the results of a verification performed at DWD in 2011 over a 2 months parallel run with COSMO-EU (*Raschendorfer, 2011*). In that, the main differences over the COSMO-EU domain were on biases of near surface temperature, wind speed and pressure respectively (for the latter the bias was always reduced). The root mean square errors (rmse) of the three variables remained almost unchanged or they improved slightly.

As a supplement, we now present an analysis of the impact on the structure of the whole troposphere. For that purpose we have interpreted the differences in the wind and temperature fields with and without this additional term in different meteorological conditions represented by some cases. The first case is a 3 days period in January 2012, characterized by stable anticyclonic conditions. The second case is a 2 days period in May 2012, characterized by unstable conditions with a cold frontal passage and associated precipitation. The case studies have been performed for the COSMO-I7 domain using the COSMO5.0 version with a namelist configuration similar to that of COSMO-EU [1]. COSMO's initialization and boundary conditions came from

[1] Differently from COSMO-EU, the sea ice and lake formulations were not activated.

ECMWF analysis and no data assimilation was activated. For each case study, we obtained a COSMO run with the *ltkesso* option set off and on. We focus on the differences between the 2 runs over Northern Italy, which contains regions with high and low SSO (e.g. the Alps and the Po Valley respectively).

The direct impacts of *ltkesso* on turbulence and the indirect effect on the dynamical fields are described in sections 3 and 4. Further on, we verified the experimental and control runs against the stations network of Northern Italy for both the cases, distinguishing between stations with high and low SSO (sect. 5). Finally, the results are summarized in sect. 6. In the next section there is a short description of the idea behind the additional TKE source term.

2. Background and parameterization description

The presence of the Subgrid-Scale Orography (SSO) induces additional pressure forces (form drag) to the mean flow, which are firstly related to a direct sink term in the budgets of the mean horizontal momentum components (blocking effect). Further, a small part of the Mean Kinetic Energy (MKE) of the flow is converted into vertically propagating gravity waves. As soon as they break, they cause a disturbance of the mean flow, associated with an additional sink term in the mean momentum budgets. In the COSMO model, these sink terms are parameterized following Lott and Miller's approach (*Lott and Miller, 1997; Schulz, 2009*), providing the related sink terms of horizontal momentum in the following form:

$$\left.\frac{\partial \overline{\rho} u_i}{\partial t}\right|_{SSO} = \left.\frac{\partial \tau_i}{\partial z}\right|_{SSO}, i = x, y \tag{1}$$

In eq. (1), $\tau_i|_{SSO}$ is a virtual vertical flux density of horizontal momentum (stress), which includes both the stress by gravity-waves and blocking. The scheme further provides a local dissipation heating term to be considered in the temperature equation.
The new development of M. Raschendorfer considers that all sink terms in the budget of the mean momentum vector are always associated to sink terms in the budget of the Mean Kinetic Energy (MKE), which in turn correspond to source terms in the budget of subgrid-scale Kinetic Energy (SKE) according to the following fomula (see e.g. *Raschendorfer, 2011*):

$$\partial_t MKE|_{SSO} = \overline{u_i} \cdot \partial_z \tau_i^{SSO} = -\partial_t SKE|_{SSO} \tag{2}$$

Formally, $\partial_t SKE^{SSO}$ (2) contains also the energy production of the gravity waves, which takes place below the SSO effective height together with the blocking and which is then transformed in drag where the waves break. Neglecting the remote character of this part of SKE release, $\partial_t SKE|_{SSO}$ thus describes the direct conversion of MKE into SKE, as wake production. As those motions typically are not in accordance with the closure assumptions of a turbulence scheme, they cannot be treated as a part of the latter. Based on a formal scale separation, M. Raschendorfer developed the concept of Separated Turbulence Interacting with (non-turbulent and still unresolved) Circulations (STIC), which is also part of the COSMO Science Plan for the current year. In the framework of this approach, which is so far only described in an internal paper, the Sub-Grid Scale (SGS) motions induced by SSO themselves produce kinectic energy of scales that can be described by the turbulence scheme(*Raschendorfer, 2011*).

Thus in a first approximation, $\partial_t SKE|_{SSO}$ can be treated as an additional production term of TKE, which intensifies the vertical turbulent mixing for all prognostic variables whenever the SSO scheme is active. Hence by this extension, the kinetic energy extracted from the mean flow by the action of SSO is not immediately dissipated into inner energy. Rather it is transported through all SGS motions until it is finally dissipated.

3. Effects on turbulence

The additional source term in the TKE equation appears with the largest increment at model grid points at pronounced SSO (often corresponding with high altitude of resolved orography), mainly within the following three ranges of altitude: at the lowest model levels, at the top of the troposphere (around $10km$ height) and at the highest model levels (Fig. 1). Obviously the effect at the lowest model levels refers mainly to the direct blocking component, while the middle and highest levels are affected by the breaking gravity waves.

In these regions, a large increase of TKE and diffusion coefficients due to the SSO effect is simulated by the model (Fig. 1; diffusion coefficients not shown). This significant effect demonstrates the potential of this measure to simulate strong signals of Clear Air Turbulence (CAT) above structured orography, which also has valuably improved the turbulence forecast for aviation (*M. Raschendorfer and A. Barleben, 2014*).

At model grid points above low SSO, the additional source term in the TKE equation and the consequent impact on values of TKE and diffusion coefficients is very small (not visible in Fig. 1). However, in the stable stratified atmosphere a non-negligible feedback in terms of destabilization may appear.

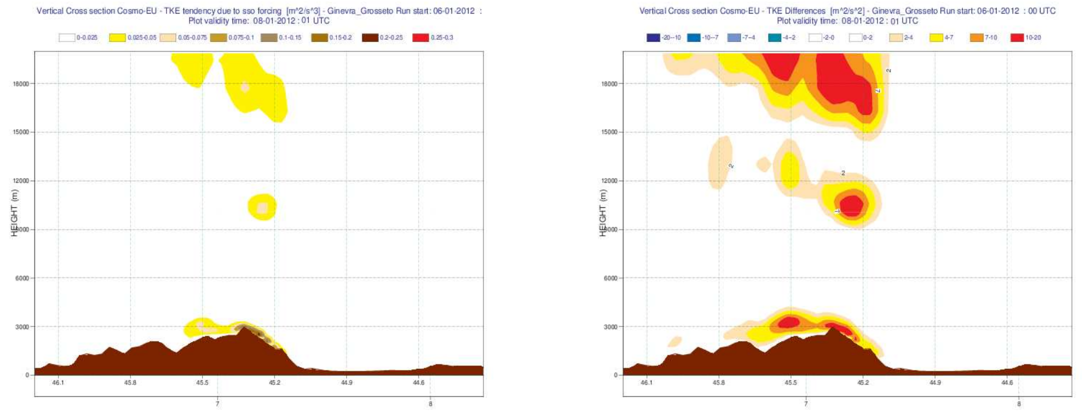

Figure 1: Cross vertical sections of the additional term into TKE equation (left) and the difference in TKE between the case with *ltkesso* enabled and without (right). The plots refer to the January case study (08/01/2012-01:00). The cross sections are parallel to the main component of the geostrophic flow (from North-NorthWest), in the plot coming from the left side.

4. Effects on dynamical variables

The case study of January is used to analyze the situation (Fig. 2). The geostrophic flow comes from North-North-East and crosses the Alps (from the left side in Fig. 2). Gravity waves are developed and break at the tropopause producing a slowing down of wind. In the lee of the mountain, the flow weakly interacts with the SBL located at the mountain feet, being dragged only slightly.

The main impact of *ltkesso* appear at model grid points above considerable SSO (which mainly is the case, if gridscale orography is pronounced as well) and at points downflow to the latter where flat SSO is prevailing. One grid point for each of these regions has been selected (see black dashed line in Fig. 2). For these two points, vertical profiles of potential temperature θ, horizontal wind speed $\overline{u}$ and TKE between the surface and 14km are shown in Fig. 3. Above that level, the impact of *ltkesso* on those profiles is negligible.

At point above high SSO, the vertical gradients of θ and $\overline{u}$ are reduced in correspondence with the turbulent mixing increases (surface-4 km and 8-14 km).

Conditions of a stably stratified atmosphere (generally scarcely diffusive) are the ones being most sensitive to the increase of turbulent mixing. In those cases, the reduction of the vertical θ gradient causes a warming in the lower part and a cooling above, as it is visible between the lowest model level and 4km in Fig.2. Similarly, the positive vertical gradient of wind speed at the lowest levels reduces, leading to stronger wind close the surface and weaker above. Moreover, the combination of intensified wind speed and higher diffusivity produces a higher surface momentum flux, which subtracts kinetic energy to the mean flow, causing a further reduction of it in the upper layers. At the level of breaking-waves, the increased mixing planes out the perturbation of the wind and θ profiles generated by the SSO scheme.

At point above low SSO downflow to the high-SSO region, it is supposedly the advection that leads a layer of colder air with weaker horizontal wind speed and higher TKE between 2 and 4km in the run with *ltkesso* activated (Fig. 3). Similarly above 4km, the increase of $\overline{u}$ refers to the smoothing of the gravity-wave-breaking perturbation.

The downward flow along the mountain slope has a non-sufficient MKE to significantly interact with the SBL underneath. Thus, in the mountain lee a more intense thermal inversion develops (Fig. 3). However, notice that this is a local effect, since at a proper distance from the mountain slope it is the the slight increase of mixing at the lowest model levels that dominates the modification on the vertical boundary layer profiles, as a direct effect of *ltkesso* (visible also in TKE profile in Fig. 3). As in the previous case, the impact is mostly visible in the SBL, where the thermal stratification slightly reduces, leading to a near surface warming and a cooling above. In the case study of May, the geostrophic flow comes from South and the main deviations in θ and $\overline{u}$ appear over the Alps and in their downflow on the Swiss side (graphs not shown). As the additional source of TKE equation is smaller compared to the one of January, this holds also for the magnitude of its feedbacks on the other prognostic model variables. Nevertheless, the same tendencies have been observed.

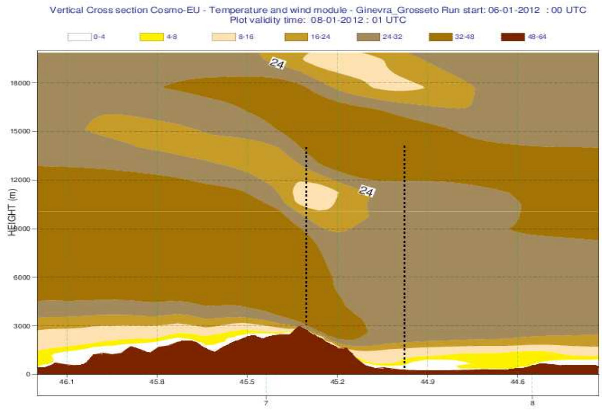

Figure 2: Vertical cross section of the horizontal wind speed $[m/s]$ in the run without *ltkesso* enabled in the January case study. The section is parallel to the geostrophic flow (from North-NorthWest), in the plot coming from the left side. Time: 08/01 01:00. The two dottet lines correspond to the profiles plotted in Fig.3

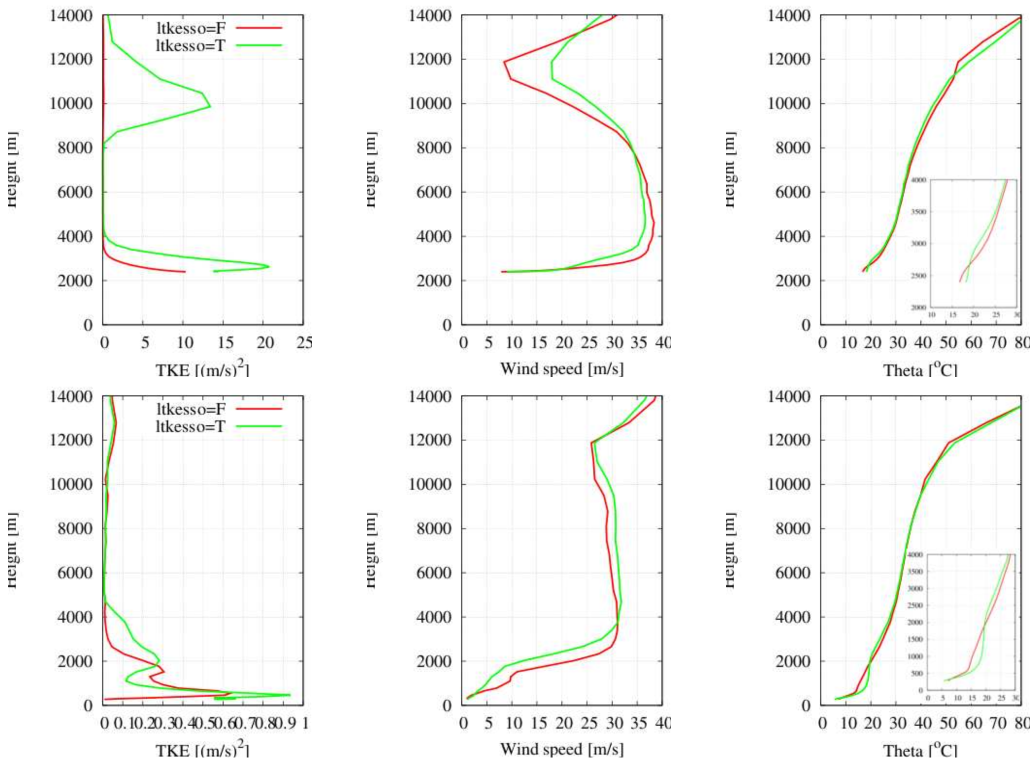

Figure 3: Simulated vertical profiles of TKE (left), horizontal wind speed (middle) and potential temperature (right) in a model grid point with high SSO (lat=45.3, lon=7.2; top line) and in a point downflow (lat=45.0, lon=7.5; bottom line) simulated with and without *ltkesso*. Time: 08/01 01:00

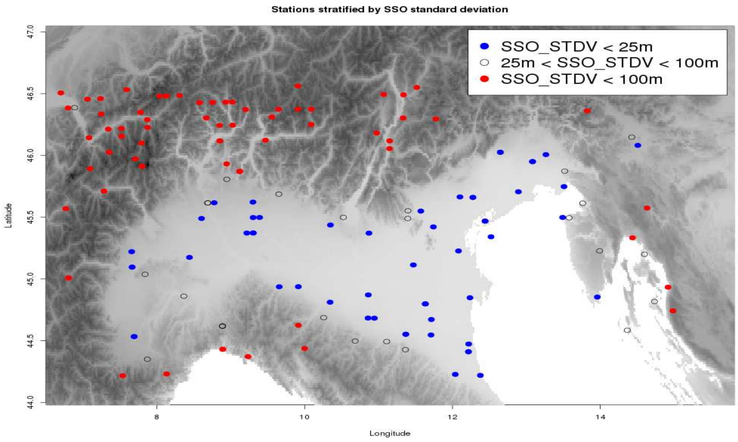

Figure 4: Stations used in the verification aggregated on the base of the sso_stdv value of the closer model gridpoint

5. Verification

The verification is performed by aggregating model grid points with similar SSO standard deviation (sso_stdv), as an indication of the presence of SSO [2]. Two categories are considered: stations which nearest model grid point has sso_stdv-values below 25m in the first category, and above 100m in the second one (Fig. 4). The geographical pattern of sso_stdv broadly corresponds to that of the grid-scale orography, however this is not always true (e.g. the highlands have high altitude but small sso_stdv). The verification of 2m temperature (Fig 5) at high sso_stdv points outlines how the negative bias is mitigated, mainly by the effects of the increased mixing at the lowest model levels (see sect. 4). In the January case, the bias and rmse decrease is about $1 - 1.5K$, while in the May case the improvement is smaller ($\leq 0.5K$), due to the lower impact of *ltkesso*.

At low sso_stdv points, a light warming up is visible, but only in the January case. During day this mitigates the negative bias, however during night it enlarges the positive bias. This nocturnal positive bias is correlated to the over-diffusive turbulence scheme in the SBL, related to some un-physical limits in turbulence code preventing the TKE to fade out (*Cerenzia et al., 2014*). Hence, the activation of an additional source of TKE (despite its small entity) further promotes the over-mixing. However, this induced destabilization in SBL demonstrates the potential of *ltkesso* to sustain the turbulent diffusion even above points with low SSO. Thus, this measure will be beneficial in order to substitute the still present additional unphysical mixing in the scheme.

The verification scores of the wind speed at 10m (Fig 5) in points at high sso_stdv are improved by the intensification due to the increased mixing at the lowest model levels (see sect. 4). The improvement is about $0.5m/s$ in the January case, and less in the May case, for the same reason mentioned above. The verification in points at low sso_stdv provides a very small signal, which is difficult to interpret. The verification performed against all the stations (Fig 5, 6, top line) shows a general improvement by the application of the *ltkesso*-option in terms of 2m temperature, 10m wind speed and mean sea level pressure (the latter not shown for brevity). The observed intensification of temperature and wind speed, and lowering of pressure (all at the near surface levels) are in agreement with the results obtained over the full COSMO-EU domain in 2011 (*Raschendorfer, 2011*).

[2] sso_stdv is a constant field employed in COSMO model in the SSO scheme and it can be retrieved from the model output.

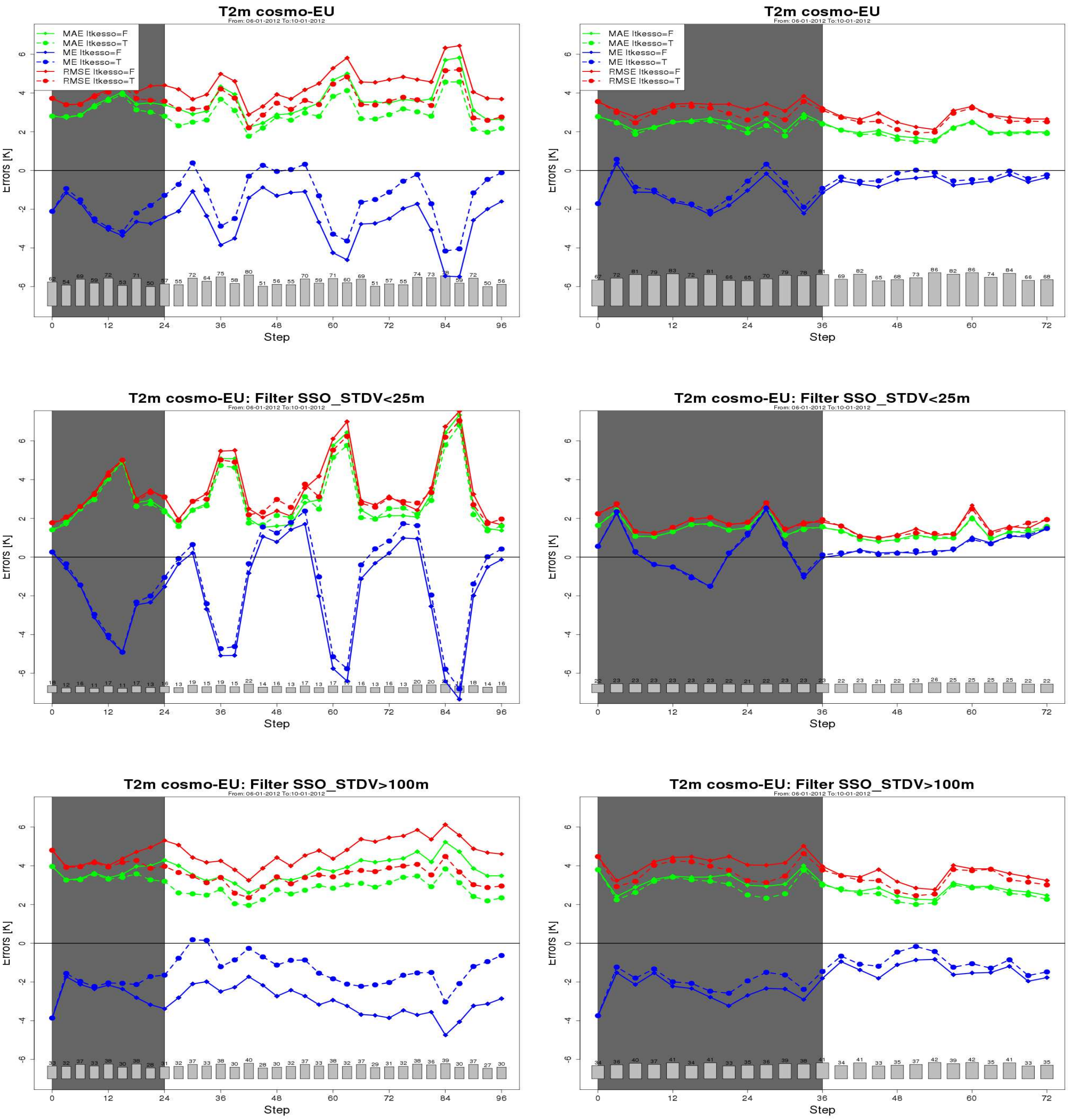

Figure 5: Verification of 2m temperature in the January and May cases (left and right respectively). All North Italian stations (top line), only North Italian stations which nearest model grid point has sso_stdv below 25m (middle line) and only North Italian stations which nearest model grid point has sso_stdv above 100m (bottom line). The histograms represent the sample size for each time range. The grey shaded area is considered as spin-up time and it is not involved in the analysis.

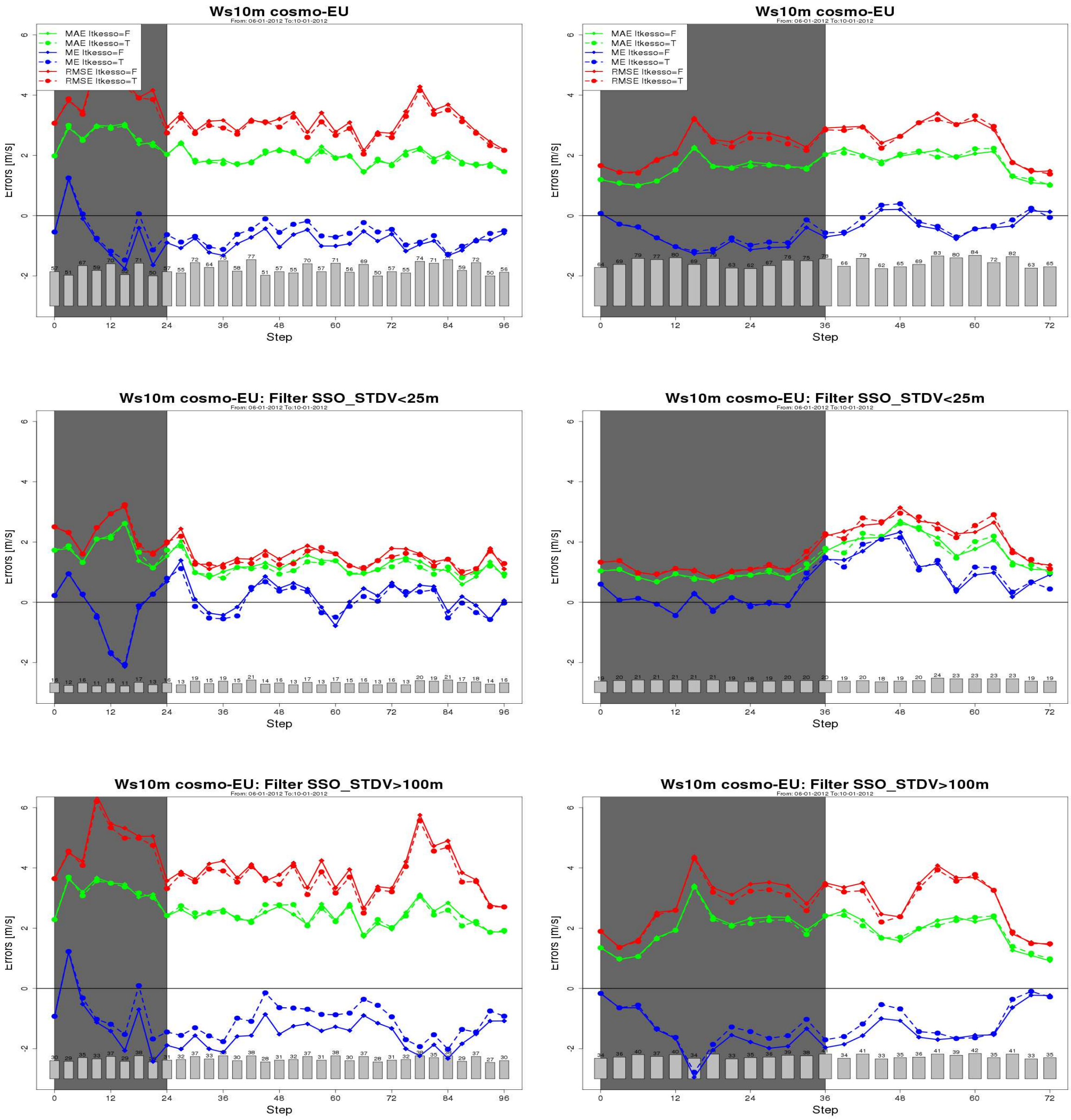

Figure 6: As in Fig.5 but for 10m wind speed.

6. Conclusions

We studied the effect of the additional source for TKE, derived from the sink term of momentum generated by the SSO scheme. It is based on the hypothesis that Sub-Grid Scale (SGS) motions induced by SSO themselves produce kinectic energy, that can be treated by the turbulence scheme. This hypothesis belongs to the framework of the Separated Turbulence Interacting with (non-turbulent and still unresolved) Circulations, developed by M. Raschendorfer.

The analysis of the case studies underlines that a large additional amount of turbulent kinetic energy is generated due to the additional TKE source mainly at three ranges of altitude above areas of pronounced SSO: at the lowest model levels, at the top of the troposphere and at the highest model levels. The first one is associated to the blocking effect on flow by SSO, while the other two to the gravity-wave breaking.

We evidenced that the related increase of turbulent vertical mixing at the lowest levels produces significant feedbacks on the wind profile above those areas. As a primary effect the vertical positive gradient at the lowest levels is reduced, intensifying the near surface wind speed and slowing it above. Since the surface momentum flux intensifies as well, by the increase of the low-level wind speed and diffusivity, effectively more momentum is extracted from the upper layers. In terms of temperature, the impact is significant mainly in cases in which the turbulence activity is weak, e.g. in SBL. In those cases the profile destabilizes, leading to a near surface warming and a cooling above. The effects on the near surface variables are very beneficial by comparing the simulations with the data collected in North Italy stations located in sites at pronounced SSO (sso_stdv higher than 100m). The negative biases of wind and temperature are reduced in both the case studies considered, although the effect is more evident in the case characterized by stable anticyclonic conditions.

Moreover, the significant TKE production at the top of the troposphere is in accordance with the results of Raschendorfer and Barleben (2014) above structured orography and confirms the potential of this measure to reproduce the Clear Air Turbulence occurrences.

A minor impact on the simulation has been observed also at areas above low SSO. It is partially associated to the advection downflow of the modifications generated at points above pronounced SSO, and partially directly induced by an increase of diffusivity at the lowest levels due to the additional TKE-source. Neglecting the local effect of the downflow, only stable boundary layers appear sensitive to this intensified diffusivity, because the increment is comparable with the typical values for stable stratifications. At the moment, the effect is detrimental on the near surface temperature, in comparison with data collected at sites above low SSO (sso_stdv lower than 25m). This may be associated to the fact that the SBL is already over-mixed, due to the use of some un-physical limits in the turbulence code. Nevertheless, the potential of this measure to sustain the turbulent mixing in conditions of weakly diffusive background is an actractive feature. Therefore, we suggest that this kind of physical based additional terms in the TKE equation will help to prevent the use of the current undesired numerical limits in the turbulence scheme.

In order to confirm the results obtained from these two case studies, a verification based on the same thresholds of sso_stdv is currently performed over the COSMO Common Area. The results will be available in the next Common Plots report.

References

[1] I. Cerenzia, F. Tampieri, M.S. Tesini, 2014. *Diagnosis of Turbulence Schema in Stable Atmospheric Conditions and Sensitivity Tests*, Cosmo Newsletter 14.

[2] F. Lott, M. J. Miller, 1997. *A new subgrid-scale orographic drag parametrization: its formulation and testing.* Q. J. R. Meteorol. Soc.,123, 101–127.

[3] M. Raschendorfer, 2011. *Ergebnisse der Experimente mit aktiver Nachlaufwirbelturbulenz durch SSO.* DWD, Routine-Sitzungen im Februar u. April 2011

[4] M. Raschendorfer, A. Barleben, 2014. *Vorhersage fluggefährdender Turbulenz und ihre Registrierung,* DWD, promet 39 No. 1/2 pp 23-35

[5] J.P. Schulz, 2009. *Introducing sub-grid scale orographic effects in the COSMO model*, Cosmo Newsletter 9.

Implementation and Significance of TKE-Advection in COSMO 5.0 for itype_turb=3 and Other Turbulence-Related LES-like Sensitivity Studies Including 3D Turbulence

Ulrich Blahak, Deutscher Wetterdienst

Frankfurter Str. 135, 63067 Offenbach

1 Introduction

Up to now the advection of TKE was only implemented for the alternative turbulence schemes from the LLM-project (`itype_turb=5...8`). It can be activated by by choosing `lprog_tke=.TRUE.` and is only possible when using the Runge-Kutta-Core. This process has now also been implemented for the "standard" scheme (`itype_turb=3`), still only for Runge-Kutta-dynamics. This document describes the technical implementation and some simulations to investigate the significance of the process for simulations at 3 km horizontal grid spacing (today's "high resolution" weather forecasting) as well as for an LES-like setup for explicit shallow convection simulations at 200 m grid spacing.

Note that the switch `lprog_tke=.TRUE.` has a slightly different meaning in the different schemes, as will be explained below. Whereas it only denotes the advection process of TKE for `itype_turb=3`, it also switches on the vertical and horizontal TKE diffusion (depending on switch `l3dturb`) for the schemes `itype_turb=5...8`. The latter processes are active in `itype_turb=3` independent of `lprog_tke`.

For the LES-like setup, besides the effects of including TKE-advection, we will also investigate in more general the settings of other turbulence-related parameters, in particular in combination with considering full 3D turbulence effects (`l3d_turb=.true.`). This is relevant for future LES-like very high resolution simulations in idealized or real-case configurations, because it gives hints on how to properly choose and configure the turbulence scheme(s).

Although we mention the schemes `itype_turb=5/6` above and sometimes below, their use is not recommended!

Just to mention, the difference between `itype_turb=7` and `8` respectively `5` and `6` is that the latter employ moist conserved liquid water potential temperature instead of ordinary potential temperature to take into accound the effects of phase changes on local stability within clouds.

2 Implementation and technical testing

The implementation is along the lines of the COSMO tracer advection schemes. Semi-lagrange advection, flux-form density-based advection (Bott et al.) or the traditional formulation with divergence correction can be used.

For `itype_turb=3`, the transported quantity is the turbulent velocity scale $q = \sqrt{2\ \mathrm{TKE}}$, but for `itype_turb=5...8` it is directly the TKE. For the flux-form density-based advection schemes, the transported quantities are multiplied with the total density before the advection operator — to transform them to densities for the advection operator — and divided by the advected density afterwards, same as for the tracers. Because TKE is defined on half levels, the density values to multiply with have to be vertically interpolated to the half levels, which is done by linear interpolation. The same applies for the advected density to be divided by afterwards.

Technically, the advection is done slightly differently for the different turbulence schemes:

- `itype_turb=3`: The advective tendency $\mathrm{TEND}_{adv} = (q_{after} - q_{before})/\Delta t$ is stored on a new global field `tket_adv(1:ie,1:je,1:ke)` and added to q in the call to the subroutine `turbdiff()` in the next timestep, together with the other physical tendencies of q.
- `itype_turb=5...8`: "update in place" of the advected quantity on timelevel `nnew`

A slight complication arises for `itype_turb=3` because of the exponential filtering of q to damp numerical local oszillations during time integration. The relevant namelist parameter is `tkesmot`, which is the weight a in the recursive exponential time filter

$$q_{n+1} \;=\; (1-a)q^*_{n+1} \;+ aq_n \qquad (1)$$

where q_n is the "old" value, q_{n+1} the "new" and q^*_{n+1} is the result of an implicit time integration step,

$$q^*_{n+1} = \text{fct}\,(q_n, q^*_{n+1}, \text{TEND}(q_n), \Delta t) \quad (2)$$

It is obvious that, if we would include the advection in the total tendency $\text{TEND}(q_n)$, the transport velocity of TKE structures would be reduced by the factor a, which is physically wrong. To mitigate this problem and at the same time to keep the possibility for time smoothing, the procedure is modified. In a first explicit Euler-Forward-step, only the advective tendency $\text{TEND}_{adv}(q_n)$ is applied to obain a provisional value q^{**}_{n+1},

$$q^{**}_{n+1} = q_n + \text{TEND}_{adv}(q_n)\Delta t \quad (3)$$

Then, the implicit scheme is applied to this provisional value, neglecting the advective tendency,

$$q^*_{n+1} = \text{fct}\,(q^{**}_{n+1}, q^*_{n+1}, \text{TEND}(q_n) - \text{TEND}_{adv}(q_n), \Delta t) \quad (4)$$

followed by the time filtering

$$q_{n+1} = (1-a)q^*_{n+1} + aq^{**}_{n+1} \quad (5)$$

In this way, the time filtering is only applied to the non-advective part of the TKE-changes.

Note that, for the diffusion process of TKE, there is a similar problem with the spatial propagation speed of the diffusion signal, and in the future, the diffusion tendendy should also somehow be removed from the time filtering.

As a first testing step, a simple 2D idealized test case (flow over hill) has been set up. A cuboid package of high TKE values (50 m^2s^{-2}) is artificially introduced near the inflow boundary of the domain, and the output is analyzed every timestep. The spatial resolution was $\Delta X = 1.1$ km, the time step $\Delta T = 10$ s and 40 vertical levels up to 22 km height have been chosen. The initial wind speed is a constant $U = 10$ ms^{-1} everywhere (no lateral and vertical motion) and the temperature decreases linearily with height at the ICAO standard atmosphere gradient. With that, we have a stable stratification and very low windshear and expect pure horizontal transport.

This setup has been run for both `itype_turb=3` and `itype_turb=7` to test the two above-mentioned different implementations of TKE advection. Fig. 1 to 4 show the results for both runs for different simulation times, starting with the initial state (Fig. 1) and ending with 15 min (Fig. 4). Slight differences in the initial state are due to the fact that the output of TKE in the first timestep includes or excludes the time-changes during the first time step. For `itype_turb=7`, the output is on timelevel "nnow" as for the other prognostic model variables, so no changes occured. But in case of `itype_turb=3`, the local changes due to some TKE sources and sinks (not the advection and diffusion and possibly some others!) have already been added in the first time step.

One can see that in both cases the TKE-cuboid is transported with about the same speed, but there are differences in the vertical. Therefore, the advection is implemented properly and happens at the expected speed. We expect no advection errors in the other transport directions, because the same well-tested subroutines as for the tracers are applied in the same way.

However, the vertical differences require some more consideration. It turns out that these are due to differences in the turbulent diffusion of TKE. Note that the values of the Richardson Number $Ri = N^2/S^2$ (N = Brunt-Väisälä frequency, S = total shear) are quite high, so that in reality, we expect the TKE to die out very soon, associated with low turbulent mixing. This "stable" case is treated differently in both turbulence schemes. For `itype_turb=7`, the diffusion coefficients are simply set to a low value (0.1 m^2s^{-1}) regardless of the TKE, whereas they are still a function of stability and TKE in case of `itype_turb=3`. This explains why the blob of spuriously high TKE is strongly diffused in the latter case and nearly not diffused in the former.

The use of the already existing namelist parameter `lprog_tke` to switch on the advection of TKE for `itype_turb=3` requires some clarification, because its meaning is slightly different in case of the alternative schemes `itype_turb=7/8`. And in combination with the parameter `l3dturb` ("3D-turbulence"), different terms of the TKE-equation are actually considered. Tab. 1 summarizes these considered terms for `itype_turb=3` and Tab. 2 for `itype_turb=7` and 8. Note in particular that for `itype_turb=7/8` the metrical terms in horizontal differentials in case of `l3dturb=.true.` due to the terrain following coordinate system are not considered. This means that this scheme is strictly only valid for flat terrain, although the errors in case of "not too hilly" terrain should be tolerable.

Additionally Tab. 3 shows which processes are active for "3D-turbulence" in the other model equations for T, p, $\vec{v}$ and tracer(s), depending on `l3dturb` and the switch `l3dturb_metr`, which concerns the metrical terms due to terrain following coordinates in the horizontal diffusion part of the equations. In case of hilly terrain it is advisable to set `l3dturb_metr=.true.` if `l3dturb=.true.`.

Table 1: `itype_turb=3`: Considered processes in the TKE-equation for the different combinations of `lprog_tke` and `l3dturb`.

`lprog_tke`	**.false.**	**.false.**	**.true.**	**.true.**
`l3dturb`	**.false.**	**.true.**	**.false.**	**.true.**
∂_t	X	X	X	X
Therm. prod.	X	X	X	X
Horiz. Shear prod.		X		X
Vert. Shear prod.	X	X	X	X
Dissipation	X	X	X	X
Horiz. diffus.				X
Vert. diffus	X	X	X	X
Advection			X	X
Metrical terms in horiz. differentials in TKE-equation due to terrain following coordinates		X		X

Table 2: Same as Tab. 1, but for `itype_turb=7` and `8`.

`lprog_tke`	**.false.**	**.false.**	**.true.**	**.true.**
`l3dturb`	**.false.**	**.true.**	**.false.**	**.true.**
∂_t			X	X
Therm. prod.	X	X	X	X
Horiz. Shear prod.		X		X
Vert. Shear prod.	X	X	X	X
Dissipation	X	X	X	X
Horiz. diffus.				X
Vert. diffus			X	X
Advection			X	X
Metrical terms in horiz. differentials in TKE-equation due to terrain following coordinates				

Table 3: `itype_turb=3`: Considered processes in the equations for T, p, $\vec{v}$ and tracer(s) depending on `l3dturb` and `l3dturb_metr`.

`l3dturb`	**.false.**	**.true.**	**.true.**
`l3dturb_metr`	**(not relevant)**	**.false.**	**.true.**
Vertical diffus. of T, p, $\vec{v}$ and tracer(s)	X	X	X
Horizontal diffus. of T, p, $\vec{v}$ and tracer(s)		X	X
Metrical terms in horiz. differentials in diffusion tendencies of T, p, $\vec{v}$ and tracer(s) due to terrain following coordinates			X

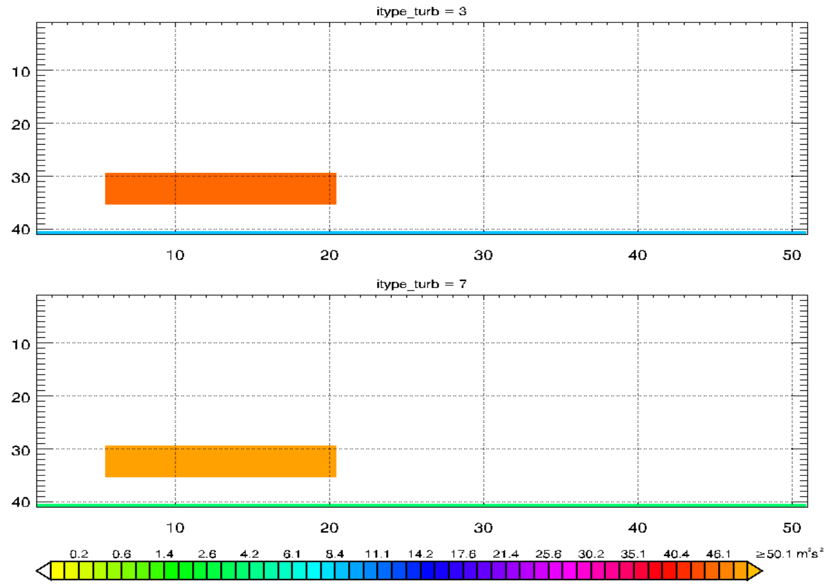

Figure 1: Simple test of the TKE advection for `itype_turb=3` and `7`. X-Z-cut along the 2D flow, $U = 10$ ms^{-1} everywhere from left to right, stable stratification (ICAO-standard atmosphere). Initial values for the TKE.

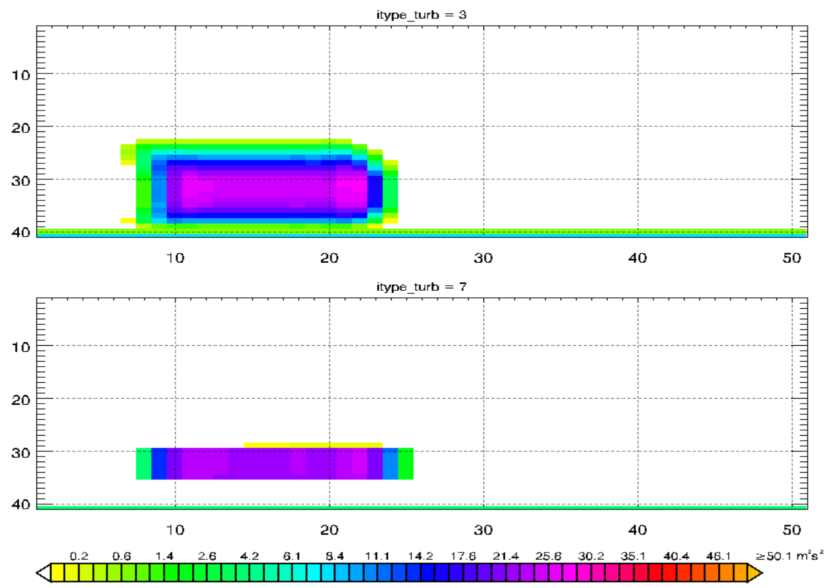

Figure 2: Same as Fig. 1 but after 2 minutes.

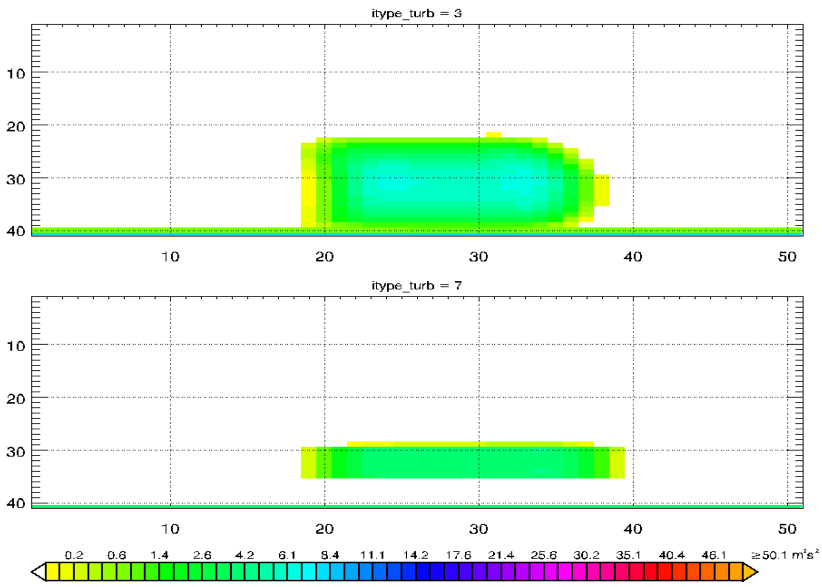

Figure 3: Same as Fig. 1 but after 10 minutes.

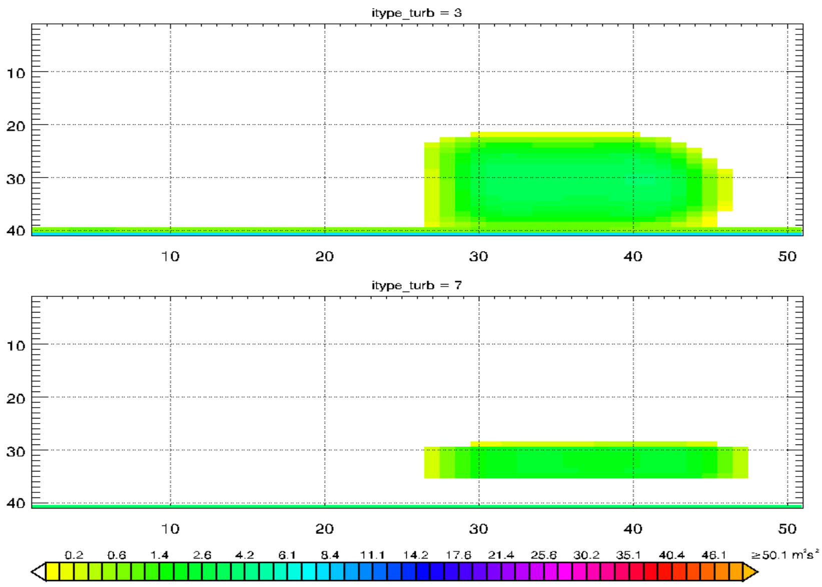

Figure 4: Same as Fig. 1 but after 15 minutes.

3 Meteorological significance for $\Delta X \sim 3\,\mathrm{km}$

For `itype_turb=3`, the activation of `lprog_tke` has been tested by a real case COSMO_DE hindcast of 31.5.2011, 12 UTC +21 h, driven by the operational COSMO_DE-analyses (`l3dturb` remained `.false.`). Two model runs were performed, one with `lprog_tke=.false.` and the other with `.true.`. The 3D-turbulence was deactivated, consistent with the operational setup of COSMO_DE. The only difference between the two runs is thus the consideration of TKE-Advection (cf. Tab. 1, first and third column).

Fig. 5 shows T_2M (upper row) and accumulated total precipitation (lower row) after 21 h at the end of the forecast. The left column is without TKE-Advection, the middle column with TKE-Advection and the right column is the difference with minus without. No significant differences for the T_2M can be observed, only a wave-like pattern, perhaps indicating spatial shifts, is visible in the difference plot.

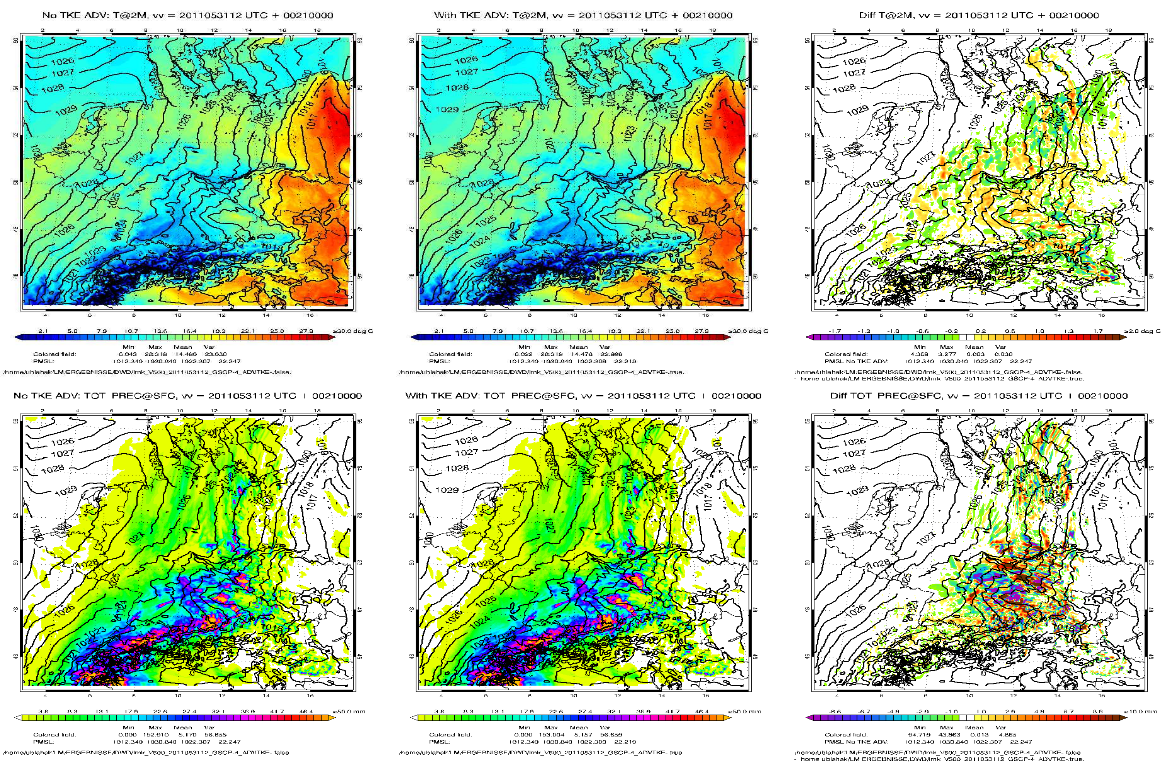

Figure 5: COSMO_DE hindcast, 31.5.2011 12 UTC + 21 h, `itype_turb=3`.
Upper left: T_{2m}, no TKE advection.
Upper middle: T_{2m}, TKE advection.
Upper right: Difference middle to left.
Lower left: Total precip, no TKE advection.
Lower middle: Total precip, TKE advection.
Lower right: Difference middle to left.

This is generally similar also for the total precipitation, except for a region south of the Erzgebirge, Eastern Bavaria and Western Czechia. Here, the consideration of the TKE-Advection shifted the precipitation pattern a little to the South.

However, for both quantities, the domain averaged systematic difference is very very small. The effect of considering the TKE-Advection has therefore no significant effect on the weather forecast in this case. However, this has to be checked by a longer term experiment.

4 Dependence on the different subswitches for 3D LES-like simulations

To further illustrate the effects of the different switches/processes in Tab. 1 and Tab. 2 on very high resolution runs, a series of idealized LES-like simulations with a horizontal grid spacing of $\Delta X = 200\,\mathrm{m}$ has been performed. The runs are characterized by 125 x 125 grid points in the horizontal, 64 levels in the vertical up to 15 km height, periodic boundary conditions, flat terrain, condensation and cloud microphysics switched off, soil model switched off, radiation switched off, deep and shallow convection parameterization switched off, usage of the new fast waves solver in the Runge-Kutta core, and a forced constant sensible heat flux of $H_0 = 300\,\mathrm{Wm}^{-2}$ at the surface.

The initial T-profile in the PBL is slightly stable with a T lapse rate of $\approx -0.007\,\mathrm{Km}^{-1}$, and the wind profile is $U(z) = U_\infty \tanh(z/z_{ref})$ with $U_\infty = 5\,\mathrm{ms}^{-1}$ and $z_{ref} = 3000\,\mathrm{m}$. Some small random noise on T and w is added at simulation start in the lowest 100 hPa of the atmosphere to initiate motions on different scales from which shallow convection will spin up later.

For each of the 4 possible combinations of the switches `lprog_tke` and `l3dturb` and each of `itype_turb=3` and `7`, a model run has been performed out to +4 h. To make both turbulence schemes comparable, the full 3D isotrophic shear production of TKE has been switched on for `itype_turb=3` by choosing `itype_sher=2`. Fig. 6 shows horizontal cross sections of w at a height of about 700 m after 4 h for each of the 4 switch combinations in case of `itype_turb=3`. Fig. 7 is the same, but for `itype_turb=7`.

From convection theory and measurements, one would expect to see coherent and organized up- and downdraft structures with a more cellular pattern close to the ground and more isolated updrafts above ("Thermals") , growing from the cell corners with converging horizontal motions.

The updraft regions should be smaller than the downdraft regions, and the maximum updrafts "stronger" than the maximum downdrafts, but not more than, say, 5 – 6 ms^{-1}. The diameter of the cellular patterns respectively the average distance between the thermals should scale with the boundary layer height and be about 2 - 5 times this height.

With this in mind, an inspection of Fig. 6 for `itype_turb=3` shows clearly that without 3D turbulence effects (upper row), the coherent structures are strongly overlayed by spurious noise, which turn out to be $2\Delta x$ waves caused by spurious energy accumulation at the smallest grid scales ("under-diffusive" turbulence scheme). Setting `l3dturb=.true.` completely changes the picture (lower row). The added horizontal diffusion effects (cf. Tables 1 and 3) cause a very strong smoothing of the structures, eliminating any $2\Delta x$ waves. The w structures seem qualitatively realistic, although in the opinion of the author somewhat overly smooth. A closer look at power spectra could shed more light on this in the future.

Clearly, considering TKE advection (by setting `lprog_tke=.true.`) is a second-order effect compared to the combined action of all other 3D effects (maybe because of the quite low windspeed).

The situation in Fig. 7 for `itype_turb=7` is slightly different. The $2\Delta x$ waves vanish here when setting `lprog_tke=.true.` and `l3dturb=.true.` (lower right panel). Then, the w structures look very realistic (considering the relatively coarse grid resolution for this phenomenon) and are not overly smoothed. The author considers this as the best simulation of the series.

As mentioned previously, concerning the different behaviour of the two turbulence schemes, the meaning of the two switches `l3dturb` and `lprog_tke` is different among the two turbulence schemes (Tables 1 and 2). Whereas for `itype_turb=3`, `lprog_tke` concerns only the TKE-advection and the TKE horizontal diffusion in case of `l3dturb=.true.`, it is connected to the prognostic treatment of TKE and to its advection and diffusion for `itype_turb=7`. Additionally, `l3dturb=.true.` switches on the horizontal diffusion of all other prognostic variables.

From the different behaviour visible in Figures 6 and 7, one possible conclusion is that mainly the consideration of the horizontal diffusion (`l3dturb=.true.`) of the model variables, including in the TKE-equation the TKE shear production and TKE diffusion, enhances the quality of the results in the presented case.

The different "degree of smoothing" of the w structures between the two turbulence schemes, perhaps associated with a different behaviour of the power spectra, deserves a closer look. As previously mentioned, the author considers the simulation with `itype_turb=7` and `lprog_tke=.true.` and `l3dturb=.true.` (Fig. 7, lower right) as the best simulation of the series. For the standard scheme `itype_turb=3`, an unrealistically smooth w field was obtained here (Fig. 6, lower right). To improve the simulation here, M. Raschendorfer suggested, on physical grounds, to limit the horizontal length scale for 3D-turbulence by $0.5\Delta X$ instead of the current $1\Delta X$.

This can be motivated by the fact that each one of a pair of contrariwise rotating eddies, which are not resolved by the grid, can have a maximum horizontal diameter of $0.5\Delta X$. If the most energetic non-resolved eddies are assumed to be even smaller, the factor should also be smaller than 0.5.

To be separated from the vertical length scale, the factor 0.5 has been introduced in the code only at the 2 following places:

- `turbulence_utilities.f90`, subroutine `turb_param()`:

  ```
  l_scal=MIN( 0.5*l_hori, tur_len )
  ```

- `turbulence_diff.f90`, subroutine `turbdiff()`:

  ```
  IF (itype_sher.GE.2 .OR. PRESENT(tket_hshr)) THEN
  !Separate horizontale Scherungsmode soll berechnet werden:
    DO j = jstart, jend
    DO i = istart, iend
      src(i,j)=(a_hshr*0.5*l_hori)**2 * hlp(i,j,k)**z1d2 !related horiz. ...
    END DO
    END DO
  ```

Fig. 8 compares a corresponding test simulation (right) with "standard" `itype_turb=3` (upper left; same as Fig. 6 lower right) and with the abovementioned best simulation `itype_turb=7` (lower left; same as Fig. 7

lower right). The w field of the test simulation appears much similar to the one from `itype_turb=7`, although still a little more smooth. However, the reduction of the limiting horizontal length scale by half is clearly an improvement. The question if the value should be even smaller than 0.5 should be addressed in the future, e.g., by inspection of the corresponding power spectra.

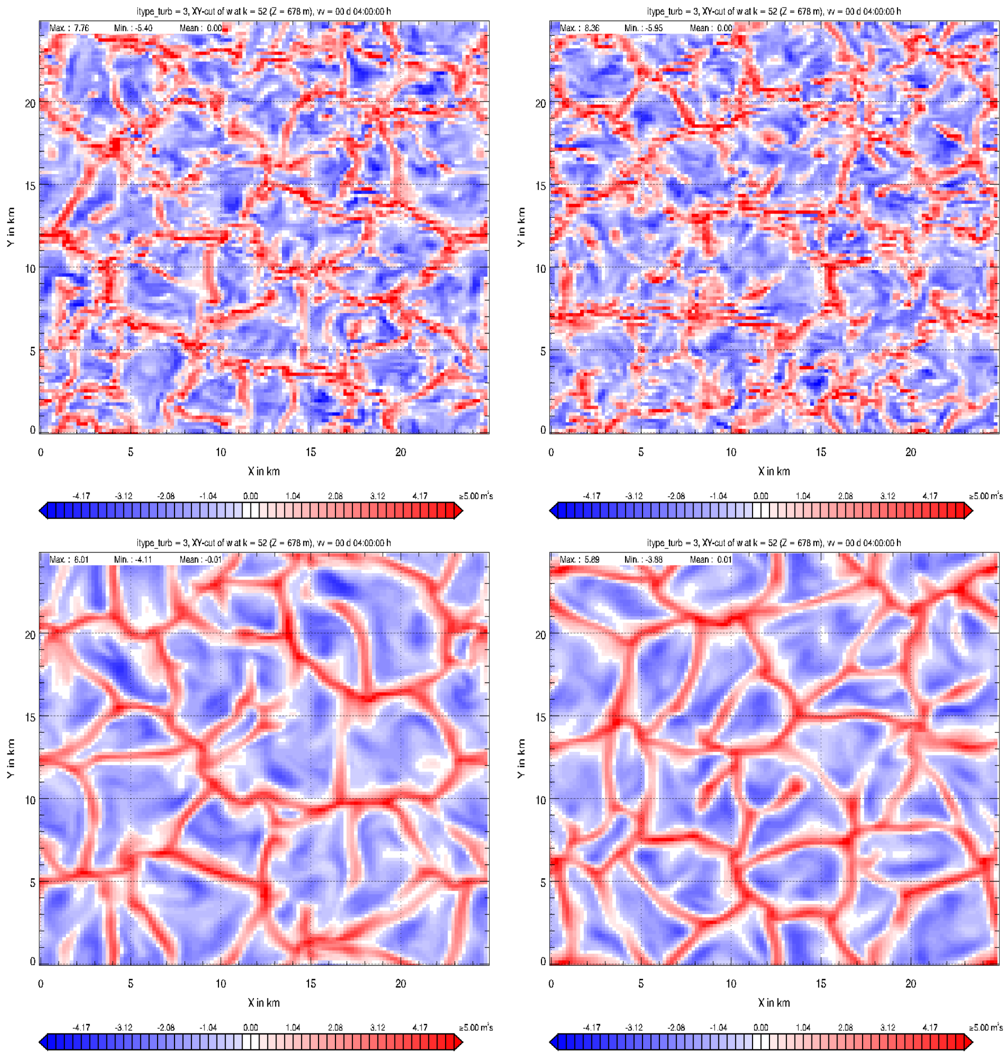

Figure 6: LES experiment: $H_0 = 300\,\mathrm{Wm}^{-2}$, $\Delta X = 200\,\mathrm{m}$, 4 h after simulation start, `itype_turb=3`, horizontal cross section of w at $Z = 678\,\mathrm{m}$.
Upper left: `lprog_tke=.false.`, `l3dturb=.false.`.
Upper right: `lprog_tke=.true.`, `l3dturb=.false.`.
Lower left: `lprog_tke=.false.`, `l3dturb=.true.`.
Lower right: `lprog_tke=.true.`, `l3dturb=.true.`.

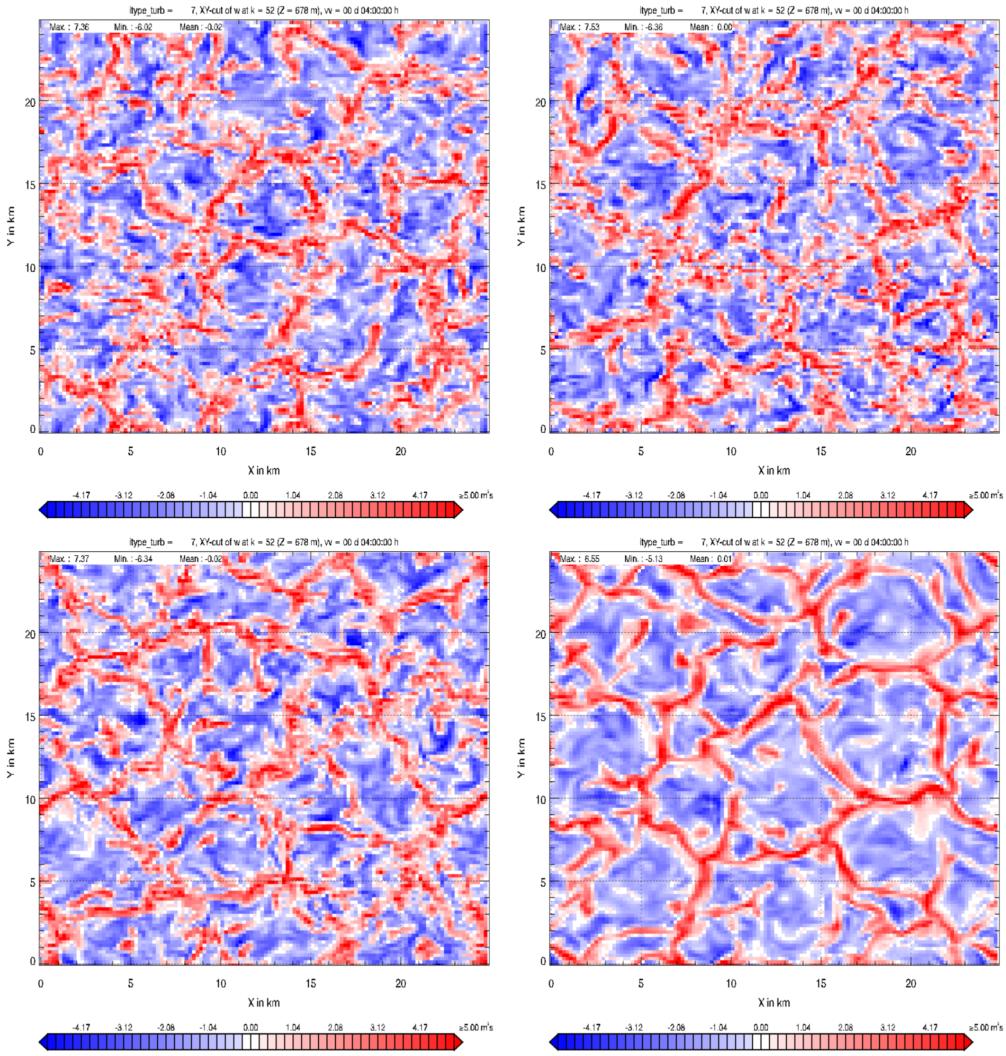

Figure 7: LES experiment: $H_0 = 300\,\mathrm{W m^{-2}}$, $\Delta X = 200\,\mathrm{m}$, 4 h after simulation start, `itype_turb=7`, horitonal cross section of w at $Z = 678\,\mathrm{m}$.
Upper left: `lprog_tke=.false.`, `l3dturb=.false.`.
Upper right: `lprog_tke=.true.`, `l3dturb=.false.`.
Lower left: `lprog_tke=.false.`, `l3dturb=.true.`.
Lower right: `lprog_tke=.true.`, `l3dturb=.true.`.

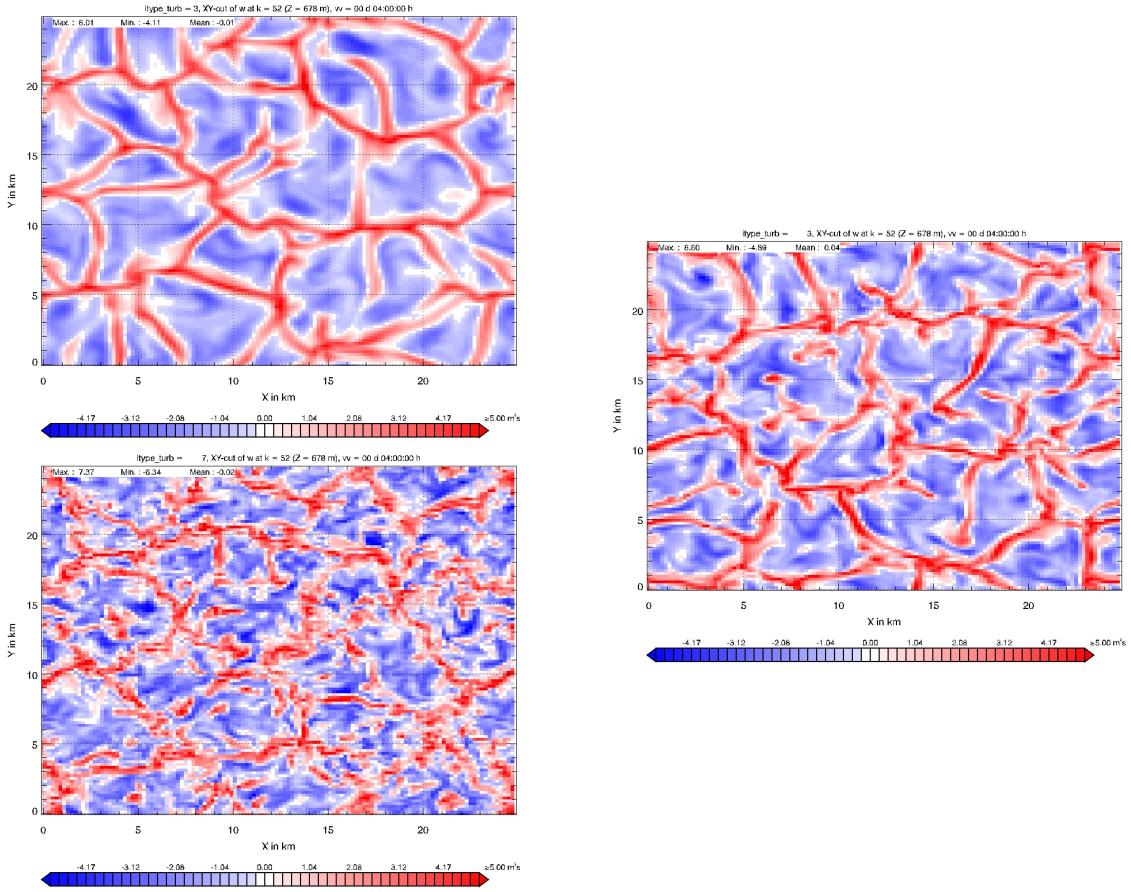

Figure 8: LES experiment: $H_0 = 300\,\mathrm{W m^{-2}}$, $\Delta X = 200\,\mathrm{m}$, 4 h after simulation start, `lprog_tke=.true.`, `l3dturb=.true.`.
Upper left: `itype_turb=3` with original turbulent length scale formulation, same as Fig. 6 bottom right.
Lower left: `itype_turb=7` same as Fig. 7 bottom right, ("best" simulation).
Right: `itype_turb=3`, but with limitation of the horizontal length scale by $0.5\Delta X$ instead of $1\Delta X$. **Clear improvement compared to upper left!**

5 Summary and Outlook

The advection of TKE has been implemented into the COSMO-model for the standard turbulence scheme `itype_turb=3`, where it has not been present before. The implementation details have been described in Section 2. Section 3 shows that for todays "high resolution" NWP at a horizontal grid spacing of $\sim 3\,\mathrm{km}$ and the operational COSMO-DE configuration, its consideration does not lead to significant changes, although there might be some differences on small scales.

Further, for LES-like studies with the COSMO-model and full 3D turbulence closure, also the influence of other namelist configuration parameters for the turbulence scheme has been investigated. Here, in particular the consideration of horizontal diffusion (`l3dturb=.true.`) of all model variables (including in the TKE-equation the TKE shear production `itype_sher=2` and TKE diffusion) enhances the quality of the results in the presented case.

Here, the alternative hybrid Smagorinsky-/TKE turbulence scheme `itype_turb=7` lead to the most plausible and "realistic" results in terms of structure and smoothness of the w fields for shallow convection simulations. `itype_turb=3` produced overly smoothed structures. However, reducing the upper horizontal length scale limit from $1\Delta X$ to $0.5\Delta X$ leads to a considerable improvement towards the results of `itype_turb=7` and is promising for the future. It will have to be investigated in more detail, whether the reduction factor should be even smaller than 0.5 and how the corresponding power spectra behave.

If, for `itype_turb=3`, the spectra would follow reasonably well the -4/3 law without too much energy loss at small scales an without too much spurious buildup at $2\Delta X$, the COSMO-model would posess a universal turbulence scheme, usable from operational forecasting down to grid spacings in the LES range.

A new leaf phenology for the land surface scheme TERRA of the COSMO atmospheric model

Jan-Peter Schulz1,3,*, Gerd Vogel2, and Bodo Ahrens3

1LOEWE Biodiversity and Climate Research Centre, Senckenberganlage 25, D-60325 Frankfurt am Main, Germany
2Deutscher Wetterdienst, Meteorological Observatory Lindenberg – Richard-Aßmann-Observatory, D-15848 Tauche OT Lindenberg, Germany
3Goethe University Frankfurt, Institute for Atmospheric and Environmental Sciences, Altenhöferallee 1, D-60438 Frankfurt am Main, Germany
**Corresponding author: Jan-Peter Schulz, affiliation now: Deutscher Wetterdienst, Frankfurter Straße 135, D-63067 Offenbach am Main, Germany*

1 Introduction

The terrestrial biosphere has a significant impact on near-surface atmospheric phenomena by modifying the energy and water balance at the land surface. In particular, it determines the evapotranspiration and therefore the latent and sensible heat fluxes over land, and thus can considerably affect atmosphere and land characteristics, such as near-surface temperature and humidity, low-level clouds and precipitation (Arora, 2002).

In soil-vegetation-atmosphere transfer (SVAT) schemes the role of vegetation in controlling the energy and water balance is considered by taking into account its physiological properties, in particular, leaf area index (LAI, the ratio of leaf to ground area), stomatal resistance, and rooting depth. However, many SVAT schemes do not describe the vegetation as a dynamic component. The seasonal evolution of its physiological properties is prescribed as a climatology, being the same for each year of a simulation (see e. g. ECMWF, 2014).

This is also the case for the SVAT scheme TERRA of the Consortium for Small-scale Modeling (COSMO) mesoscale atmospheric model (Steppeler et al., 2003). There are different options for specifying the seasonal cycle of the LAI. In one method, a minimum and a maximum value of the LAI are specified, depending on land use, representing vegetation at rest and during the growing season, and the seasonal cycle is prescribed by a sinusoidal fit for the transitions between these values in spring and autumn (Doms et al., 2011). This is currently the default in the COSMO model for numerical weather prediction (NWP). In another method, climatological monthly mean values of the LAI are specified which are based on satellite retrievals. A shortcoming of these methods is that the model can not account for inter-annual variations of the seasonal evolution of the vegetation. In some years the spring and growing season start earlier, in some years they are delayed. In these cases, the state of the vegetation is not accurately represented in the model when prescribing the leaf phenology by a climatology, leading to errors in for instance the evapotranspiration. In this study, two phenology models are presented, based on Polcher (1994) and on Knorr et al. (2010), which allow the vegetation in TERRA to adapt to the simulated seasonal and inter-annual variations in weather and climate, as well as to habitat factors, such as elevation.

2 Model description

The COSMO model (Steppeler et al., 2003; Doms et al., 2011) is a nonhydrostatic limited-area atmospheric prediction model, which is developed and maintained by the COSMO consortium (http://www.cosmo-model.org). It is designed for both operational numerical weather prediction and various scientific applications on the $meso-\beta$ and $meso-\gamma$ scale. Furthermore, the COSMO model was expanded by the CLM community(http://www.clm-community.eu) to become applicable as a regional climate model, called COSMO-CLM (e. g. Rockel et al., 2008).

A variety of physical processes is taken into account by parameterization schemes, including the soil and vegetation model TERRA (Doms et al., 2011). It simulates the energy and water balance at the land surface and in the ground, providing the land surface temperature and humidity as lower boundary conditions for computing the energy and water fluxes between surface and atmosphere. In TERRA, all processes are modelled one-dimensionally in the vertical, no lateral interactions between adjacent soil columns are considered.

The soil temperature is calculated by the heat conduction equation, while the soil water content is predicted by the Richards equation. Both equations are discretized by a multi-layer scheme using the same layer depths for both temperature and water content. This allows to include the freezing and thawing of soil water or ice, respectively. At the interface between surface and atmosphere, the surface energy balance equation is solved, yielding the new surface temperature. It takes into account the total surface net radiation, the sensible and latent heat flux, and the ground heat flux. The atmospheric energy fluxes constitute the upper boundary condition of the soil heat conduction equation.

Precipitation reaching the ground is separated into infiltration or surface runoff. The simulation of the water vapour flux, returning moisture from the ground back to the atmosphere, depends on the land use. For vegetated areas, transpiration from the vegetation is computed, taking into account the plant physiological properties, and for non-vegetated areas, bare soil evaporation is computed. The total moisture flux, the evapotranspiration, at a grid element is calculated as an area weighted average of the individual fluxes. In the standard model configuration, the formulations of both components of the evapotranspiration are based on BATS (Dickinson, 1984). During this study, it turned out that the bare soil evaporation based on BATS is overestimated. Therefore, it was replaced by a formulation based on ISBA (Noilhan and Planton, 1989), yielding, for instance, a more realistic simulation of the annual cycle of soil moisture. The snow pack is simulated by a single-layer snow model, taking into account snow ageing with respect to albedo and density.

In TERRA, the vegetation is described basically by three parameters, i. e. the vegetation ratio (the fractional area of a grid element covered by vegetation), the LAI, and the rooting depth. The different options for specifying the seasonal cycle of the LAI and the vegetation ratio compared in this study are decribed in section 3. For the comparison, here the same exponential root profile is used for the different options, which is constant in time.

3 Seasonal cycle of the LAI

The parameter values describing the vegetation at a particular element of the model grid are determined by the dominant land use class as given by a land use dataset (Smiatek et al., 2008; Smiatek, 2014). In TERRA, the following parameters are needed: Minimum and maximum vegetation ratio ($\sigma_{min} and \sigma_{max}$), representing winter and summer conditions, minimum and maximum LAI ($LAI_{min} and LAI max$), and rooting depth.

3.1 Current parameterization (sinusoidal fit)

In order to specify a seasonal cycle of the LAI and the vegetation ratio, in the currently used standard configuration of the COSMO model for NWP a simple empirical analytical function is prescribed to interpolate between their minimum and maximum values (Doms et al., 2011). This function depends on the latitude φ and the altitude of the location, and on the initial Julian day J_d of the forecast. It is computed by the preprocessing procedure INT2LM which provides the initial and boundary conditions for the model (Schättler, 2014).

The Julian day V_s, when the vegetation period starts, and its length V_l (in days) are estimated by the following formulae:

$$V_s = max(1.0, 3(|\varphi| - 20^\circ)) \tag{1}$$

$$V_l = min(365.0, 345.0 - 4.5(|\varphi| - 20^\circ)) \tag{2}$$

The following reduction factor f_h depending on surface geopotential height Φ_S describes the effect of an increasing altitude:

$$f_h(\Phi_S) = exp(-5 \cdot 10^{-9} \cdot \Phi_S^2). \tag{3}$$

The seasonal cycle of the LAI (and of the vegetation ratio in a similar way) is given by:

$$LAI(\varphi, \Phi_S, J_d) = LAI_{min} + (LAI_{max} - LAI_{min}) \cdot f_v \cdot fh(\Phi_S), \tag{4}$$

with

$$f_v = max(0.0, min(1.0, 1.12 \cdot sin(\pi \cdot max(0.0, (J_d - V_s)/V_l)))). \tag{5}$$

3.2 Dynamic phenology adapting to meteorological conditions

The phenology is mainly determined by three meteorological, or climatological, conditions: temperature, day length, and water availability. Whenever one or more of these factors are not sufficiently supplied, the vegetation will experience "stress", limiting its ability to fully get developed. Beside these, there exist other limiting factors, for instance the net primary productivity (NPP), which is the result of photosynthetic activity and respiration of the vegetation and requires the treatment of CO_2 concentrations and fluxes in the atmospheric model (see e.g. Arora, 2002). There are several dynamic global vegetation models which make use of NPP dependent formulations of phenology, for instance, JSBACH (see e. g. Raddatz et al., 2007), CLM (Oleson et al., 2013), or ORCHIDEE (Krinner et al., 2005). But, since the COSMO atmospheric model does not include a carbon cycle we restrict ourselves to schemes without the need of NPP. Two phenology models are compared in this study, a diagnostic and a prognostic one, based on Polcher (1994) and on Knorr et al. (2010). They were both implemented in the TERRA offline model.

In order to describe the stress with respect to temperature, a phenology determining temperature T (based on Knorr et al., 2010) is defined by:

$$T(t) = \frac{\int_{-\infty}^{0} T_S(t+\widetilde{t})e^{\frac{\widetilde{t}}{\tau}}\,d\widetilde{t}}{\int_{-\infty}^{0} e^{\frac{\widetilde{t}}{\tau}}\,d\widetilde{t}} \tag{6}$$

where τ is the averaging period for the surface temperature T_S, and t is the time. This formula uses exponentially declining weights when going back into the past, which is equivalent to an exponentially declining memory of the plants for the surface temperature. The averaging period is chosen to be 15 days, this makes sure that the diurnal cycles and other short-term fluctuations of T_S are sufficiently dampened, while not making the evolution of T(t) too inert which would delay the vegetation period.

3.2.1 Polcher (1994)

Here, a purely temperature-limited LAI is adopted in modified form from Polcher (1994):

$$LAI(t) = \begin{cases} LAI_{min} & if\ T(t) \le T_1 \\ LAI_{min} + \frac{T(t)-T_1}{T_2-T_1}(LAI_{max} - LAI_{min}) & if\ T_1 < T(t) \le T_2, \\ LAI_{max} & if\ T_2 < T(t) \end{cases} \tag{7}$$

where T_1 is the minimum limiting temperature, and T_2 the maximum limiting temperature. These two parameters depend on the phenology type.

Knorr et al.(2010)

The phenology model by Knorr et al.(2010),includes limiting factors due to temperature, day length, and water availability. But, for the comparison with Polcher (1994), here the focus is set on the temperature, while excluding the day length and water limitations. This leads to:

$$\frac{dLAI(t)}{dt} = \begin{cases} k_{grow}(LAI_{max} - LAI(t)) if\ T(t) \ge T_{on/off} \\ k_{shed}(LAImin - LAI(t)) else \end{cases} \tag{8}$$

where $T_{on/off}$ is the leaf onset and offset temperature, and k_{grow} and k_{shed} are the growth rate and the shedding rate, respectively. These parameters depend on the phenology type.

4 Experiments and observational data

In order to compare the three phenology schemes described in section 3, experiments with the land surface scheme TERRA in offline mode were carried out. This methodology is described e.g. by Chen et al.(1997) or Schulz et al. (1998). For this comparison, TERRA was forced in each simulation with a set of identical atmospheric observations, which are downward shortwave and longwave radiation, total precipitation, near-surface wind speed, air temperature, and specific humidity. For this study, observations from the boundary layer field site Falkenberg were used, providing the atmospheric forcing variables as mentioned before, as well as several quantities for model validation, such as e.g. surface latent heat flux.

Falkenberg is a site at the Meteorological Observatory Lindenberg – Richard-Aßmann-Observatory – of the German Meteorological Service (Deutscher Wetterdienst), located about 5 km south of the observatory. It is a grass land site representative for farmland surfaces in the heterogeneous rural landscape typical for large parts of northern central Europe (Neisser et al., 2002; Beyrich et al., 2006). It is in continuous operation since 1998 with a main focus on the near-surface boundary layer and soil processes. A detailed description of the measurement conditions, instrumentation, data acquisition and the comprehensive quality control procedures is given by Beyrich and Adam (2007).

The offline simulations were carried out for five selected years between 2006 and 2013. They represent very different seasonal cycles in terms of temperature and precipitation. Some years had a very warm spring, e.g. 2007, and some years a cold one, e.g. 2013. It is expected that, in contrast to the current parameterization, the two temperature-dependent phenology schemes presented here will respond to these different seasonal cycles. A warm spring may lead to an early begin of vegetation activity, a cold one to a late begin. The main land surface parameter values needed to appropriately describe the Falkenberg site within TERRA are given in Table 1. They were based on measurements and estimates adapted to the site conditions. The predominant vegetation species are perennial ryegrass *(Lolium perenne)* and red fescue *(Festuca rubra)*. For these grass species an albedo value of 0.18 was used.

The soil texture especially prevailing at the radiation measurement spot is dominated by sandy pale soil *(Eutric Podzoluvisol)*, (see Hierold, 1997) according to the FAO soil classification (FAO, 1988), for which an albedo value of 0.2 was used. The prescribed albedo values are in good agreement with experimental findings for this site described by Beyrich and Adam (2007). Although the meadow of the site is mowed several times a year to keep the vegetation height below 20 cm, the impact of the surrounding crop fields on the 10 m wind speed was represented by a slightly increased roughness length z_0 of 0.03 m on annual average. The additional parameter values needed for the phenology models by Polcher (1994) and Knorr et al. (2010) were estimated as follows: $T_1 = 2°\mathrm{C}$, $T_2 = 15°\mathrm{C}$, and $T_{on/off}$= 5°C, $k_{grow} = k_{shed} = 0.07^{d-1}$.

Table 1: Main land surface parameter values in TERRA representing the Falkenberg site.σ_{min} and σ_{max} are the minimum and maximum vegetation ratio, representing winter and summer conditions for grass.LAI_{min} and LAI_{max} are the respective values but for the leaf area index.α_{gr} and α_{bs} are the surface albedos for grass and bare soil, and $z_{0.gr}$ and $z_{0.bs}$ are the turbulent roughness lengths for grass and bare soil, respectively.

Parameter	σ_{min}	σ_{max}	LAI_{min}	LAI_{max}	α_{gr}	α_{bs}	$c^{(m)}$	$z_{0,bs}^{(m)}$
Value	0.55	0.80	0.50	2.5	0.18	0.2	0.03	0.03

5 Results

The phenology models adopted from Polcher (1994) and Knorr et al.(2010) are compared to the current parameterization of the LAI, using the land surface scheme TERRA in offline mode by applying the methodology as described in section 4. Figure 1 illustrates the annual cycles of the 2m temperature as measured at Falkenberg during the years 2006, 2007, 2008, 2012, and 2013. They show a considerable inter-annual variability. Some years have a very warm spring, e. g. 2007, and some years have a cold one, e.g. 2013. In autumn, the differences are smaller, but there are also warm years, e.g. 2006, and cold years, e.g. 2007.

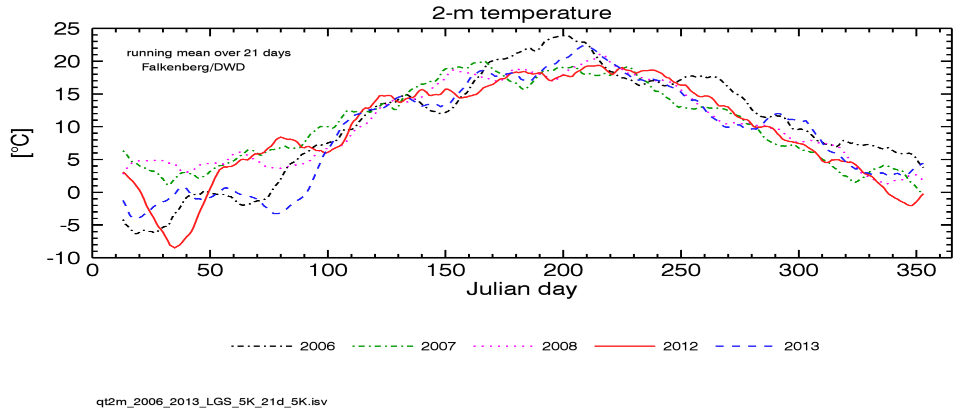

Figure 1: Annual cycles of the 2 m temperature as measured at Falkenberg during the years 2006, 2007, 2008, 2012, and 2013. A running mean over 21 days was applied to the data.

When running the land surface scheme TERRA in offline mode, using the phenology model based on Polcher (1994), it results in five different annual evolutions of the LAI. As shown in Fig.2 a warm spring such as in 2007 leads to an early rise of the LAI, or an early begin of vegetation activity, and a cold spring such as in 2013 results in a late rise of the LAI. A warm autumn, on the other hand, leads to a late decline of the LAI, e.g. in 2006, and a cold autumn results in an early drop of the LAI, e.g. in 2007. This means that the phenology model allows the vegetation in TERRA to adapt to the simulated seasonal and inter-annual variations in weather and climate. This is a clear improvement compared to the sinusoidal fit of the current parameterization, shown in Fig.2 for reference, which can not account for this variability.

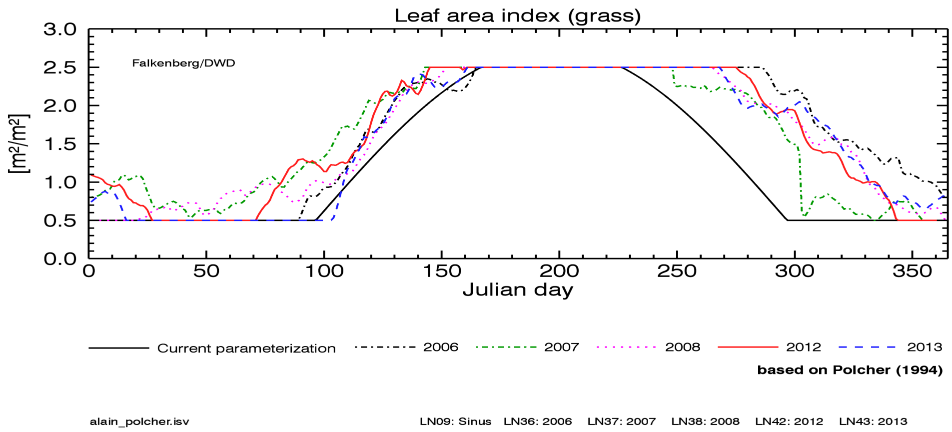

Figure 2: Annual cycles of the LAI at Falkenberg during the years 2006, 2007, 2008, 2012, and 2013 based on Polcher (1994). For comparison, the sinusoidal fit of the current parameterization is shown.

A shortcoming of a diagnostic model such as the one by Polcher (1994) may be that the LAI has to always closely follow the evolution of the driving quantities, here the temperature. This can lead to a drop of the LAI during its rising phase in spring which may not be realistic for many species. In contrast, in a prognostic model such as the one by Knorr et al. (2010), the LAI will keep on rising once the trigger for leaf onset is set. The underlying concept is that the initial leaf development relies on the buds and the reserves from the previous year. Leaf unfolding and growth will continue even if the surface stays cool for a while, as long as it does not return to frost or winter conditions.

The result is shown in Fig. 3. Once the leaf onset temperature is exceeded in spring, leaf unfolding and growth start, and the LAI starts rising asymptotically towards its maximum value. In autumn, this works in opposite direction. The order of the years is almost similar in Figs. 2 and 3. The warm spring in 2007 leads to an early rise of the LAI also for the phenology model based on Knorr et al. (2010), and the cold spring in 2013 results in a late rise of the LAI. A similar order of the years is also found in autumn, for instance, for the early dropping LAI in 2007 and the lately declining LAI in 2006. An exception is the year 2008 in which the LAI starts rising much earlier based on Knorr et al. (2010) than based on Polcher (1994). This shows the need for a careful calibration of the various threshold values, for instance for temperature, for the different phenology types.

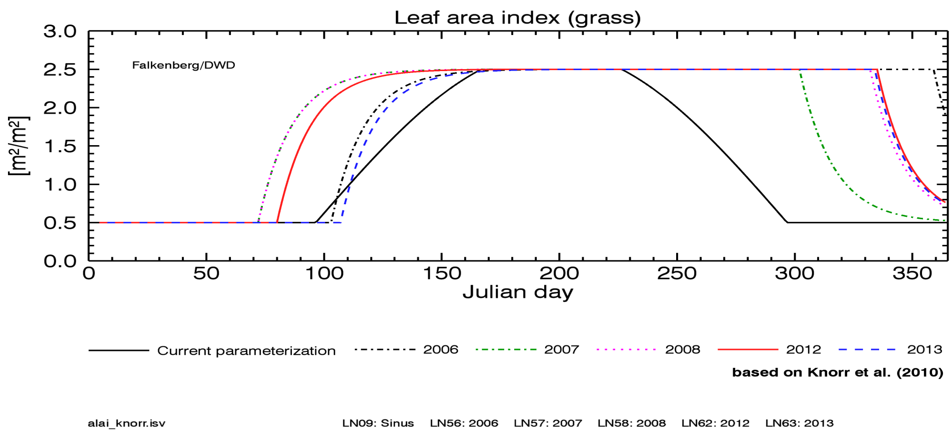

Figure 3: Same as Fig. 2 but for Knorr et al.(2010).

Due to the lack of in-situ observations of the LAI at Falkenberg, here an attempt for an indirect validation of the different models is made, using measurements of the surface latent heat flux at Falkenberg. Figure 4 compares the diurnal cycles of the observed and the simulated latent heat fluxes, averaged over the spring period of 1-20 April 2007 (Julian day 91-110). During this period, the LAI of the current parameterization increases from 0.5 to about 1.0, the LAI based on Polcher (1994) rises within the range of about 1.2 to 1.8 (both see Fig. 2), and the LAI based on Knorr et al. (2010) is already in the range of about 2.0 to 2.3 (see Fig. 3). As a consequence of these differences in LAI based on the three phenology models compared here, the transpiration and therefore the latent heat flux as simulated by TERRA show distinct differences as well. As depicted by Fig. 4, the maximum of the latent heat flux as simulated by the current parameterization is at about 90 W/m^2, which is clearly underestimating the measurement, the maximum based on Polcher (1994) is increased to about 120 W/m^2, while the one based on Knorr et al. (2010) reaches about 150 W/m^2.

The latter is very similar to the measurement. These results suggest that the current parameterization of the LAI is not able to accurately describe its early rise during the warm spring of 2007, while the two temperature-dependent phenology models based on Polcher (1994) and on Knorr et al. (2010) provide an earlier and more realistic increase of the LAI.

Qualitatively similar results are found for a period of leaf shedding in the autumn of 2007, as illustrated in Fig. 5.

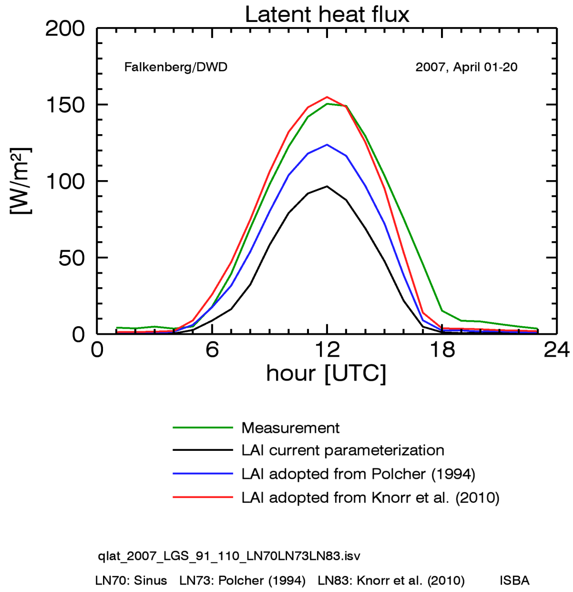

Figure 4: Mean diurnal cycles of the surface latent heat flux as measured at Falkenberg on 1-20 April 2007 (Julian day 91-110) compared to the results of the current parameterization of the LAI, and the results based on Polcher (1994) and on Knorr et al.(2010).

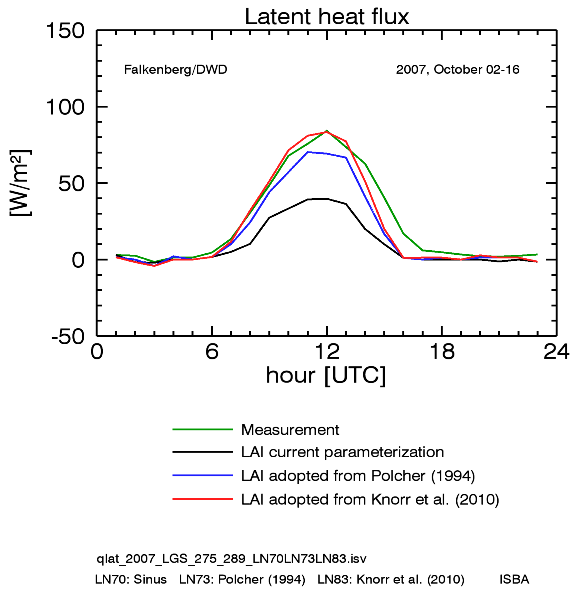

Figure 5: Same as Fig. 4 but for 2-16 October 2007 (Julian day 275-289).

6 Conclusions

Two temperature-dependent phenology models based on Polcher (1994) and on Knorr et al. (2010) were compared to the current parameterization of the LAI as used in the land surface scheme TERRA of the COSMO atmospheric model. Currently, in TERRA a minimum and a maximum value of the LAI are specified, depending on land use, representing vegetation at rest and during the growing season, and the seasonal cycle of the LAI is prescribed by a sinusoidal fit for the transitions between these values in spring and autumn. As a consequence, the model can not account for inter-annual variations of the seasonal evolution of the vegetation, leading to errors in for instance the evapotranspiration.

The two modified versions of TERRA, including the phenology models based on Polcher (1994) and on Knorr et al. (2010), allow the vegetation in TERRA to adapt to the simulated seasonal and inter-annual variations in weather and climate, as well as to habitat factors, such as elevation. Polcher (1994) uses a diagnostic approach, directly relating the LAI to temperature, while Knorr et al.(2010) follow a prognostic approach, utilizing the concept of growth and shedding rates. The latter appears to be generally favourable. Experiments with TERRA in offline mode, using observations from the boundary layer field site Falkenberg, have shown that the current parameterization of the LAI tends to significantly underestimate the surface latent heat flux during the transition periods in spring and autumn. In the case of the year 2007, this behaviour was found to be substantially improved by the model based on Polcher (1994). Furthermore, the simulated diurnal cycles of latent heat flux based on Knorr et al.(2010) were found to be very close to the observations, in terms of amplitude as well as phase.

This study was restricted to the temperature limitation of the LAI. The next step will be the extension of the phenology model to the limiting factors due to day length and water availability. This is already prepared in the work by Knorr et al. (2010). Furthermore, for global applicability, an extension to more phenology types, beside grass, is needed, for instance shrubs and trees (deciduous and evergreen). Finally, the phenology model needs to be transfered and implemented into the three-dimensional coupled COSMO model code.

Acknowledgements

The authors thank Udo Rummel, Deutscher Wetterdienst, for his assistance with the Lindenberg observational data. We further acknowledge funding from the Hessian initiative for the development of scientific and economic excellence (LOEWE) at the Biodiversity and Climate Research Centre (BiK-F), Frankfurt am Main. This work was supported by the German Federal Ministry of Education and Research (BMBF) under grant MiKliP: DECREG/01LP1118B, DEPARTURE/01LP1129D.

References

[1] Arora, V., 2002: *Modeling vegetation as a dynamic component in soil-vegetation-atmosphere transfer schemes and hydrological models.* Rev. Geophys., 40(2), 1006, doi:10.1029/2001RG000103, **26 pp**.

[2] Beyrich, F., and W. K. Adam, 2007: *Site and data report for the Lindenberg reference site in CEOP – Phase 1.* Berichte des Deutschen Wetterdienstes No. 230, Offenbach am Main, **55 pp**. ISBN/EAN:978-3-88148-422-0.

[3] Beyrich, F. (Ed.), S. H. Richter, U. Rummel, and U. Weisensee, 2006: *Ausgewählte Ergebnisse von Bodenfeuchtemessungen am Meteorologischen Observatorium Lindenberg.* Deutscher Wetterdienst – Forschung und Entwicklung: Arbeitsergebnisse Nr. 84, Offenbach am Main, **46 pp**. ISSN 1430-0281.

[4] Dickinson, R. E., 1984: *Modeling evapotranspiration for three-dimensional global climate models*: Climate processes and climate sensitivity. Geophys. Monogr., 29, Maurice Ewing Volume 5, 5,*58–72*.

[5] Doms, G., J. Förstner, E. Heise, H.-J. Herzog, D. Mironov, M. Raschendorfer, T. Reinhardt, B. Ritter, R. Schrodin, J.-P. Schulz, and G. Vogel, 2011: *A description of the nonhydrostatic regional COSMO model.* Part II: Physical parameterization. Deutscher Wetterdienst, Offenbach, **154 pp**. (Available at http://www.cosmo-model.org/).

[6] ECMWF, 2014: IFS documentation – Cy40r1. Part IV: Physical processes. European Centre for Medium-Range Weather Forecasts, Reading, **190 pp**. (Available at http://www.ecmwf.int/).

[7] FAO, 1988: Soil map of the world. Food and Agriculture Organization of the United Nations, Rome,**119 pp**.

[8] Hierold, W., U. Schumacher, R. Ziethen, and D. Becker, 1997: Kartierbericht. Ergebnisse der bodenkundlichen Kartierung zum Messfeld Falkenberg des Meteorologischen Observatoriums Lindenberg des DWD. Deutscher Wetterdienst, Internal report, Lindenberg, **26 pp**.

[9] Knorr, W., T. Kaminski, M. Scholze, N. Gobron, B. Pinty, R. Giering, and P.-P. Mathieu, 2010: *Carbon cycle data assimilation with a generic phenology model.* J. Geophys. Res., 115, G04017, doi:10.1029/2009JG001119, **16 pp**.

[10] Krinner, G., N. Viovy, N. de Noblet-Ducoudré, J. Ogée, J. Polcher, P. Friedlingstein, P. Ciais, S. Sitch, and I. C. Prentice, 2005: *A dynamic global vegetation model for studies of the coupled atmosphere-biosphere system.* Global Biogeochem. Cycles, 19, GB1015, doi:10.1029/2003GB002199, **33 pp**.

[11] Neisser, J., W. Adam, F. Beyrich, U. Leiterer, and H. Steinhagen, 2002:*Atmospheric boundary layer monitoring at the Meteorological Observatory Lindenberg as a part of the "Lindenberg Column"*: Facilities and selected results. Meteorol. Z., 11, **241–253**.

[12] Noilhan, J., and S. Planton, 1989: A simple parameterization of land surface processes for meteorological models. Mon. Wea. Rev., 117,**536–549**.

[13] Oleson, K. W., D. M. Lawrence, G. B. Bonan, B. Drewniak, M. Huang, C. D. Koven, S. Levis, F. Li, W. J. Riley, Z. M. Subin, S. C. Swenson, P. E. Thornton, A. Bozbiyik, R. Fisher, C. L. Heald, E. Kluzek, J.-F. Lamarque, P. J. Lawrence, L. R. Leung, W. Lipscomb, S. Muszala, D. M. Ricciuto, W. Sacks, Y. Sun, J. Tang, and Z.-L. Yang, 2013: *Technical description of version 4.5 of the Community Land Model (CLM).* National Center for Atmospheric Research, Technical Note NCAR/TN-503+STR, Boulder, CO, **420 pp**.

[14] Polcher, J., 1994: *Etude de la sensibilité du climat tropical à la déforestation.* Thèse de doctorat, Univ. Pierre et Marie Curie, Paris.

[15] Raddatz, T. J., C. H. Reick, W. Knorr, J. Kattge, E. Roeckner, R. Schnur, K.-G. Schnitzler, P. Wetzel, and J. Jungclaus, 2007: *Will the tropical land biosphere dominate the climate-carbon cycle feedback during the 21st century?.* Climate Dyn., 29, **565–574**.

[16] Rockel, B., A. Will, and A. Hense, 2008: *The regional climate model COSMO-CLM (CCLM).* Meteorol. Z., 17, **347–348**.

[17] Schättler, U., 2014: *A description of the nonhydrostatic regional COSMO model.* Part V: Preprocessing: Initial and boundary data for the COSMO model. Deutscher Wetterdienst, Offenbach, **74 pp**. (Available at http://www.cosmo-model.org/).

[19] Smiatek, G., 2014: *Time invariant boundary data of regional climate models COSMO-CLM and WRF and their application in COSMO-CLM.* J. Geophys. Res. Atmos., 119, **7332–7347**.

[19] Smiatek, G., B. Rockel, and U. Schättler, 2008: *Time invariant data preprocessor for the climate version of the COSMO model (COSMO-CLM).* Meteorol. Z., 17, **395–405**.

[20] Steppeler, J., G. Doms, U. Schättler, H.-W. Bitzer, A. Gassmann, and U. Damrath, 2003: *Meso-gamma scale forecasts using the nonhydrostatic model LM.* Meteor. Atmos. Phys., 82, **75–96**.

Fresh snow depth postprocessing at Hydrometcenter of Russia (exemplifying COSMO-Ru)

E.V. Kazakova, M.M. Chumakov and I.A. Rozinkina

1 Introduction

Present-day atmospheric models make it possible to get quite accurate forecasts of meteorological characteristics.Various kinds of precipitation take an important place among meteorological elements. Success in prediction of more and more realistic values of precipitation sums are particularly connected with rapidly developing technologies of operational numerical forecast based on non-hydrostatic mesoscale models with grid resolution about several km.

Due to modeling algorithms of atmospheric link of hydrological cycle, model precipitation is considered to be a mass of water which reached earth surface (taking into account its phase state) for given time period, i.e. accumulated water equivalent. According to WMO regulations, information about fallen precipitation is received from synoptic measurement network in the same terms, as well as general-purpose weather forecasts are made.

Due to stated structure "data-numerical forecast-general-purpose weather forecast", in case of falling of solid or mixed precipitation users (transportation, electricity supply networks, community facilities, organization of winter sports events, etc.) are not provided with greatly demanded information about depth of snow layer after snowfall which has already taken place or predicted. As a rule, for fresh snow depth determination simple empirical dependences based on assumption of constant values of its density are used in operational synoptic practice. Differences in density depending on air temperature are not considered (review in [1]). Use of more valid difficult dependencies should be provided on the basis of automated technology.

Snow depth measurements are held at hydrometeorological stations (HMS) and sent once a day through communication link in international exchange. Such a discreteness of measurements is not satisfactory for exact determination of snow depth in the train of snowfalls, as during this period of time snow cover could experience significant changes (snow could dense, melt, be blown by wind). In some regions there are automated meteorological stations (AMS), for example, in Sochi region in Russia, which measure snow depth with high time discreteness (once in 10 minutes). Yet, as the practice of their using has shown, these data should have thorough quality control because reliability of these data is very sensitive to accuracy of setting, operation conditions and regularity of technical service of AMS. That's why information about snow from AMS can't always be directly used in operational practice.

Nowadays results of calculations of non-hydrostatic mesoscale atmospheric models with grid resolution about several km are widely used by specialists while weather forecast forming. For visual representation of atmospheric modeling results postprocessing is applied. Calculation of density of falling snow with the use of parametric dependencies may be included into systems of postprocessing of operational modeling technologies. The work is dedicated to the description of technological chain in the framework of postprocessing of COSMO-Ru system and aspects of testing of results done for the mountain cluster region of winter Olympic Games Sochi-2014 for the period of its holding based on that chain.

2 Goals

The main goal was to propose users of mesoscale forecast system COSMO-Ru output a new type of information – snow increment for several hours. In order to achieve this goal a number of algorithmic and technological issues needed to be solved.

Forming of suggestions and testing of algorithm for fresh snow density calculation (hence, its layer thickness) referred to algorithmic tasks, combination of calculation of this characteristic with existing elements of postprocessing of COSMO-Ru operational system – to technological. Additional task was to analyze success of fresh snow depth calculation due to COSMO-Ru (with the proposed algorithm included into its postprocessing) on snow observations at AMS and HMS of North-Caucasian region during the period of winter Olympic Games Sochi-2014 holding. Technological aspects consist in work over combination of calculations according to the proposed module with operationally functioning postprocessing systems of COSMO-Ru.

COSMO-Ru postprocessing allows providing users with model output as tables and meteograms of a wide range of meteorological elements changing in time for given points as well as forming fields of different meteorological elements on grids in the form of maps of these elements' fields. While forming tables-meteograms, fresh snow depth could be calculated on the basis of elements' values included in the table.

The peculiarity of technological changes during present work was the fact that in the framework of preparation of meteorological support for Sochi-2014 at Hydrometcenter of Russia algorithm of model air temperature (2 meters) correction for mountain region based on moving amendments connected with differences between model and actual relief heights (for points for which meteograms are prepared) was proposed and implemented. It's obvious that when big differences occur, such a temperature amendment should be taken into account in calculations of fresh snow depth, especially at temperatures close to zero.

For output processing in grid nodes the program module of universal postprocessing FieldExtr[3] with very wide set of functions and possibilities (interpolation on different grids, diagnostic calculations of different characteristics, comparison and correction of some meteorological elements and so on) was developed in COSMO consortium.

One of the tasks of the present work was to adapt and to implement the proposed algorithm of fresh snow depth calculation on the basis of air temperature data into FieldExtra, what in future could allow providing users with calculated information in the form of maps.

3 Results of algorithm of fresh snow depth calculation implementation into COSMO-Ru system postprocessing

Before the start of winter Olympic Games Sochi-2014 since 3 February 2014 prognostic maps of fresh snow depth began to prepare at Hydrometcenter of Russia based on forecasts of precipitation sums obtained from COSMO-Ru model versions with grid resolution of 7 km (COSMO-Ru7), 2.2 km (COSMO-Ru2) and 1.1 km (COSMO-Ru1). Maps were formed according to operational forecasts data at 00, 06, 12 and 18 UTC.

Also values of fresh snow depth were recorded in meteograms for stations situated in North-Caucasian region. Prognostic values were calculated taking height-corrected air temperature into consideration.

The technological branch of fresh snow postprocessing and its output in the framework of COSMO-Ru system postprocessing are shown in figure 1.

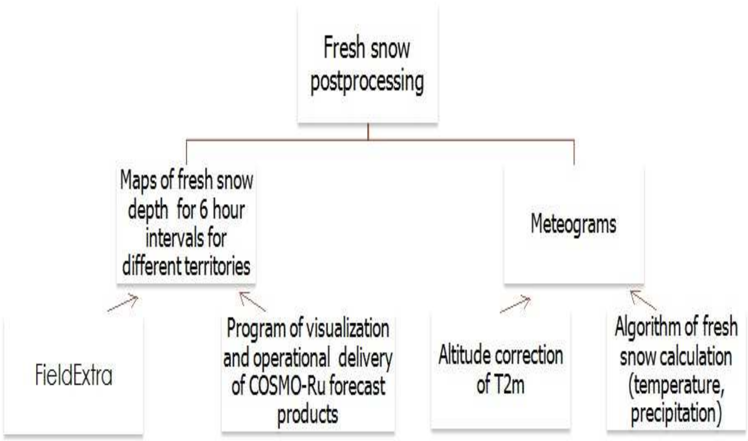

Figure 1: The scheme of fresh snow depth calculation at Hydrometcenter of Russia (based on mesoscale model COSMO-Ru).

Output is meteograms for stations and maps of fresh snow depth for 6-hour intervals prepared for versions COSMO-Ru7, COSMO-Ru2 and COSMO-Ru1 four times a day with the use of FieldExtra.

As can be observed in figure 2 there are significant differences in calculations according to different COSMO-model versions.

The fact that relief detailing and its model heights for this region turned to be principled for precipitation phase prediction, as here large elevation and temperature drops are observed.

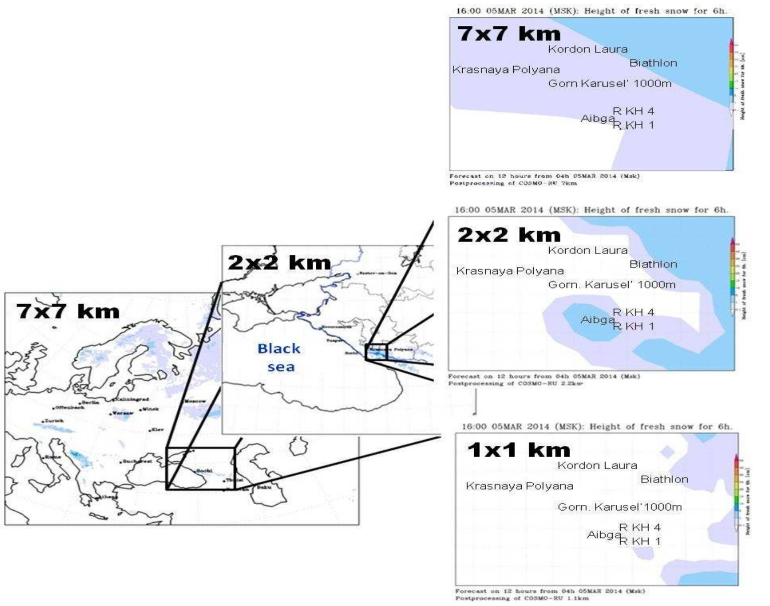

Figure 2: 12h-forecasts of fresh snow fallen for the last 6 hours according to COSMO-Ru7, COSMO-Ru2 and COSMO-Ru1. Start – 00 UTC 5 March 2014

And while relief smoothing in case of coarser resolution (COSMO-Ru7), area with negative air temperatures occurred to be larger in comparison with more detailed modeling (COSMO-Ru2, COSMO-Ru1), when definition of relief led to more accurate specification of extended valleys and relatively small highlands regions, for which snow falling was typical.

In addition testing done in [2] pointed out to lower precipitation sums formed by COSMO-Ru1 in comparison with COSMO-Ru2. Maps of fresh snow depth and meteograms were used for initial quality estimation of work of the proposed system as well as hourly measurements from AMS situated at different levels on the mountain resort Roza Khutor and daily measurements from three HMS (Aibga, Kordon Laura, Gornaya Karusel'-1500) located in the region of winter Olympic Games Sochi-2014 holding.

Complexity of testing realization was determined by several factors: firstly, snowfalls were observed only several times during winter season 2013/2014; secondly, model data could be compared with measurements only at some stations.

During winter Olympic Games Sochi-2014 holding there were three cases with significant snowfalls: 17-19 February, 21 February and 26-28 February. Let's have a look at the main peculiarities in fresh snow depth reproduction by COSMO-Ru in the region of winter Olympic Games Sochi-2014 holding.

Preliminary results showed a big variability of snowfall forecasts for the same period started at different instants of time, and the latest forecast was not always the best in comparison with others started before. Based on quite detailed analysis of time-distribution intensities inside snowfall period it's turned out impossible to conclude forecast with what lead time is more successful and what forecast is more accurate: obtained by model version with the resolution of 2.2 km or 1.1 km.

Yet in general the best agreement with snowfall measurements was observed in case of all realizations averaging. Comparison with similar calculations found at website *www.snow-forecast.com* [4] showed systematic underestimation of represented fresh snow values and results more close to reality calculated in the framework of COSMO-Ru1 and COSMO-Ru2 systems. Example of analysis of one snowfall case according to observations at Roza Khutor is shown in table 1.

The proposed system gives more successful fresh snow depth forecast with account of hight-corrected air temperature than in case of using of air temperature received from standard version of COSMO-Ru model. The example is shown in fig.3 for station Aibga. Before noon and partly during afternoon 4 March 2014 COSMO-Ru2 predicted precipitation in the form of rain.

Yet height-corrected temperature turned to be a little bit lower than initially calculated temperature, that's why fresh snow depth was reproduced in postprocessing system. According to observations in the night from 3 to 4 March 2014 precipitation under weakly negative temperature were observed, and snow depth didn't

Table 1: Fresh snow depth (cm) according to observations at AMS Roza Khutor 4, forecasts from COSMO-Ru2 and COSMO-Ru1 and data from website www.snow-forecast.com. 18 February 2014.

Observations	Forecast start (day hour)						Website data
	mean	17 00	17 06	17 12	17 18	18 00	
28.2	COSMO-Ru2						12.0
	27.6	30.0	39.5	22.1	25.4	21.3	
28.2	COSMO-Ru1						12.0
	23.8	17.0	24.9	40.8	19.9	16.8	

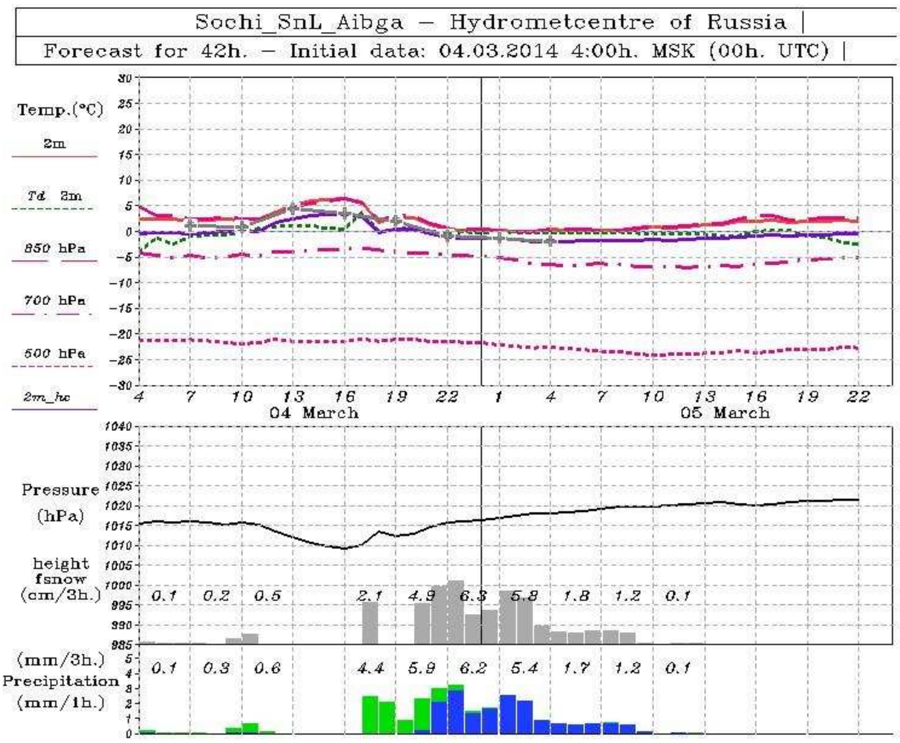

Figure 3: The example of meteogram obtained from COSMO-Ru2 model for station Aibga. Forecast start – 00 UTC 4 March 2014. Grey columns show hourly sums of fresh snow, numbers above – its 3-hour sums. Blue columns indicate hourly precipitation sums in the form of snow, green – in the form of rain. Height-corrected air temperature is pictured in solid violet line, air temperature – in solid pink line

change during the day. This proves the fact that postprocessing system properly predicted type of precipitation (snow): in case of rain falling snow depth had to reduce (snow sank). 12-hour precipitation sum at 3 UTC 5 March was 4 mm and gave 2 cm increment in snow depth for the day.

In the evening 4 March and in the morning 5 March observes fixed snow showers at temperatures from weakly positive to weakly negative. So, the proposed algorithm of fresh snow depth calculation on the basis of height-corrected air temperature reproduced the fact of snow falling rather realistically.

Maps of fresh snow depth can be created for any territory which coincides with the calculated grids of COSMO-Ru model versions (fig.2), for example, for the region including most part of the European territory of Russia. Meteograms containing fresh snow depth forecasts were prepared in January-March 2014 for North-Caucasian region for the purpose of specifying this meteorological element at points (stations). Analogous meteograms with fresh snow depth data can be obtained for stations located in other regions.

The testing showed that the developed system reproduces fresh snow depth quite realistically. Note that

COSMO-Ru provides the fact of precipitation falling as snow reliably, but quantitative estimations depend on forecast interval.

4 Conclusions

The system of prediction of fresh snow depth in the framework of COSMO-Ru postprocessing is developed and realized at Hydrometcenter of Russia. The system includes preparation of fresh snow depth maps for 6-hour intervals four times a day according to model versions with the resolutions of 7, 2.2 and 1.1 km, as well as fresh snow forecasts for stations as an addition to meteodrams.

Preliminary analysis of snowfalls occurred in North-Caucasian region in February 2014 showed that COSMO-Ru output connected with fresh snow characteristics could be used when weather forecast making. This output was used by weather forecasters in the framework of meteorological support of winter Olympic Games Sochi-2014, in particular for completion of daily bulletins and competitions planning.

References

[1] Kazakova E.V., Chumakov M.M., Rozinkina I.A. The algorithm of fresh snow depth calculation intended for postprocessing of atmospheric modeling systems (exemplifying COSMO) *Proc. of Hydrometcenter of Russia*, 2013, no. 350, **164-179**(in Russian).

[2] Shatunova M.V., Rivin G.S. Model COSMO-Ru1 with high space resolution: influence of external parameters on modeling results *Proc. of Hydrometcenter of Russia* , 2014, no. 352, **150-167**(in Russian).

[3] http://www.cosmo-model.org/content/support/software/default.htm

[4] www.snow-forecast.com

An application of SRNWP data pool radiation data with VERSUS software

Gofa F.1, Raspanti A.2, Tzeferi D.1

Hellenic National Meteorological Service, NWP Division, Athens, Greece
Italian Meteorological Service, Pratica di Mare, Italy

Abstract

In the verification field it is particularly important the exploitation of any kind of existing, controlled and homogenous set of surface and near surface observations. This becomes even more crucial in the Planetary Boundary Layer (PBL) where usually very limited dataset are available and observation concerning fluxes, radiation and soil characteristics are rarely available. In the EUMETNET framework of SRNWP programme an action has taken place with the aim to collect organize and control specialized observations in the PBL from selected stations all over Europe. In this study, the particular characteristics of these available observations are briefly described and their use in verification activities, through the verification system VERSUS, is presented. As a first application, an overview of the performance of the Italian and Greek implementations of COSMO model, as compared to the observed parameters, mainly surface fluxes and radiation, is discussed as well as specific case studies and applications of the conditional verification technique.

1 Introduction

Over the last years, limited area models as COSMO have increased their spatial horizontal and vertical resolution with the goal to achieve a better representation of the real topography and to resolve explicitly physical processes that otherwise would be of the sub-scale kind and would need a specific treatment (parameterization) of the corresponding equations. For this reason, usually, the increment of levels has mainly an impact on the planetary boundary layer (PBL) where turbulence, convection, fluxes of heat and moisture and radiation play all together, combined and separately, a major role. The improvement in the representation of PBL processes is of course, or can be, evident from the assessment of the general quality the forecast and from there the quality of forecasted fluxes or radiations balances can be inferred, having a look to the quality of 2mT forecast for example. At the same time the direct verification of such parameters is extremely important for modellers in the effort to focus the attention to the source of the physical process and not to one of the effect, which can be partially or even misleadingly representative.

Unfortunately this kind of information, organized as extensive dataset, are not usually available, while in the verification field it is particularly important the exploitation of any kind of existing, controlled and homogenous set of surface and near surface observations. Clearly, due the peculiarity of the processes, becomes even more crucial in the PBL, where usually observation concerning fluxes, radiation and soil characteristics are rarely available. Nevertheless in the EUMETNET framework of SRNWP programme, an action took place in the last years with the aim to collect, organize and control specialized observations in the PBL from selected stations all over Europe (Fig. 1). Data have been collected in a standard ASCII format since 2006, even if not complete, and made available to EUMTNET community for scientific purposes. These data have been used in this study to compare COSMO model to some of the available observations in the PBL, from some selected stations, and in particular: long and short wave radiation (upward and downward components) (LW and SW), latent and sensible heat flux (LHF and SHF).

The chosen stations are Cabauw, Lindenberg, Fauga-Muzac, Payerne, Debrecen and S.Pietro Capofiume, for the completeness of their datasets and because all of them are included in the model domain. Datasets have been made available on the COSMO Consortium website to the scientific community.

The main goal of this work, was to perform all the necessary adjustments in COSMO verification software (VERSUS), in order to be able to handle this kind of radiation data and to provide to the users some first examples of their application with the conditional verification feature for diagnostic studies.

2 Methodology of Comparison

For this application, the complete dataset 2011-2012 for both observations and forecasts has been used and compare with different methodologies. As forecasts parameters were given as an average from the reference time of the model run, a homogenising pre-processing phase with the observation was performed and hourly datasets created.

The comparison between model output and observations has been carried out mainly through long term time series and daily cycle. This choice has been adopted in order to be able to compare, from a more general point of view, the ability of the model to reproduce the parameters behaviour without paying attention to statistical score values.

The plots have been initially calculated over a stratification including all the set of stations described in the previous paragraph and afterwards some consideration focusing on the Italian station of S. Pietro Capofiume will be shown.

In this last part also some peculiar situations connected also to the usual weather parameters, like 2m temperature and total cloud cover, will be shown and discussed in the perspective of a conditional verification technique.

In the following Table 1 the association between the observations used and the model outputs is shown:

Table 1: Association of observations with model output parameters. Radiation observation balances have been calculated as they are not available from the datasets.All parameters in $W/m2$.

OBS Data	FCS Data
RSWD: incoming solar radiation	ASWDIR_S: Average direct downward SW rad Surface
RSWU: reflected solar radiation	ASWDIFD_S: Average diffuse downward SW rad Surface
(RSWD-U balance)	Averaged Balance of SW
RLWD: incoming thermal radiation	ALWD_S: Average downward LW radiation at the surface
RLWU: outgoing thermal radiation	ALWU_S: Average upward LW radiation at the surface
(RLWD-U balance)	Averaged Balance of LW
HS: sensible heat flux	ASHFL_S: averaged sensible heat flux
LE: latent heat flux	ALHFL_S: averaged latent heat flux

All the results shown in the present study, the calculations and the graphs have been produced using the VERSUS software. The initial ascii files of observations have been ingested and processed internally in order to produce the average values of LW and SW radiation and the appropriate association of forecast and observation parameters has been included in the respective configuration tables.

Figure 1: Geographical distribution of SRNWP data pool stations.

3 Results

It is useful, for the understanding of the basic physical processes in the PBL, to summarize, in Fig. 2, the annual radiation and heat balance of the Earth.

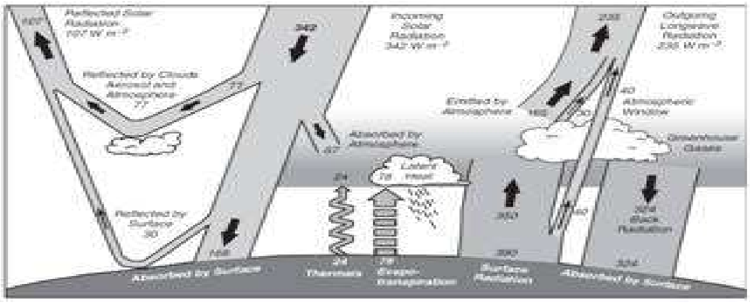

Figure 2: The mean annual radiation and heat balance of the Earth (Houghton et al 1996).

Fig.3 shows the daily cycles of long and short wave radiation and the LHF and SHF averaged on the period 2011-2012 for all the stations considered. The long period daily cycle is able to filter out seasonality and asses the general quality of the model. It is evident the general accordance between the model output and the observation, where the model overpredicts the LW upward radiation and the maxima of SHF (overestimated during the day and underestimated early morning and evening) and LHF (underestimated during the day) precede the observation.

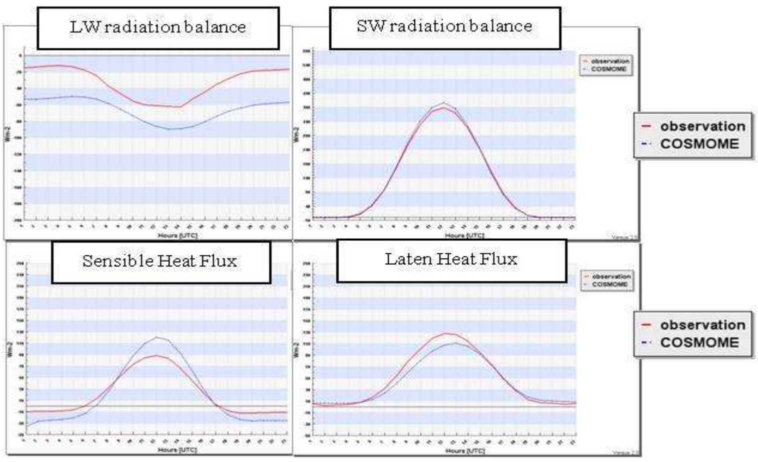

Figure 3: Daily Cycle LW and SW radiation – SHF and LHF for 2011-2012 – All SRNWP stations.

Focusing the attention on S. Pietro Capofiume station and comparing the previous parameters with daily cycles of 2mT (Fig.4) and total cloud cover (Fig.5), some other interesting considerations arise.

The typical COSMO model tendency to overestimate the 2mT during night and early morning is reflected also in the overestimation of negative (downward) flux of SH, taking in account that the SHF can be seen as proportional to $(T_{surf}\breve{\ }T_{atm})$ if 2mT is considered representative of Tatm.

The light underestimation of 2mT during the day is less evident and the correspondent overestimation of positive flux (upward) could be due mainly to the surface heating produced by solar radiation (not present during the night). The connection between LW radiation and total cloud cover shown in figure 5 is even more interesting.

The overestimation of TCC in the daily cycle results clear also in the light underestimation of SW radiation during the central part of the day, while the higher amount of upward LW radiation compared with observation seems to be in contrast with this conclusion, as the presence of clouds, especially during the night, should result in a LW radiation balance closer to zero than the one showed below.

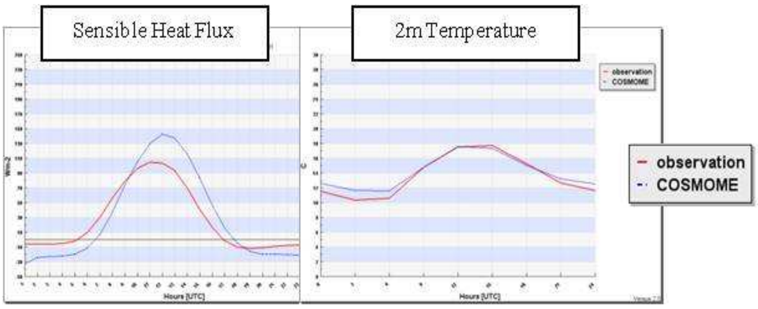

Figure 4: Daily Cycle of SHF and 2mT for 2011-2012 S. Pietro Capofiume.

Actually (see Fig. 6) also 2011-2012 winter scatter plots show an evident overestimation of the upward component of LW radiation balance, especially during the night (Step 24).

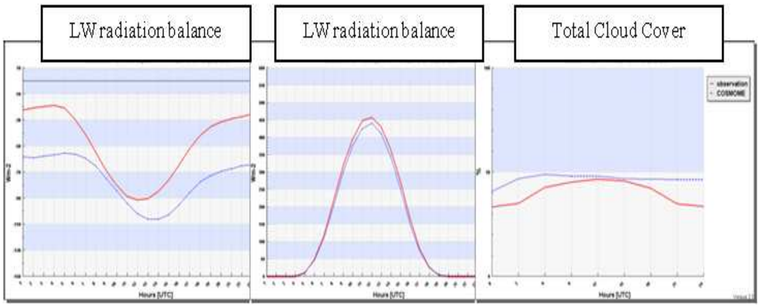

Figure 5: Daily Cycle of LW and SW radiation and TCC for 2011-2012 - S. Pietro Capofiume.

Under the reliable hypothesis of a several number of days with high amount of cloud cover and in connection with the daily cycles of TCC shown in Fig.5, the conclusion can be only that COSMO model predicts less thick clouds and/or less amount of low and medium clouds, able to maintain the LW radiation balance close to zero during the winter nights.

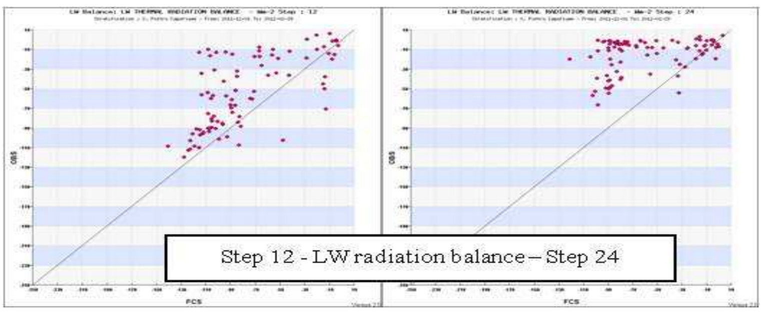

Figure 6: DJF scatter plots of LW radiation balance – Step 12 and 24 – S. Pietro Capofiume.

Another very interesting example, in the perspective of the application of conditional verification to these special observations in order to discover connection between physical processes and weather parameters behaviour, is shown in Fig.7.

Here in the time series of LW radiation balance it is shown and highlighted the period from 10.01.2011 to 20.01.2011. It is evident the mismatch between the observed LW radiation balance, that is almost zero, and the predicted one that has clear fluctuations of quite high magnitude. In this situation the examination of TCC time series and daily cycle is revealing of the problem.

The model predicted a complete wrong amount of cloud cover in those days, even up to 90-100% of error and the correspondent daily cycle shows the gap between forecast and observation. In this situation the whole predicted atmospheric column will be affected by the error and other parameters, not shown here, will present similar deficiency.

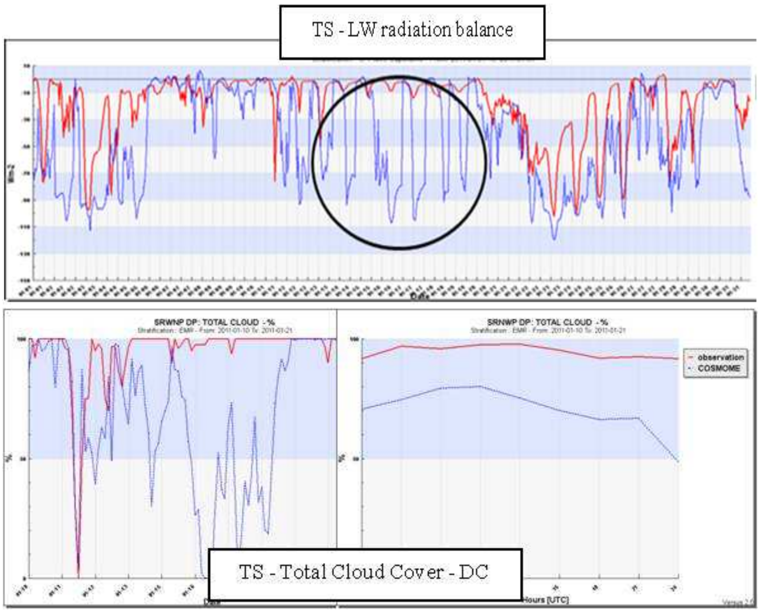

Figure 7: Time series of LW radiation and TCC, DC of TCC – 10-20 Jan 2011- S.Pietro Capofiume.

4 Conclusions

The exploitation of controlled and homogenous set of surface and near surface observations is fundamental in any verification process in the framework of NWP. This is even more crucial when the field of application of such activity is the PBL and the effort is to explore directly the sources of the physical processes. The availability of datasets like the one used here gives to the verificators and the modellers the possibility to check directly some specific model outputs and to cross-check them in connection with the usual weather parameters, also using the conditional verification techniques.

In this work it has been briefly shown how, radiation data can be utilized in VERSUS software together with other surface measured parameters in order to extract valuable information for COSMO model performance. As a first indication, COSMO generally predicts well LW and SW radiation balance and fluxes, with some exception, especially for LW radiation. It has been also explained how also the different aggregations of results can be revealing of the reason of model deficiencies, like the contemporary use of time series, daily cycle and scatter plots.

The overprediction of negative sensible heat flux has an impact also on the prediction of 2mT, mainly during the night and the early morning, while the shift of maximum in latent heat flux should be better investigated connected with dew point and specific humidity prediction. The model tends to steadily overpredict the upward LW radiation for both the complete station stratification and S. Pietro Capofiume, with almost the same behaviour. It has been shown how in two specific situations this can be due to different reason: the wrong representation of TCC in terms of percentage and/or in terms of cloud layer thickness.

Finally the use of conditional verification technique should be applied in order to find connection between specific significant thresholds, for which these fields become more significant, and the usual weather parameters.

References

[1] Gofa F, Raspanti A, Charantonis T (2010) Assessment of the performance of the operational forecast model COSMOGR using a conditional verification tool. *In: Proc. 10th COMECAP Conference of Meteorology, Patras. Greece, Hellenic Meteorological Society*, **70-77**.

[2] Fleagle RG, Businger JA (1980) An Introduction to Atmospheric Physics Vol. 25 Academic Press.

[3] Wilks DS (1995) Statistical Methods in the Atmospheric Sciences. Academic Pres.

Neighborhood verification of convection in the Swiss COSMO models with radar and satellite measurements

Thomas Leutert, Daniel Leuenberger and Francis Schubiger

MeteoSwiss, Operation Center 1, CH-8058 Zurich Airport

1 Introduction

Increasing the resolution of numerical weather prediction (NWP) models is a promising approach to improve weather forecasts on local and regional scales: High-resolution models better represent topography, boundary layer and land surface processes, and avoid uncertainties due to convection parameterizations (e.g., Ban et al., 2014). Several studies confirm a benefit in simulating precipitation for high-resolution models at convection-resolving scales in comparison to coarser-resolution models (e.g., Langhans et al., 2013; Prein et al., 2013; Kendon et al., 2012; Langhans et al., 2012; Knote et al., 2010; Hohenegger et al., 2008). However, conventional skill scores often do not capture the higher realism from increased resolution due to small spatial or temporal shifts of the forecast (double penalty effect). Therefore, a neighborhood verification approach which does not only take into account individual grid points, but also rewards closeness in space, time and other relevant aspects (e.g., Ebert, 2008) has to be used for the evaluation of high-resolution forecasts.

Assessing forecasts of three configurations of the non-hydrostatic limited-area atmospheric prediction model from the Consortium for Small-Scale Modelling (COSMO) with grid sizes of 1.1 km (COSMO-1), 2.2 km (COSMO-2) and 6.6 km (COSMO-7), we evaluate the role of model resolution for the quality of convection simulations for summer 2014 in Switzerland. The main objectives of this study are as follows:

- Compare the diurnal cycle of convective precipitation in COSMO-1, COSMO-2 and COSMO-7 against gridded precipitation estimates from combined radar and rain gauge observations. Is there a significant difference between convection-permitting and convec-tion-parametrizing models?
- Extend the neighborhood verification framework from precipitation data to brightness temperatures measured by satellites. What are reasonable brightness temperature threshold values to verify convective clouds in NWP models?
- Assess the NWP models of MeteoSwiss against radar and satellite observations. How well does COSMO-1 simulate clouds in comparison to COSMO-2 and COSMO-7? On which spatial scales does model performance benefit from increased resolution?

2 Verification approach

A better representation of reality by high-resolution models in comparison to models with a lower resolution does not necessarily imply greater accuracy. In case of high-resolution forecasts, traditional verification methods tend to overemphasize errors on small spatial scales, leading to an unfair double penalty effect (Roberts and Lean, 2008). Taking into account more than one grid point helps to reduce this double penalty effect. Neighborhood verification assesses forecast skill scores for different spatial windows and thresholds, allowing for the identification of the scales and thresholds where model quality reaches highest values.

Ebert (2008) summarizes the main neighborhood verification methods. They represent different decision models to assess the usefulness of a forecast. The Fractions Skill Score (FSS) is well suited for the verification of high-resolution forecasts (Eckert, 2009) and evaluates the simulated fraction exceeding/falling below a certain threshold. It is calculated via Fractions Brier Score (FBS) from the fractions of observed (P_{obs}) and forecast (P_{fcst}) grid points which exceed/fall below a certain threshold (e.g., Weusthoff et al., 2010):

$$FBS = \frac{1}{N} \sum_{N} (P_{fcst} - P_{obs})^2 \tag{1}$$

$$FSS = 1 - \frac{FBS}{\frac{1}{N}\left(\sum_N P_{fcst}^2 + \sum_N P_{obs}^2\right)} \tag{2}$$

For precipitation data, threshold exceedances are assessed, whereas we use threshold undercuts for brightness temperature. The FSS asymptotically approaches a value that depends on the frequency bias (1 if no bias). According to Roberts and Lean (2008), useful spatial scales of a forecast are characterized by FSS > FSS_{useful} ($FSS_{useful} = 0.5 + f_{obs}/2$ where f_{obs} is the observed fractional coverage for a given threshold over the domain). A simulation with a useful FSS provides additional benefit in comparison to the forecast of a constant ratio of events to non-events. The skill scores were calculated with the neighborhood verification package from Ebert (2008) for a domain covering Switzerland.

In order to assess precipitation, the thresholds 0.1 mm/h, 0.2 mm/h, 0.5 mm/h, 1 mm/h, 2 mm/h, 5 mm/h, 10 mm/h and 20 mm/h have been used. We chose the following brightness temperature thresholds: 210 K, 220 K, 230 K, 240 K, 250 K and 260 K. This brightness temperature range prevents an influence by surface temperatures in Swiss summers and at the same time covers the relevant spectrum of tropospheric cloud temperatures. All skill scores were calculated for square neighborhoods with different sizes (COSMO-1: 1×1, 2×2, 6×6, 18×18, 30×30, 54×54 and 90×90 grid points; COSMO-2: 1×1, 3×3, 9×9, 15×15, 27×27 and 45×45 grid points; COSMO-7: 1×1, 3×3, 5×5, 9×9 and 15×15 grid points).

3 Observational data

CombiPrecip is a suitable product to verify quantitative precipitation forecasts. It is produced with a mesh size of 1 km and combines information from the Swiss radar composite based on 4 Doppler radars and ~180 automatic rain gauges measuring each 10 minutes. The large observation errors of the spatially dense radar precipitation estimates are reduced by rain gauge point measurements by means of co-kriging with external drift (Sideris et al., 2014). Hourly accumulations from CombiPrecip are used to assess convective precipitation in the complex Alpine topography. The CombiPrecip data have been interpolated to the grids of COSMO-1, COSMO-2 and COSMO-7 by averaging over all grid points lying inside a model grid box.

In order to estimate the skill of forecasting convective clouds, observational satellite imagery from the Spinning Enhanced Visible and Infrared Imager (SEVIRI) located onboard Meteosat Second Generation (MSG) (Schmetz et al., 2002) is compared to simulated satellite images from the COSMO models using the NWP-SAF RTTOV forward operator (Keil et al., 2006; Keil and Tafferner, 2003). The focus lies on brightness temperatures computed from Channel 9 (10.8 μm). They are closely correlated with the target temperatures and thus can be used to distinguish between (cold) clouds and the warmer Earth's surface (e.g., Böhme et al., 2011; Schmetz et al., 2002). For the verification, we assume an inverse relationship between brightness temperature and the top height of convective clouds: High, convective clouds are cold, low clouds are warmer. The satellite data set with a resolution of 3.2 km (west-east) × 5.4 km (north-south) over Switzerland (Schmetz et al., 2002) has been interpolated to the COSMO model grid by means of bilinear interpolation. Spatial scales below ~5 km are ignored in the interpretation of the brightness temperature verification results.

4 Model data

We validated and verified three Swiss COSMO configurations: COSMO-1 (1.1 km), COSMO-2 (2.2 km) and COSMO-7 (6.6 km). The configurations differ in horizontal resolution and in physical parameterizations: COSMO-7 uses a mass-flux convection scheme with equilibrium closure based on moisture convergence for shallow to deep convective clouds (Tiedtke, 1989). COSMO-1 and COSMO-2 are assumed to explicitly resolve deep convection, but rely on a parameterization for shallow convection. COSMO-7 is driven by the Integrated Forecasting System (IFS) of the European Center for Medium-Range Weather Forecasts (ECMWF). COSMO-1 and COSMO-2 are nested into COSMO-7. The model domain for the assessment of convection has been chosen to fully cover the domain of Switzerland. COSMO-2 and COSMO-7 are run in operational mode, while COSMO-1 still runs in experimental mode. Here, all 00 UTC model runs of the verification period are considered up to a lead time of 24 h.

5 Verification of the 12th June 2014 case

First, a typical convection day is analyzed. A flat pressure distribution over central Europe, warm temperatures and moist air led to favourable conditions for deep convection over Switzerland on 12th June 2014. It was a summer day characterized by a strong diurnal cycle of convection.

At the beginning of the day (01 UTC), the satellite (Fig. 1) and radar (Fig. 2) observations (interpolated to a 1.1 km grid) show cloud leftovers from the previous day (Fig. 1), but no precipitation (Fig. 2). The sky has cleared up at 10 UTC. At 11 UTC, convection is initiated over the Alps and reaches its maximum intensity around 19 UTC. Afterwards, convective activity decreases again (not shown).

The models overestimate cloudiness at 01 UTC and 10 UTC (Fig. 1). At 01 UTC, COSMO-1 and COSMO-2 predict too much clouds over the western part of Switzerland and in the southeastern corner of the domain. The overprediction is less pronounced in COSMO-7. 9 hours later, low brightness temperatures have almost completely disappeared in the observations. The models show a patchy pattern of cold temperatures over Eastern Switzerland, indicating a too early onset of convection. The granular structure in case of COSMO-7 is likely caused by the parameterization scheme for deep convection. At 19 UTC, observed brightness temperatures over Switzerland have decreased significantly. Although not perfect, the overall convective structure is well captured by COSMO-1 and COSMO-2. COSMO-7 misses the centre of convection over the northern part of Switzerland.

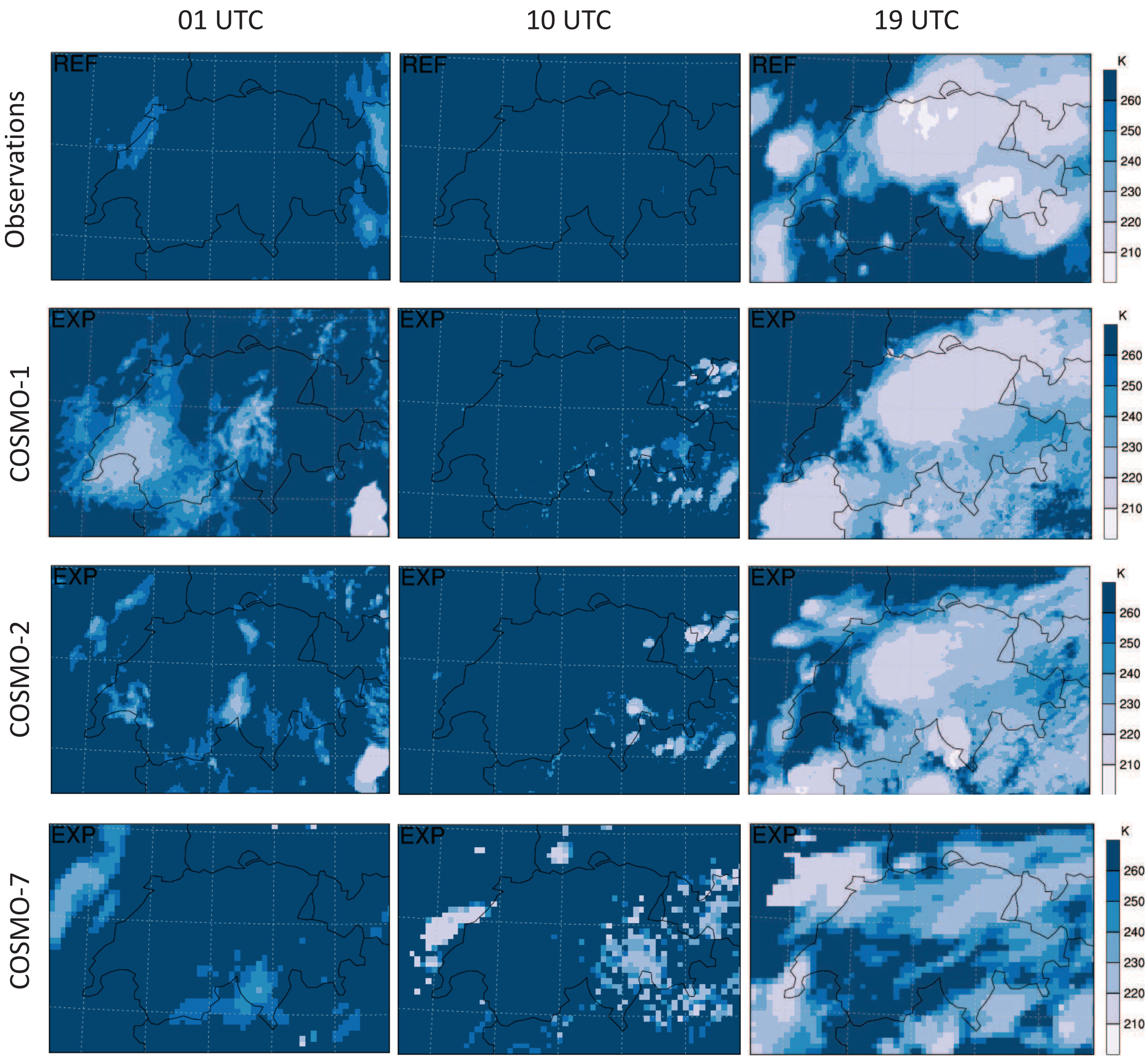

Figure 1: Brightness temperature during 12th June 2014 over Switzerland. In addition to the satellite data (interpolated to a grid with 1.1 km mesh size; upper row), the model output of COSMO-1 (middle row), COSMO-2 and COSMO-7 (lower row) is shown at 01 UTC (left column), 10 UTC (middle column) and 19 UTC (right column). Light colors indicate low brightness temperatures linked to high-altitude clouds.

Apart from the region in the northeast of Lake Constance, simulated precipitation in COSMO-1 and COSMO-2 is negligible at 01 UTC (Fig. 2). The observations and COSMO-7 show no rain at all. At 10 UTC, COSMO-1 and COSMO-2 show slight precipitation in the eastern part of the domain.

COSMO-7 overforecasts precipitation in the same zone. This overestimation of precipitation seems to spatially coincide with the granular pattern of brightness temperature (Fig. 1). As expected from the simulated brightness temperatures, convective precipitation over the Alps increases towards 19 UTC in COSMO-1 and COSMO-2. In contrast to COSMO-1 and COSMO-2, COSMO-7 heavily underforecasts precipitation over the whole domain at 19 UTC.

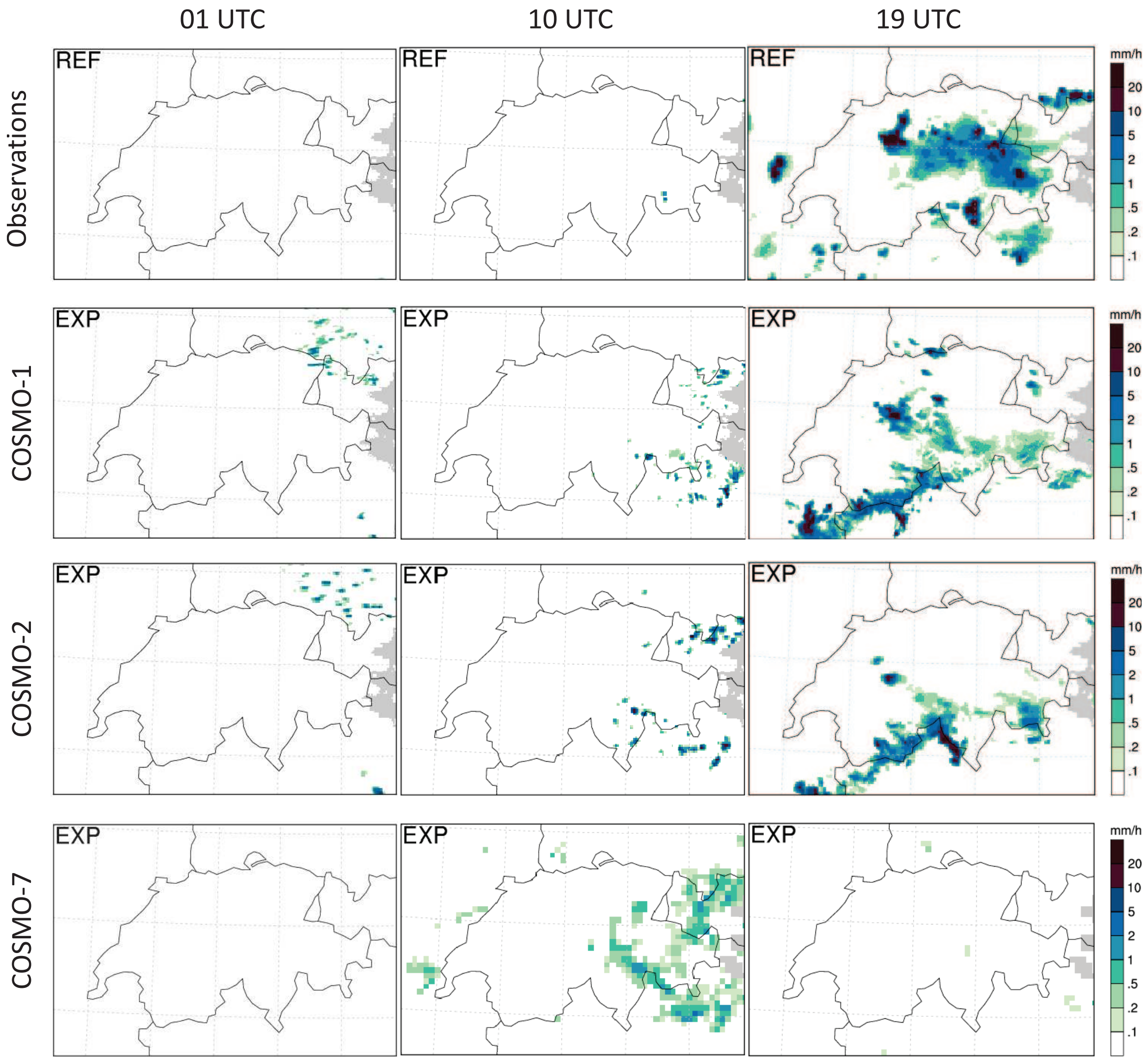

Figure 2: Precipitation during 12th June 2014 over Switzerland. In addition to the radar data (interpolated to a grid with 1.1 km mesh size; upper row), the model output of COSMO-1 (middle row), COSMO-2 and COSMO-7 (lower row) is shown for hourly sums ending at 01 UTC (left column), 10 UTC (middle column) and 19 UTC (right column). Dark colors indicate high precipitation amounts.

In all following neighborhood verification plots (Figs. 3, 4 and 7), higher skill score values indicate better performance. High skill is visualized by warm colors. The useful scales are marked by bold numbers.

Fig. 3 shows neighbourhood verification results for brightness temperature. The FSS quantifies the skill of forecasting a value below a certain threshold. Generally, the FSS tends to increase with increasing spatial scale and with increasing threshold. The best skill is obtained for high thresholds on large scales. This makes sense: (1) The requirements for a good match between model and observation are relaxed more heavily on large than on small spatial scales (e.g., Ebert, 2008). (2) A mixture of many different brightness temperature values falls below high thresholds, but only a small number of specific extreme values falls below low thresholds. Therefore, the skill at low thresholds (e.g., high clouds) is reduced in comparison to high thresholds (e.g., low clouds, no clouds).

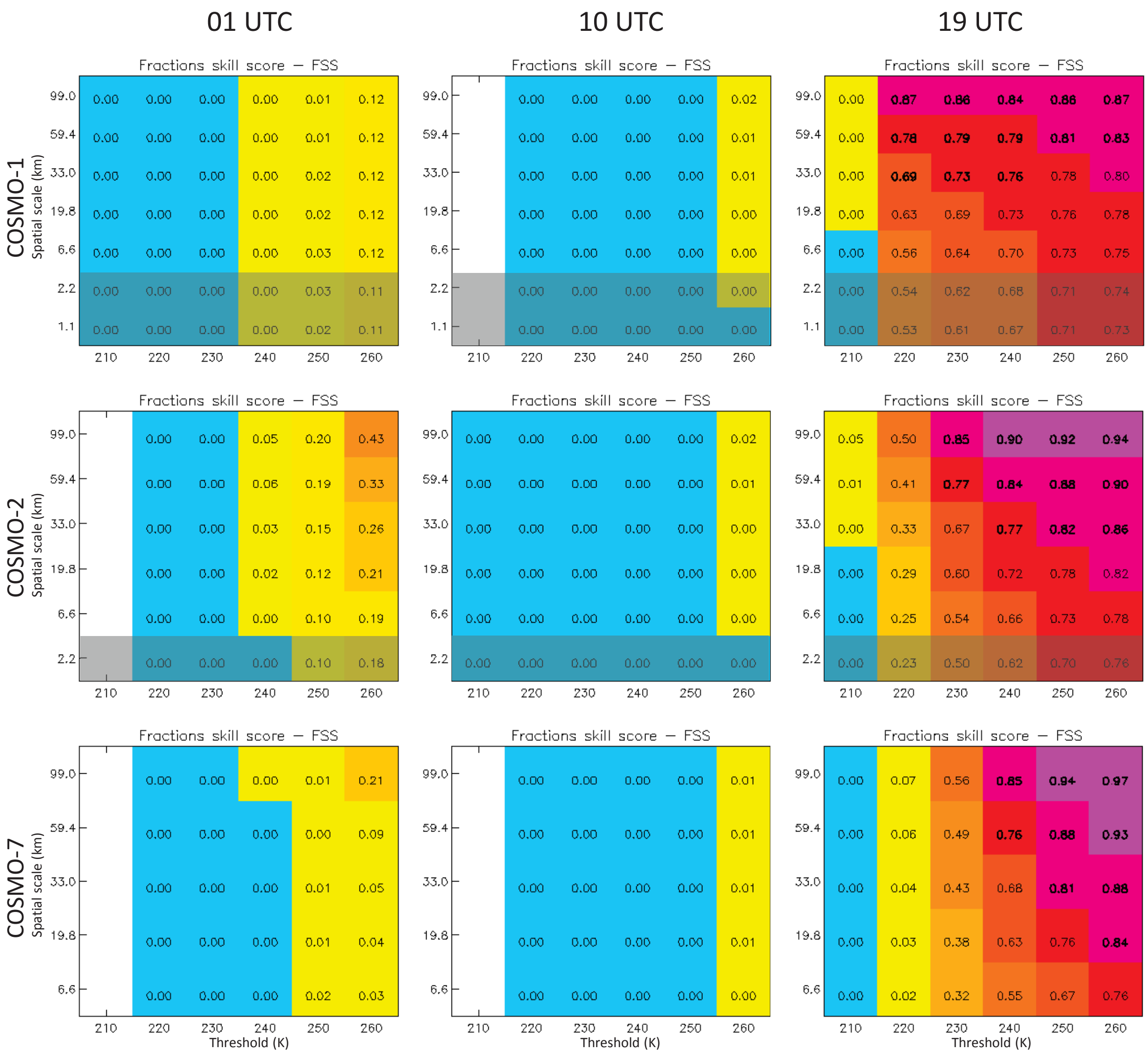

Figure 3: FSS of brightness temperatures from COSMO-1 (upper row), COSMO-2 (middle row) and COSMO-7 (lower row) at 01 UTC (left column), 10 UTC (middle column) and 19 UTC (right column) for 12th June 2014. Values shaded in gray should be disregarded since the spatial resolution of the satellite observations is about 5 km.

At 01 UTC, all models show low values of FSS in terms of brightness temperature forecasts without any useful scales at all (Fig. 3). COSMO-2 gives the best scores. 9 hours later, the FSS values are zero for most scales and thresholds, since almost no clouds are observed. In the evening (19 UTC), COSMO-1 and COSMO-2 simulate the overall brightness temperature structure better than COSMO-7, especially for low thresholds (high clouds). COSMO-7 can best discriminate between clouds/no clouds (threshold 260 K). COSMO-1 exhibits most useful scales.

In contrast to brightness temperature, threshold exceedances and not threshold undercuts are evaluated for the precipitation forecasts (Fig. 4). The neighborhood verification table of COSMO-7 is empty at 01 UTC. At this time, COSMO-7 and CombiPrecip do not show any precipitation for all spatial scales (Fig. 2). A FSS cannot be computed when the fraction of grid points exceeding a threshold is 0 in both observation and forecast (Eq. 2). Consequently, COSMO-7 correctly forecasts no rain at 01 UTC. In the morning (10 UTC) and evening (19 UTC), the precipitation forecast performance of COSMO-7 is very low. The high brightness temperature skill scores of COSMO-7 at 19 UTC are not at all reflected in the precipitation forecasts of COSMO-7. This model completely fails to predict the observed rainfall over Switzerland at 19 UTC.

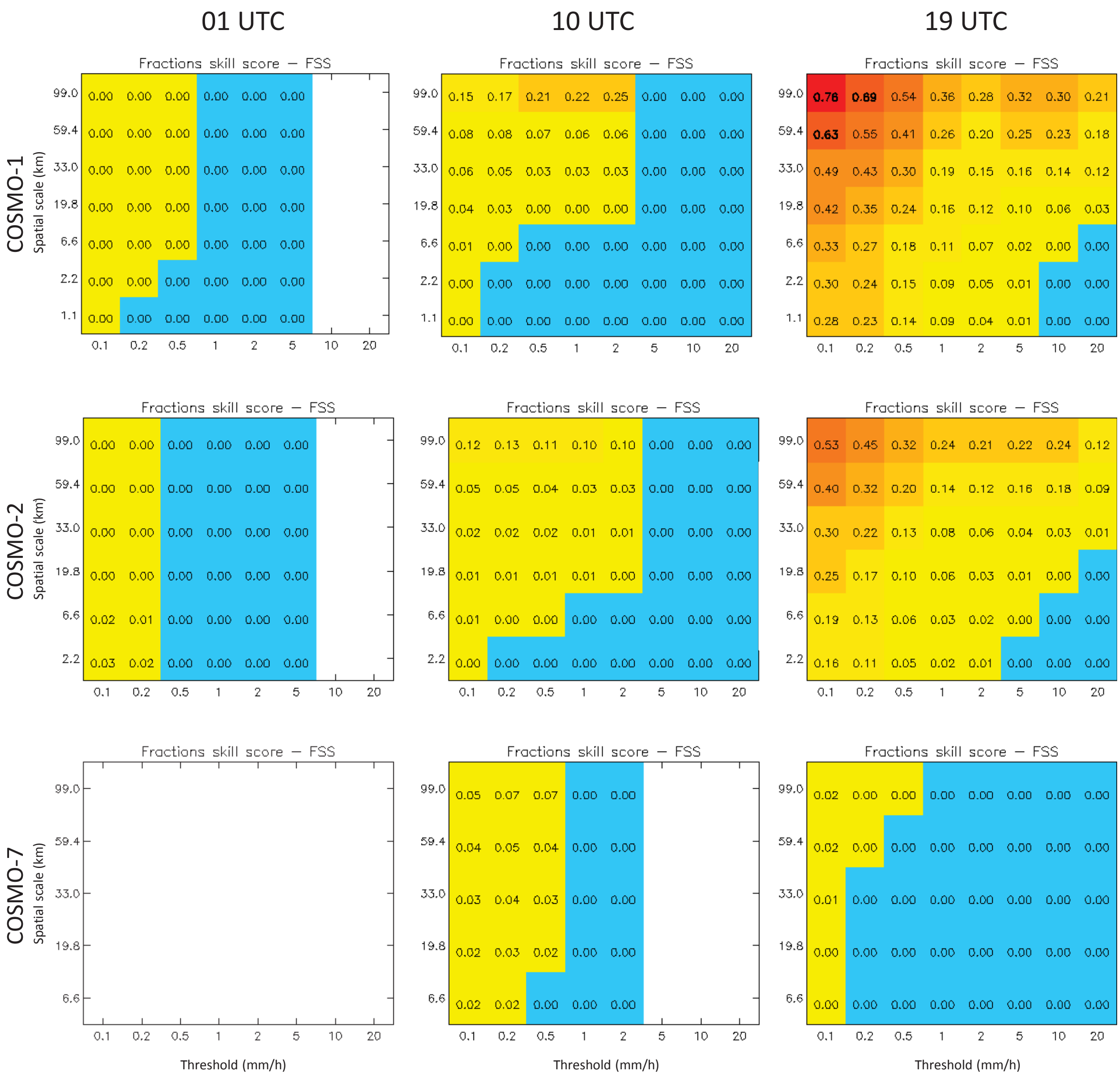

Figure 4: FSS of hourly precipitation of 12th June 2014 from 00 UTC to 01 UTC (left column), 09 UTC to 10 UTC (middle column) and 18 UTC to 19 UTC (right column) for the forecasts of COSMO-1 (upper row), COSMO-2 (middle row) and COSMO-7 (lower row).

The FSS of precipitation from COSMO-1 and COSMO-2 are low at 01 UTC and 10 UTC and rise thereafter (Fig. 4). Only COSMO-1 produces useful precipitation forecasts at spatial scales of 59.4 km and 99.0 km. It outperforms the other models for most scales and thresholds.

To sum up, the analysis of the forecasts of 12th June 2014 reveals that both COSMO-1 and COSMO-2 produce results which are closer to the observed values than those of COSMO-7. Neighborhood verification generally confirms the better skill of the convection-permitting models, as seen from visual inspection of the spatial brightness temperature and precipitation distributions. In the next chapter, the evaluation of brightness temperature and precipitation is extended to the period from June to August 2014.

6 Verification of June, July and August 2014

The end of May and the beginning of June were characterized by several cold front passages and moist conditions. After some cool days in the beginning of June, a heatwave affected Switzerland for approximately one week. Following the warm temperatures, heavy thunderstorms brought precipitation to Switzerland. Towards the end of June, a cold front and inflowing unstable air masses further intensified thunderstorm and rainfall activity. Generally, June was very warm and characterized by a high potential for convection. In contrast to June, July was cool and wet. Apart from a warm and stable weather phase (15th July to 19th July), advancing depressions and thunderstorms led to record precipitation values. Flooding and landslides caused widespread damage in Switzerland. The cool conditions over Switzerland persisted in August. Especially during the first half of the month, numerous thunderstorms associated with atmospheric disturbances led to heavy rainfall events (MeteoSwiss, 2014). Prevalent wet and convective conditions during June, July and August 2014 make this period suitable for the verification of precipitation and cloud cover forecasts.

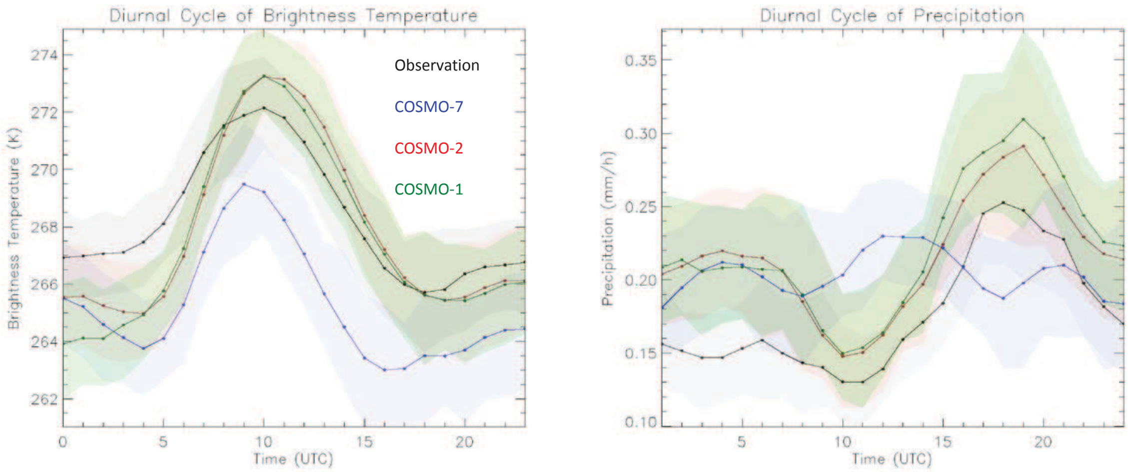

Figure 5: Mean diurnal cycles of brightness temperature (left) and precipitation (right) averaged over June, July and August 2014. Black curves denote observations, blue curves COSMO-7, red curves COSMO-2 and green curves COSMO-1 forecasts. The uncertainty estimates (shaded areas) are based on bootstrapping and represent the range between the 10th and 90th percentile.

Fig. 5 shows the mean diurnal cycles of brightness temperature and precipitation. The shaded areas denote the uncertainty represented by the range between the 10 % and the 90 % quantile of a distribution computed using bootstrapping. To this end, 100 equally sized random samples of the days were drawn from the original data of the three-month period (e.g., Boos, 2003).

In contrast to the precipitation values accumulated over 1 hour, the brightness temperature values are instantaneous. All diurnal cycles of average precipitation and brightness temperature have been computed in intervals of 1 hour from 01 UTC to 24 UTC for precipitation and from 00 UTC to 23 UTC for brightness temperature.

The observed brightness temperature values are characterized by a maximum (minimum cloud cover) around 10 UTC and a minimum (maximum high cloud cover) around 18 UTC (Fig. 5, left). COSMO-1 and COSMO-2 capture the amplitude and the timing of the observed diurnal cycle well and clearly exceed the performance of COSMO-7. Despite their good overall performance, COSMO-1 and COSMO-2 underestimate nighttime and early morning average brightness temperature. In the first half of the day, the observations indicate low rainfall (Fig. 5, right). Then, rainfall starts to increase and peaks around 18 UTC. After reaching its maximum value, precipitation decays much faster than the clouds. This is physically realistic, as clouds which have rained out tend to persist without further precipitation. COSMO-7 agrees substantially worse with the observations than COSMO-1 and COSMO-2.

The poor representation of the diurnal cycle of precipitation in COSMO-7 (too early maximum) is probably linked to the convection scheme (e.g., Dai et al., 1999). This parameterization scheme is not designed to represent individual convective showers (Kendon et al., 2012). The convection-permitting models, i.e. without parameterized deep convection, capture the diurnal cycle of precipitation much better.

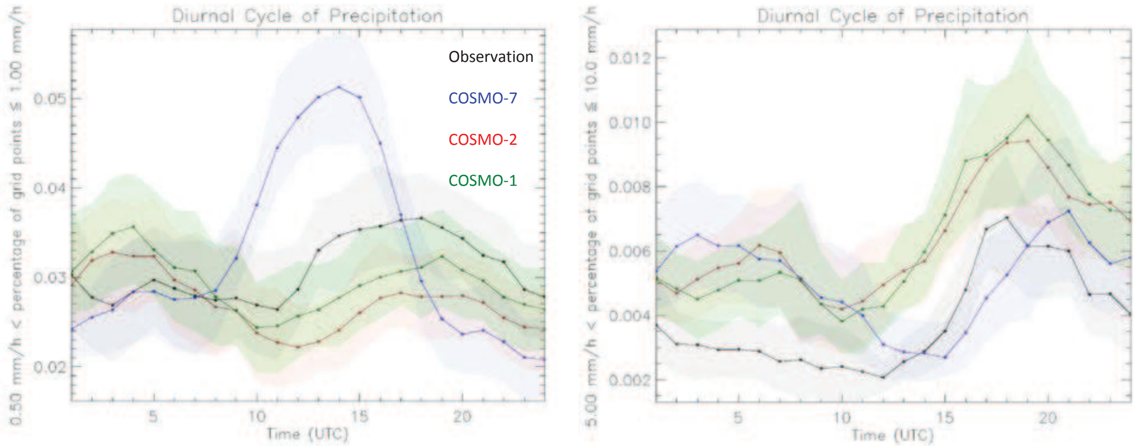

Figure 6: Diurnal cycles (June, July and August 2014) of the relative amount of grid cells with precipitation higher than 0.5 mm/h but lower/equal 1.0 mm/h (left) and precipitation higher than 5.0 mm/h but lower/equal 10.0 mm/h (right). Black curves denote observations, blue curves COSMO-7, red curves COSMO-2 and green curves COSMO-1 forecasts. The uncertainty estimates (based on bootstrapping; shaded areas) represent the range between the 10th and 90th percentile.

The too early peak of average precipitation in COSMO-7 (Fig. 5, right) is predominantly caused by light precipitation events (e.g., values between 0.5 mm/h and 1.0 mm/h; Fig. 6, left). In contrast, the maximum of heavy precipitation (e.g., values between 5.0 mm/h and 10.0 mm/h; Fig. 6, right) in COSMO-7 even occurs later than observed. Generally, the timing of the diurnal cycle of precipitation is well captured by the convection-permitting models (COSMO-1 and COSMO-2).

Fig. 7 shows neighbourhood results aggregated over June, July and August 2014. The best brightness temperature forecasts are produced by COSMO-1 and COSMO-2 (left panel). Their skill scores are similar for most spatial scales and thresholds. At spatial scales < 33 km, COSMO-1 performs marginally better than COSMO-2. COSMO-7 is beaten on all scales and for all thresholds. Useful spatial scales are observed for high brightness temperature forecasts on large scales during June, July and August 2014.

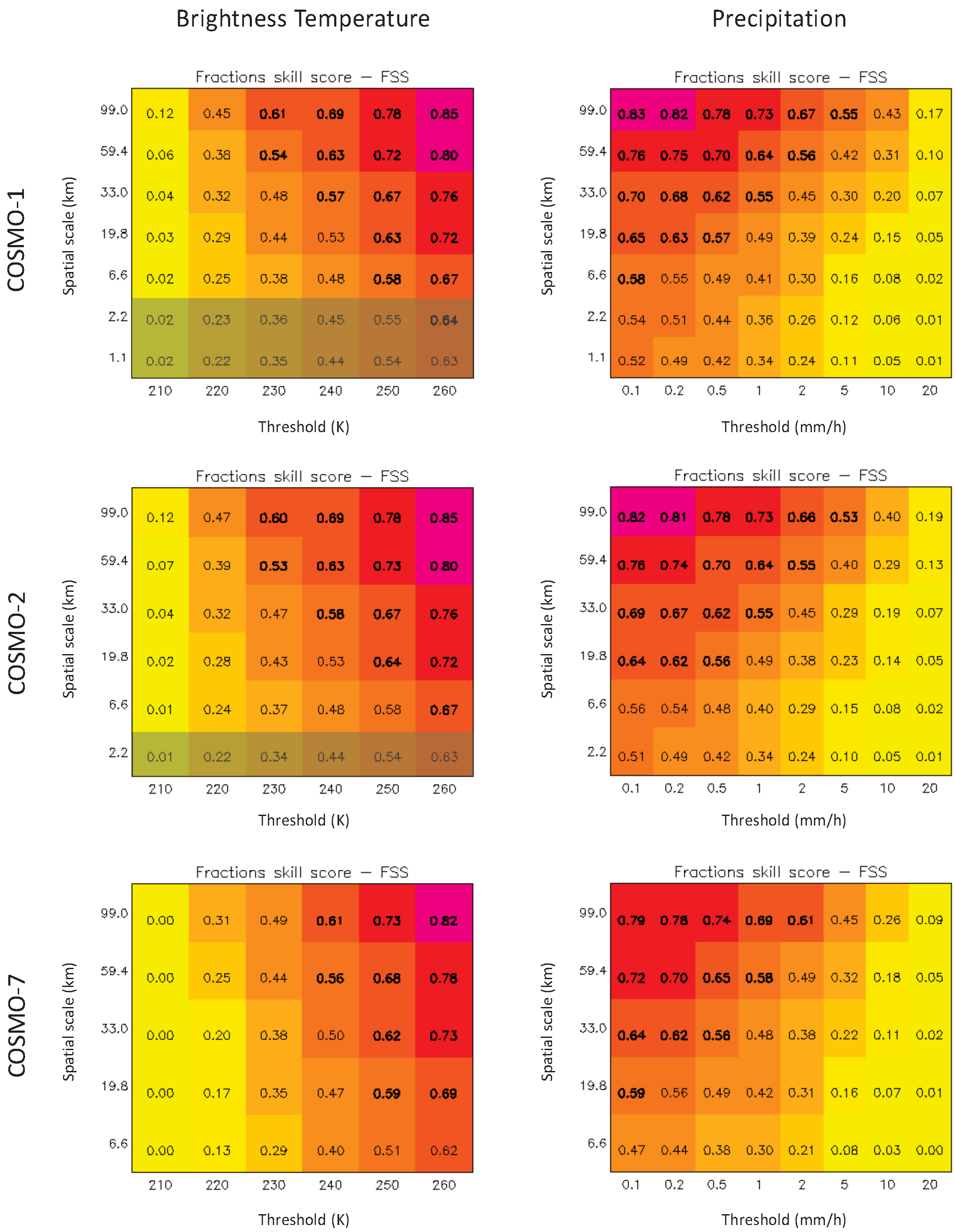

Figure 7: FSS of brightness temperature (left) and precipitation (right) as simulated by COSMO-1 (upper row), COSMO-2 (middle row) and COSMO-7 (lower row) for all 00 UTC runs from 1st June to 31st August 2014 for all hourly forecasts (hourly precipitation sums). The brightness temperature values in gray should be disregarded since the spatial resolution of the satellite observations is about 5 km.

Similar to brightness temperature, we find useful scales for all models in case of precipitation forecasts (Fig. 7, right panel). COSMO-1 outperforms COSMO-2 and COSMO-7. The simulations of COSMO-7 are clearly worst for all scales and thresholds.

We address the question whether the models forecast the correct number of grid point values within a certain brightness temperature range by means of a frequency-intensity distribution (Fig. 8). The frequency-intensity distribution is discretized into bins, using the threshold values from the neighborhood verification. The number of grid points in a bin is always computed relative to the total number of grid points in the domain in order to compare models that differ in resolution. Values above 260 K are not shown in the frequency-intensity distribution. Therefore, the values of a curve do not add up to 1. The observation values are those interpolated to the COSMO-7 grid with a resolution of 6.6 km. An overestimation of low brightness temperature values (< 250 K) occurs in all models, especially in COSMO-7, indicating too much high cloudiness. It may be caused by the parametrization of ice nucleation and/or the neglected sedimentation of cloud ice (Pfeifer et al., 2010). This positive bias of high clouds is smaller for the high-resolution models COSMO-1 and COSMO-2, confirming a benefit of the explicit resolution of convection.

Additionally, the Upscaling (UP) method was calculated using the Equitable Skill Score (ETS) (e.g., Ebert, 2008). The UP/ETS results qualitatively agree with the FSS in most cases (not shown).

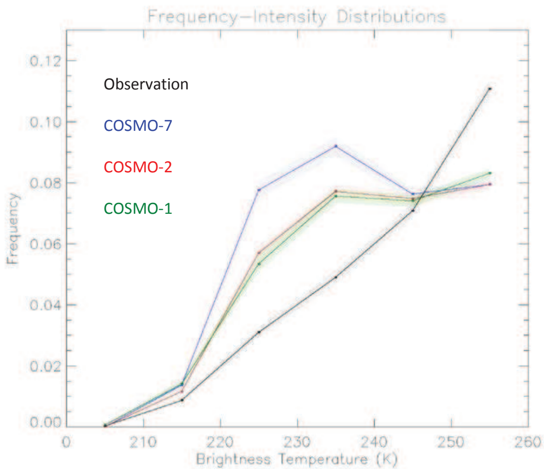

Figure 8: Frequency-intensity distributions of brightness temperature for the observations (black curve), COSMO-1 (green curve), COSMO-2 (red curve) and COSMO-7 (blue curve) during June, July and August 2014. The shaded areas represent the 80 % confidence intervals based on bootstrapping.

6 Conclusions

Precipitation and brightness temperature forecasts of COSMO-1, COSMO-2 and COSMO-7 have been assessed for a typical day with strong convective activity (12th June 2014) and for the summer 2014 (June, July and August) by means of the neighborhood verification technique for the domain of Switzerland. Thresholds of 0.1 mm/h, 0.2 mm/h, 0.5 mm/h, 1 mm/h, 2 mm/h, 5 mm/h, 10 mm/h and 20 mm/h have been used for precipitation and 210 K, 220 K, 230 K, 240 K, 250 K and 260 K for brightness temperature.

To provide a holistic view of model performance, our evaluation focused on the Fractions Skill Score (FSS) method of the neighborhood verification package, but also includes spatial distributions, frequency-intensity distributions and average diurnal cycles. Brightness temperature serves as a proxy for convective cloud activity which was intense during this period, especially in June 2014, and posed a great challenge for all NWP models.

The spatial distributions of precipitation and brightness temperature for a single convective day reveal that the high-resolution models COSMO-1 and COSMO-2 exhibit more realistic patterns than COSMO-7. This is also reflected in the results of the FSS. At 19 UTC (maximum in convective activity), the FSS indicates highest skill in COSMO-1 both for precipitation (for nearly all scales and thresholds) and for brightness temperature (for most scales and thresholds below 240 K, e.g. for deep convective clouds).

For June, July and August 2014 and averaged over all forecast hours up to +24 h, the results show the best scores for COSMO-1. No clear scale dependency of the improvements of COSMO-1 in comparison to COSMO-2 is observed. The mean daily cycles of the convection-permitting COSMO-1 and COSMO-2 models are much better in timing and amplitude than COSMO-7. However, they still overestimate nighttime and morning clouds and precipitation. The too early maximum of precipitation in COSMO-7 is caused by light precipitation events. The frequency-intensity distributions reveal that all three models tend to overestimate the number of brightness temperature values below 250 K.

The results of this study suggest that brightness temperatures of the 10.8 μm channel observed by satellites and simulated by the COSMO model can well serve as a proxy for convective clouds and have the potential to complement precipitation for the spatial verification of convective processes. It remains to be explored if brightness temperature as a verification proxy is also suited for other types of clouds like frontal or stratus clouds. All in all, our verification results confirm additional benefit for the use of convection-permitting models in comparison to coarser models with parameterized convection, further increasing confidence in the high-resolution modelling approach. A decrease in horizontal grid size from 7 km to 2 km seems to improve forecast performance more than for convection-permitting models from 2 km to 1 km.

7 Outlook

The subsequent steps could reduce the uncertainty in the assessment of the COSMO models to better understand the role of model resolution in terms of forecast skill.

- An additional temporal dimension in the neighborhood verification will allow for a relaxation of the requirements for exact matches in time (especially for hourly precipitation sums).
- The impact of using data from more than only the 00 UTC runs could be quantified for each model. Furthermore, the relationship between model skill and lead time may be assessed using all model runs.
- It would be interesting to evaluate brightness temperature and precipitation forecast performance for specific meteorological conditions and forcing factors (weather type dependent verification).
- With regard to the relation between brightness temperature and cloud top height, it has to be kept in mind that brightness temperature at 10.8 μm as recorded by satellites does not provide complete information about cloud cover in the atmosphere: Medium brightness temperatures may stem from mid-level clouds, but can also be caused by semi-transparent high-level clouds. Therefore, the analysis of satellite data could be extended to the (water vapour) channels 5 (6.2 μm) and 6 (7.3 μm).

References

[1] Ban, N., Schmidli, J., Schär, C., 2014: Evaluation of the convection-resolving regional climate modeling approach in decade-long simulations. *Journal of Geophysical Research: Atmospheres*, 13, **7889-7907**

[2] Böhme, T., Stapelberg, S., Akkermans, T., Crewell, S., Fischer, J., Reinhardt, T., Seifert, A., Selbach, C., Van Lipzig, N., 2011: Long-term evaluation of COSMO forecasting using combined observational data of the GOP period. *Meteorologische Zeitschrift*, 2, **119-132**

[3] Boos, D.D., 2003: Introduction to the bootstrap world *Statistical Science*, 2, **168-174**

[4] Dai, A., Giorgi, F., Trenberth, K.E., 1999: Observed and model-simulated diurnal cycles of precipitation over the contiguous United States. *Journal of Geophysical Research-Atmospheres*, 104, **6377-6402**

[5] Ebert, E.E., 2008: Fuzzy verification of high-resolution gridded forecasts: a review and proposed framework. *Meteorological Applications* , 1, **51-64**

[6] Eckert, P., 2009: COSMO Priority Project "INTERP"; Final Report. Technical Report, No. 16, **1-34**

[7] Hohenegger, C., Brockhaus, P., Schär, C., 2008: Towards climate simulations at cloud-resolving scales. *Meteorologische Zeitschrift*. 4, **383-394**

[8] Keil, C., Tafferner, A., 2003: LMSynSat User's Guide. Unpublished Manuscript, Institute of Atmospheric Physics, DLR-Oberpfaffenhofen, Germany

[9] Keil, C., Tafferner, A., Reinhardt, T., 2006: Synthetic satellite imagery in the Lokal-Modell. *Atmospheric Research* , 82, **19–25**

[10] Kendon, E.J., Roberts, N.M., Senior, C.A., and Roberts, M.J., 2012: Realism of Rainfall in a Very High-Resolution Regional Climate Model. *Journal of Climate*, 17 **5791-5806**

[11] Knote, C., Heinemann, G., Rockel, B., 2010: Changes in weather extremes: Assessment of return values using high resolution climate simulations at convection-resolving scale.*Meteorologische Zeitschrift* , 1, **11-23**

[12] Langhans, W., Schmidli, J., Fuhrer, O., Bieri, S., Schär, C., 2013: Long-Term Simulations of Thermally Driven Flows and Orographic Convection at Convection-Parameterizing and Cloud-Resolving Resolutions. *Journal of Applied Meteorology and Climatology* , 6, **1490-1510**

[13] Langhans, W., Schmidli, J., Schär, C., 2012: Bulk Convergence of Cloud-Resolving Simulations of Moist Convection over Complex Terrain. *Journal of the Atmospheric Sciences* , 7, **2207-2228**

[14] Pfeifer, M., Yen, W., Baldauf, M., Craig, G., Crewell, S., Fischer, J., Hagen, M., Hühnerbein, A., Mech, M., Reinhardt, T., Schröder, M., Seifert, A., 2010: Validating precipitation forecasts using remote sensor synergy: A case study approach. *Meteorologische Zeitschrift* , 6, **601-617**

[15] Prein, A.F., Gobiet, A., Suklitsch, M., Truhetz, H., Awan, N.K., Keuler, K., Georgievski, G., 2013: Added value of convection permitting seasonal simulations. *Climate Dynamics* , 9-10, **2655-2677**

[16] Roberts, N.M., Lean, H.W., 2008: Scale-selective verification of rainfall accumulations from high-resolution forecasts of convective events. *Monthly Weather Review* , 136, **78-97**

[17] Schmetz, J., Pili, P., Tjemkes, S., Just, D., Kerkmann, J., Rota, S., Ratier, A., 2002: An introduction to Meteosat Second Generation (MSG). *Bulletin of the American Meteorological Society* , 7, **977-992**

[18] Sideris, I.V., Gabella, M., Erdin, R., Germann, U., 2014: Real-time radar-rain-gauge merging using spatio-temporal co-kriging with external drift in the alpine terrain of Switzerland. *Quarterly Journal of the Royal Meteorological Society* , 680, **1097-1111**

[19] Tiedtke, M., 1989: A Comprehensive Mass Flux Scheme for Cumulus Parameterization in Large-Scale Models. *Monthly Weather Review* , 8, **1779-1800**

[20] Weusthoff, T., Ament, F., Arpagaus, M., Rotach, M.W., 2010: Assessing the Benefits of Convection-Permitting Models by Neighborhood Verification: Examples from MAP D-PHASE, *Monthly Weather Review* , 9, **3418-3433**

Setting up COSMO EPS perturbing lower boundary conditions: sensitivity and case studies

Riccardo Bonanno, Nicola Loglisci

Arpa Piemonte

1 Introduction

The present work aims to pursue the goal started in the a previous study (Bonanno et al., 2014) that is to find the best setting of a soil perturbation technique to be implemented in a high resolution ensemble system based on the Italian version of the limited area model COSMO at a resolution of 2.8 km taking into account soil surface uncertainties.

The need to investigate the role played by the soil in an ensemble system rises from a well known problem: surface atmospheric variables have a little variability as far as ensemble forecast systems are concerned.The reason of this could be find in surface conditions uncertainties not taken into account in ensemble systems (Sutton et al. (2006), Aligo et al. (2007), Quintanar et al. (2008), Klüpfel et al. (2011)).

This work is part of the COTEKINO (COSMO Towards Ensembles at the Km-scale IN Our countries) priority project aimed to develop a convection-permitting ensembles in our country. In fact, even if the sensitivity of the atmospheric moist processes to different soil condition initializations has been demonstrated in several studies previously mentioned, it can not be generalized to a completely different modeling system. To do that we completed the sensitivity started before using two different perturbation techniques applied to several case studies. This work confirms the output of Klüpfel et al. (2011) for the West Africa leading us to a final setting of soil perturbation to be used by the ensemble system. The performances of this setting have been validated studying different case studies and comparing them with the performances of the operational COSMO-LEPS system.

2 Dataset and methodology

In the previous sensitivity study (Bonanno et al. 2014) has been demonstrated that a high resolution, convection permitting ensemble system is sensitive to the initial state of the soil, as far as soil water content is concerned. This sensitivity test was based on the perturbation technique suggested by Lavaysse et al. (2013) hereafter SHP. It consists in spectral coefficients of an expansion on spherical harmonics (in the horizontal) and Fourier harmonics (in the vertical). A three-dimensional random function on the sphere $f(\lambda, \phi, \eta, t)$, correlated in space and time, with a probability density function symmetric around the mean has been described in Bonanno et al (2014).

Figure 1 shows two example of initial spatial correlated random field. Both are obtained with a perturbation intensity of $0.06m^3/m^3$, but the first one corresponds to a value of $L = 80$ (namely, to an horizontal wavelength $\lambda_L \approx 2\pi R_{earth}/L \approx 500km\lambda$), whereas the second one is obtained with $L = 160$ ($\lambda \approx 250km$).

In this work we tested another perturbation technique. Soil water content was perturbed using the a second technique based on the work done by Tsyrulnikov et al. in the framework of KENDA Priority project. It consists of a Stochastic Pattern Generator based on solution of a partial stochastic differential equation in spectral space on a 3-dimensional torus. Variance, spatial and temporal scales are tunable.

This technique construct a generic field f as the solution of a stochastic differential equation of the form:

$$\left(\frac{\partial f}{\partial t} + \mu\left(1 - \lambda^2\Delta\right)^q\right)^p f = \sigma\alpha$$

Where p and q are external parameter σ, λ and μ are parameter related to the desired variance, spatial and temporal correlation scale. α is the spatio-temporal white noise. A Fourier decomposition of f is performed and an integration of the equation in the spectral space is done. This procedure simplify the analysis because allows the decoupling of the stochastic partial differential equation into a series of ordinary stochastic differential equations that can be computed by parallel processors. After the integration, a 3D Fast Fourier Transform is applied to obtain the desired random field in physical space.

This second technique has the advantage for being less expensive from the computational point of view. A preliminary test was performed to understand the main differences in terms of spread induced by the two different perturbation techniques (SHP and SPG) with five different configuration obtained modifying the perturbation intensity and the wavelength.

Table 1: Setting of sensitivity experiments to evaluate the performances of the two perturbation techniques (SHP and SPG)

.

Test	$Fmaxsurfm^3/m^3$	$Fmaxrootm^3/m^3$	L	$\lambda^2 km$
1	0.06	0.04	400	50
2	0.06	0.04	160	125
3	0.06	0.04	80	250
4	0.06	0.04	50	400
5	0.08	0.06	80	250

The values of λ have been chose according to Lavaysse et al. (2013) while maximum values of the perturbation intensity at the surface and in the root zone have been set according to Lavaysse et al. (2013) and Mc Laughlin et al. (2006) and are comparable or smaller than the errors of the ECMWF operational soil moisture (Albergel et al. (2012), ECMWF newsletter (2012)).

As soon as the best perturbation technique with the best setting was chosen, a secondary test consisted in understanding the sensitivity of the ensemble to the initial soil moisture field. In this respect we performed a test perturbing the soil moisture fields produced by the COSMO-EU soil moisture analysis, instead of that coming from ECMWF. A third sensitivity test was conducted to understand how the ensemble is sensitive to external soil related parameters such as LAI (Leaf Area Index), roughness length and vegetation cover (Lavaysse et al. 2013).

In this case a slightly different approach was used to generate the perturbations. In fact, as suggested by Lavaysse et al. (2013) the associated perturbed fields, we used a multiplicative perturbation approach, based on the assumption that the errors are proportional to the values of the considered parameter (Lavaysse et al., 2013).

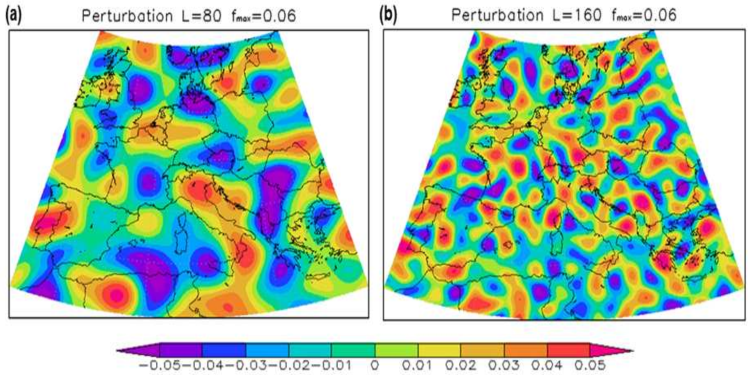

Figure 1: Examples of spatial correlated random fields obtained using two different wavelength in the SHP $L = 80$ ($\lambda_L \approx 500km$, Figure 1a) and $L = 160$ ($\lambda_L \approx 250km$, Figure 1b)

.

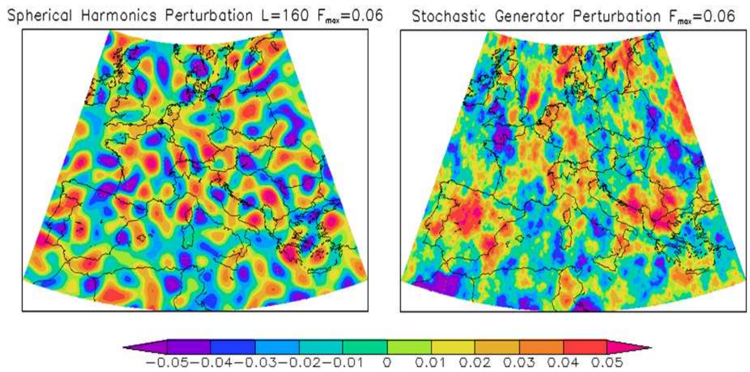

Figure 2: Comparison of a soil water content field perturbation computed by the SHP (Fig. 2a) and SGP (Fig. 2b)

.

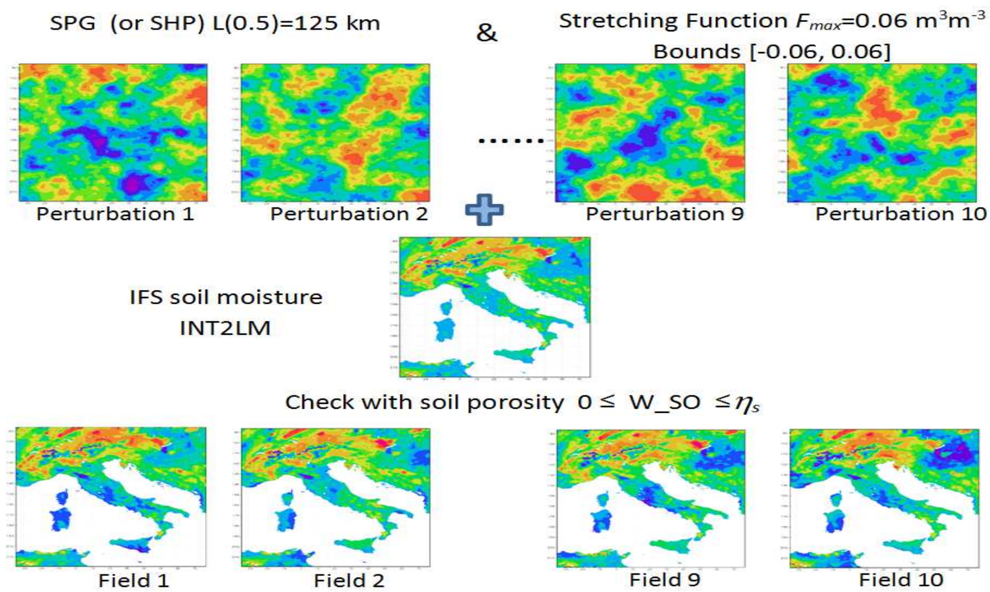

Figure 3: The procedure to create ten soil moisture initial conditions starting from ECMWF soil moisture analysis and applying SPG or SHP as additive Gaussian patterns

.

We report in Figure 4 a scheme of the above mentioned approach as far as Leaf Area Index is concerned.

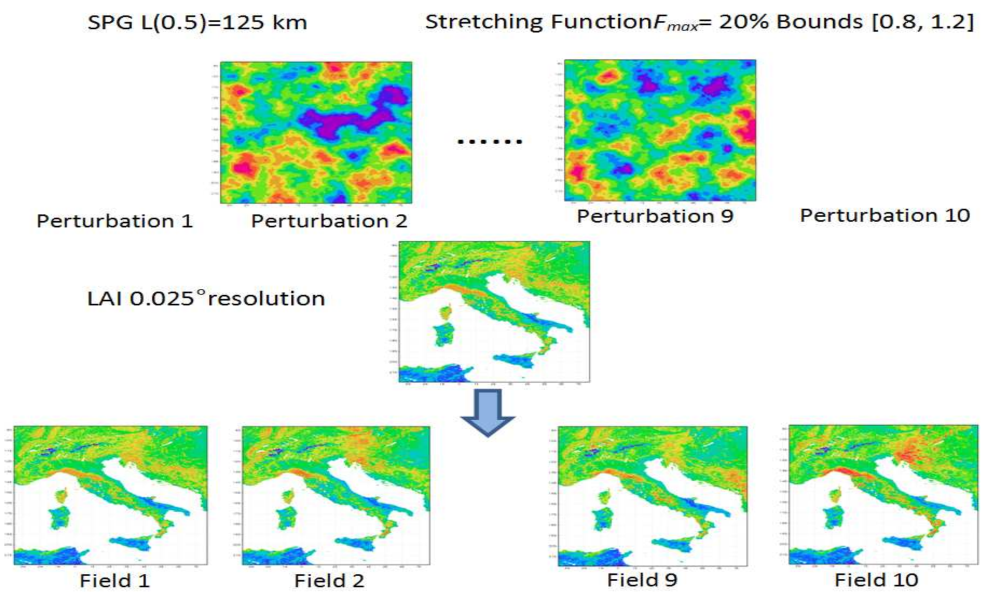

Figure 4: The procedure to create ten LAI initial conditions starting from ECMWF field and applying SPG as multiplicative perturbation

.

As result of the three tests we chose the best setting for the soil perturbation and evaluated the spread on the upper atmospheric levels in the two case studies selected as representative of two different meteorological regimes (Bonanno et al. 2014). Finally, the performances of the selected perturbation technique were compared with those coming from the operative COSMO-LEPS.

3 Simulations and results

-Selection of the best perturbation technique.

Following are the output from the first sensitivity test chosen to understand the most performing perturbation techniques and its best setting. As mentioned before we applied SHP and SPG to create the perturbed soil moisture initial conditions starting from the ECMWF soil moisture analysis of two case studies. The first one (CS1) is a case of convection induced by a strong synoptic forcing (June 29th 2011) the second one (CS2) is characterized by strong wind over the whole domain (November 10th 2013).

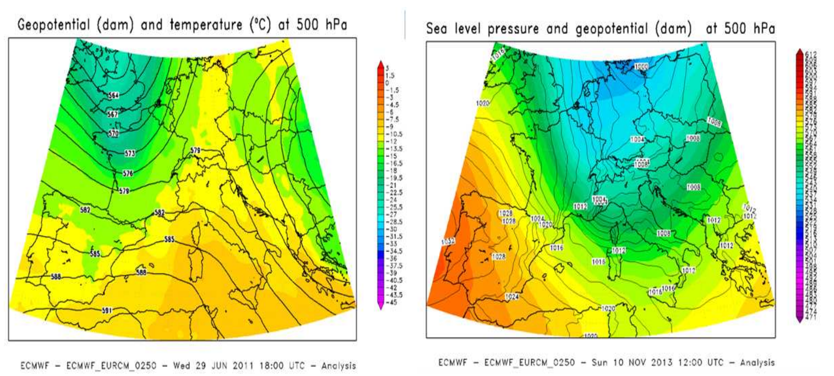

Figure 5: Case studies: convection induced by a strong synoptic forcing (left) strong wind over the whole domain.

A total amount of hundred simulation were performed (10 perturbations x 5 different settings (Tab. 1) x 2 perturbation techniques (SHP, SPG)) for each one of the two case studies.

Figure 6 shows the comparison of the spread induced by SHP (left) and SPG (right) as far as 2 meters temperature is concerned. Both the techniques produce significant spread increasing with the lead time and showing a pronounced diurnal cycle.

The differences among the 5 different settings are not appreciable whenever the perturbation intensity is kept constant. The best setting for both SHP and SPG is the one corresponding to the fifth case in Table 1, that is with the highest intensity of the perturbation considering a medium wavelength. The differences between SHP and SPG are almost negligible.

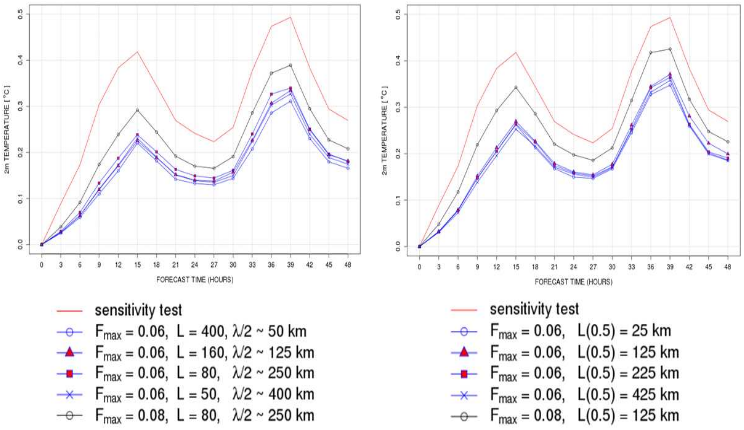

Figure 6: Comparison of the spread induced by SHP (left) and SPG (right) on 2 meters temperature for case study CS1. Solid red lines is spread obtained with the sensitivity done in Bonanno et al. (2014) using different soil moisture analysis from different GCM, LAM and LSM models.

Other variables such as 2 meters dew point, 10 meters wind speed, cloudiness, vertical velocity, precipitation soil temperature and moisture, show a similar behavior except for vertical velocity and precipitation where negligible differences are produced by all the different settings and soil moisture for which the spread, after an initial small decrease in the first hours of the run, remains almost constant throughout the entire ensemble cycle. For the sake of brevity figures are not shown.

This first step in understanding the sensitivity of the model to the initial soil moisture field led us to choose the fifth setting of Table 5 and SPG as the best setting for the soil moisture perturbation technique.

- Sensitivity to the initial soil moisture field.

A second test consisted in understanding the sensitivity of the ensemble system to the initial soil moisture field. In this respect we performed a test perturbing COSMO-EU soil moisture fields instead of that coming from ECMWF.

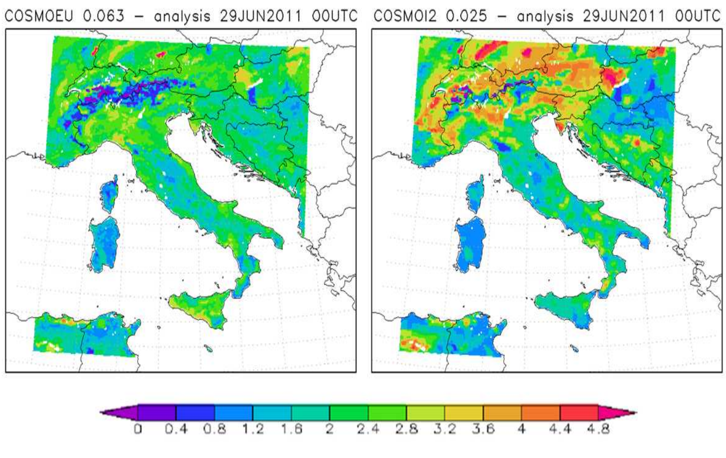

Figure 7: The initial soil moisture field interpolated on the COSMO-I2 domain from COSMO-EU (left) and ECMWF (right) for case study CS1.

In fact, as can be noticed from Figure 7, the initial soil moisture field on the COSMO-I2 domain is very different from COSMO-EU to ECMWF with the first one much drier respect to the second one.

This fact lead us to assess if this strong difference could lead to a production of different values of spread when the soil moisture is perturbed.

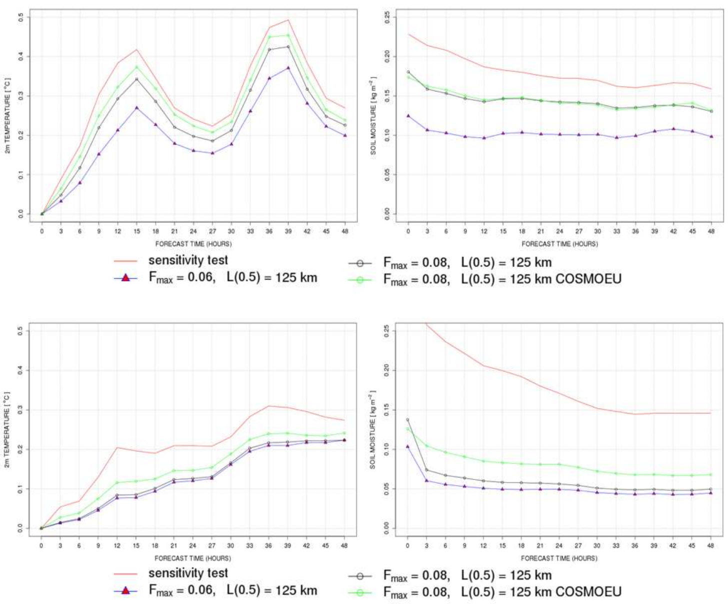

Figure 8: Case study CS1 (top panel) CS2 (bottom panel): spread produced by the ensemble system for 2 meters temperature (left) and soil moisture (right). Different lines represent different soil moisture analysis/ different SPG setting.

From Figure 8, which represents the results relative to CS1 and CS2, one can notice how a drier soil moisture analysis lead to an higher spread on 2 meters temperature due to higher fluxes at the soil-atmosphere interface.

There is not an appreciable difference as far as soil moisture spread is concerned in CS1.

Looking at other variables (not shown for the sake of brevity) such as 2 meters dew point, 10 meters wind speed, cloudiness, vertical velocity, precipitation soil temperature and moisture, similar conclusions can be inferred.

- Sensitivity to external soil related parameters.

A third and last test was performed to evaluate how sensitive the ensemble system is to the perturbation of soil related external parameters such as LAI (Leaf Area Index), roughness length and vegetation cover. Following are the comparison of the results obtained with different combinations of the perturbations.

From Figure 9 and 10 one can notice as the perturbations of the external soil related parameters do not have a great impact in the generation of spread for 2 meters temperature as well as soil moisture.

Same results have been obtained for other variables such as 2 meters dew point, 10 meters wind speed, precipitation, vertical velocity and soil temperature. Moreover, a complete perturbation accounting for uncertainties of soil moisture and soil related parameters all together, do not have an impact in generating spread on surface variables.

- Best perturbation setting choice.

The three sensitivity tests described above led us to conclude that the best setting for a soil perturbation technique is the following: Stochastic Pattern Generator was selected as the best perturbation technique.

It has the best numerical performances in terms of computational demands to compute the perturbed fields. Moreover the SPG code is already compatible with the internal code of COSMO model;

Soil Moisture is the only field to be perturbed. Perturbation of other soil related external parameters and/or a combination of them do not produce enough spread compared to the one produced by soil moisture initial condition perturbation;

Initial soil moisture field from the COSMO-EU is the initial soil moisture analysis to be perturbed. In, fact

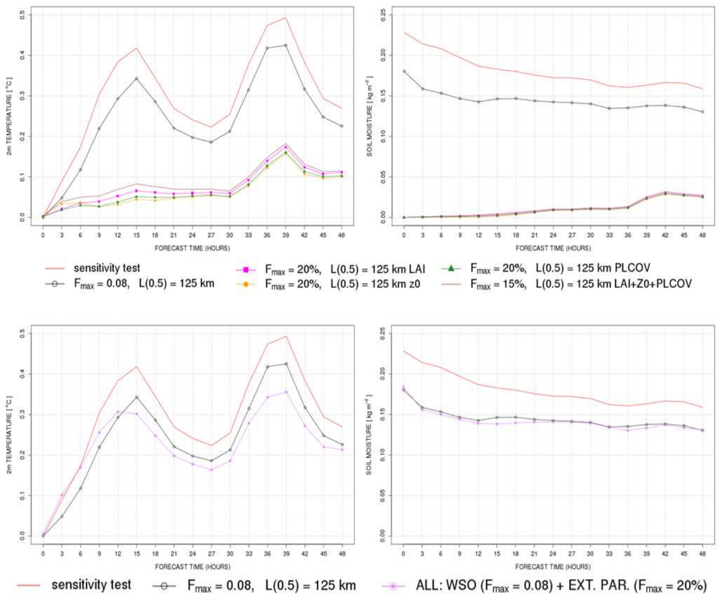

Figure 9: Comparison of different combinations of perturbations for the case study CS1.

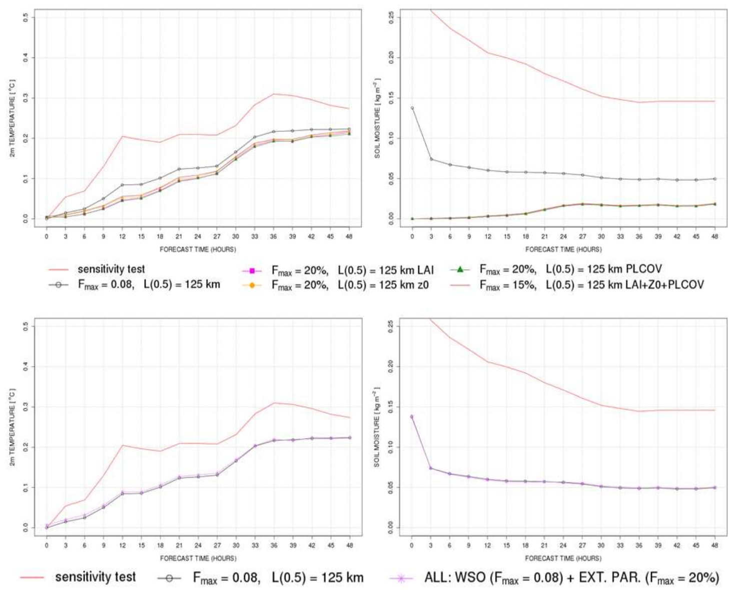

Figure 10: Comparison of different combinations of perturbations for case study CS2.

using ECMWF soil moisture analysis have a negative impact in terms of spread generation. This is partly due to the fact that ECMWF systematically overestimate the soil moisture content respect to COSMO-EU, reducing the fluxes at the soil-atmosphere interface.

- Impact of surface perturbation on upper levels of atmosphere.

The effects of an initial soil surface perturbation on surface prognostic variables have been analyzed. But does this soil initial perturbation have an effect on the upper atmospheric levels? To answer this question we plotted the cross section of main atmospheric variables over the whole domain at coordinate 11° East, 45° North (Figure 11) for the two case studies CS1 and CS2.

For sake of brevity we quote for CS1 in Figure 12. Both cross section demonstrates how the soil moisture initial condition perturbation with SPG and the selected setting is able to propagate spread from the bottom layer to middle troposphere.

-Comparison with an ensemble system with IC e BC perturbations: COSMO LEPS.

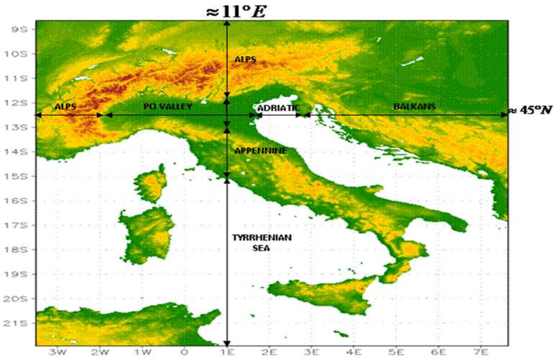

Figure 11: The COSMO-I2 integration domain with the selected latitude and longitude.

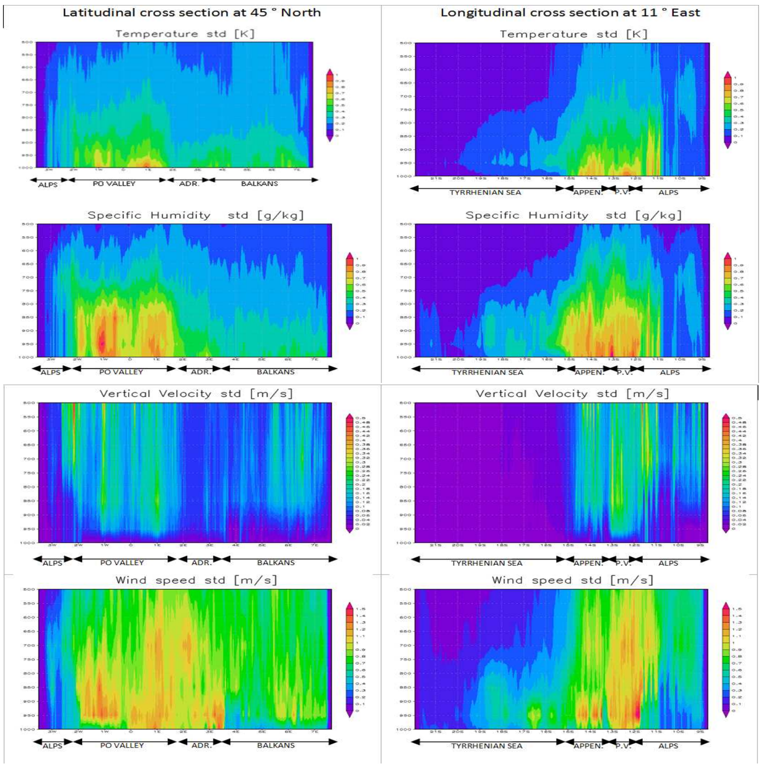

Figure 12: Latitudinal and longitudinal cross section of the time mean spread of different atmospheric variables.

In this final paragraph we compare the spread obtained with the selected soil perturbation technique with the one coming from a an ensemble system with perturbed atmospheric initial and boundary conditions, in this case COSMO-LEPS (Montani et al.,2011).

Figure 13 shows the spread obtained with the two different ensemble systems. One can notice that both systems produce comparable spread as far as inland surface atmospheric variables are concerned. In fact, the main difference between the two ensemble technique is that COSMO-LEPS is able to produce spread also over the sea. Perturbing soil moisture initial condition, in fact, has its great impact on the mainland.

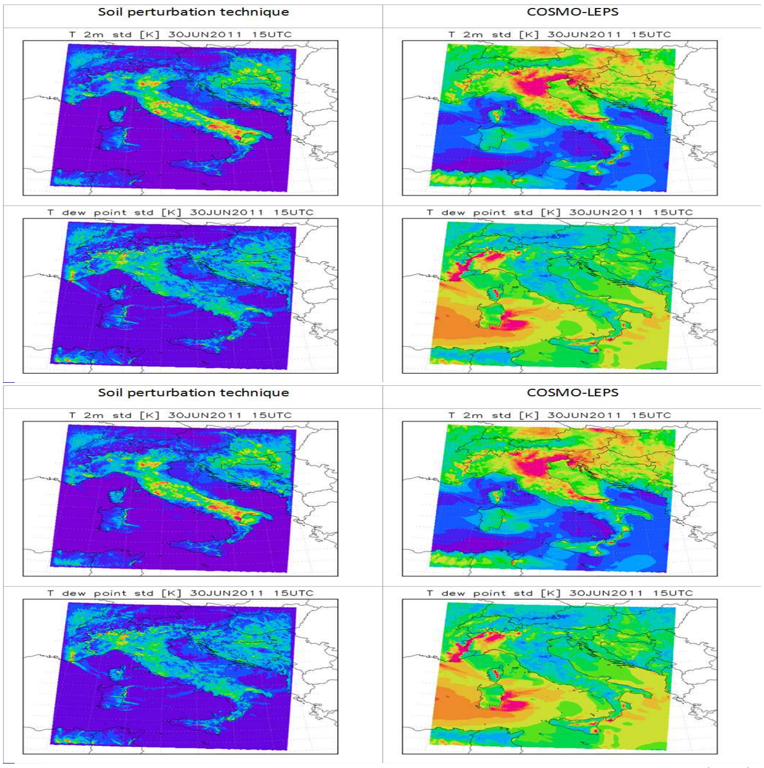

Figure 13: Comparison of the spread obtained with the soil perturbation technique (left) and with COSMO-LEPS (right).

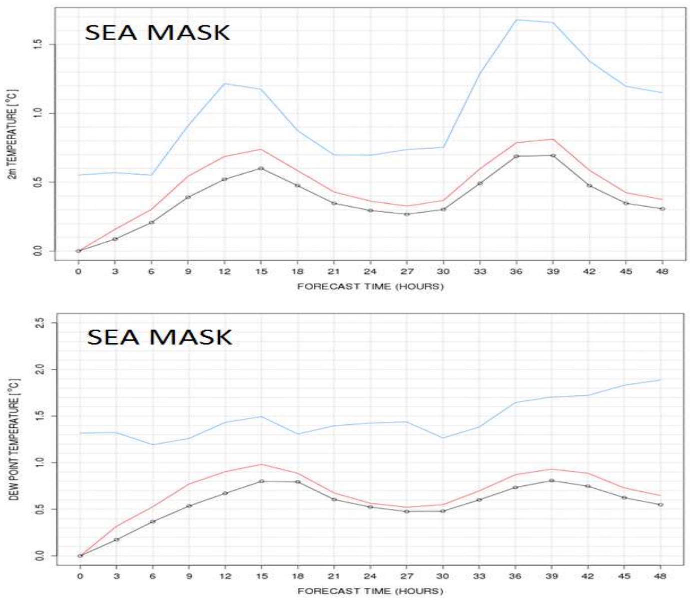

Figure 14: Comparison of the spread obtained by COSMO-LEPS (blue line) and by the soil humidity perturbation technique (black line). 2 meters temperature and dew point are plotted, Solid red lines is spread obtained with the sensitivity done in Bonanno et al. (2014).

If a land-sea mask is considered (Figure 14), the generated spread has the same order of magnitude, demonstrating that the proposed ensemble technique based on the soil moisture initial condition perturbation is able for this case to generate spread comparable with the one coming from an ensemble technique with perturbed atmospheric initial and boundary conditions.

4 Conclusions and Future developments

In this study we continue the work started in a previous study (Bonanno et al. 2013), aimed at finding the best setting of a soil perturbation technique to be implemented in a high resolution ensemble system based on the Italian version of the limited area model COSMO at a resolution of 2.8 km taking into account soil surface uncertainties.

We performed several sensitivity tests based on perturbation of soil moisture initial conditions with two different perturbation techniques and considering different initial field (soil moisture, soil related parameters such as LAI, roughness length, vegetation cover).

The perturbation of the soil using the best perturbation technique found so far produce spread of prognostic surface atmospheric variables comparable, for the case considered, with the one coming from an ensemble with perturbed initial and boundary atmospheric conditions. The proposed technique have an impact to spread of prognostic surface as well as on upper level atmospheric variables.

Future developments

Sensitivity have to be completed accounting for soil temperature perturbations. In this way also the response to initial uncertainties of this variable will be taken into account. The amplitude of soil temperature perturbation will be established according to soil temperature ECMWF bias (Albergel et al., 2014).

This technique will be tested as part of a more complete ensemble set-up, where both atmosphere and soil are perturbed (COSMO-IT-EPS ensemble). To do that, the same case studies, as well as other cases conveniently selected among those producing convection, will be analyzed using a complete perturbation technique accounting for both initial soil and upper level uncertainties. This will be done coupling the best soil perturbation technique with the perturbation of atmospheric boundary and initial conditions coming from ECMWF EPS members.

References

[1] Albergel, C., Dutra, E.,Muñoz-Sabater, J., Haiden, T., G. Balsamo, G., Beljaars, A., Isaksen, L., de Rosnay, P., Sandu, I., Wedi, N., 2014: *Soil temperature at ECMWF: an assessment using ground based 1 observations (Submitted).*

[2] Albergel, C., de Rosnay, P., G. Balsamo, G., Isaksen, L., Muñoz-Sabater, J., 2012:*Soil Moisture Analyses at ECMWF: Evaluation Using Global Ground-Based In Situ Observations. J. Hydrometeor, 13,***1442–1460**.

[3] Aligo, E. A., Gallus, W. A. and Segal, M., 2007: *Summer Rainfall Forecast Spread in an Ensemble Initialized with Different Soil Moisture Analyses. Wea. Forecasting, 22,***299–314**.

[4] Cloke, H. L., Weisheimer, A., and Pappenberger, F., 2011: *Representing uncertainty in land surface hydrology: fully coupled simulations with the ECMWF land surface scheme, in Proceedings of the ECMWF/WMO/WCRP workshop on "Representing Model Uncertainty and Error in Numerical Weather and Climate Prediction Models", 20–24 June 2011 at ECMWF, Reading, UK.*

[5] Hacker, J. P., 2010: *Spatial and Temporal Scales of Boundary Layer Wind Predictability in Response to Small-Amplitude Land Surface Uncertainty, Journal of Atmospheric Sciences, 67,***217-233**.

[6] Huffman, G. J., and Coauthors, 2007:*The TRMM Multisatellite Precipitation Analysis (TMPA): Quasi-Global, Multiyear, Combined-Sensor Precipitation Estimates at Fine Scales. J. Hydrometeor, 8,***38–55**.

[7] Klüpfel, V., Kalthoff, N., Gantner, L. and Kottmeier, C., 2011: *Evaluation of soil moisture ensemble runs to estimate precipitation variability in convection-permitting model simulations for West Africa. Atmospheric Research, 101:1-2,* **178-193**.

[8] Lavaysse, C., Carrera, M., Bélair, S., Gagnon, N., Frenette, R., Charron, M. and Yau, M. K., 2013: *Impact of Surface Parameter Uncertainties within the Canadian Regional Ensemble Prediction System. Mon. Wea. Rev., 141,***1506–1526**.

[9] Li, X., Charron, M., Spacek, L. and Candille, G., 2008: *A Regional Ensemble Prediction System Based on Moist Targeted Singular Vectors and Stochastic Parameter Perturbations. Mon. Wea. Rev., 136,***443–462**.

[10] Montani, A., Cesari, D., Marsigli, C. and Paccagnella, T., 2011:*Seven years of activity in the field of mesoscale ensemble forecasting by the COSMO-LEPS system: main achievements and open challenges. Tellus, 63A,***605-624**.

[11] Quintanar, A. I. and Mahmood, R., 2012:*Ensemble forecast spread induced by soil moisture changes over mid-south and neighbouring mid-western region of the USA. Tellus A 64:0,*.

[12] Rodell, M., Houser,P. R.,Jambor,U.,Gottschalck,J., Mitchell,K.,Meng, C.-J., Arsenault,K., Cosgrove,B. ,Radakovich,J. ,Bosilovich, M. ,Entin,J. K. , Walker,J. P. ,Lohmann,D. and Toll,D., 2004.*The Global Land Data Assimilation System, Bulletin of the American Meteorological Society, 85(3):***381-394**.

[13] Sutton, C., Hamill, T.M. and Warner. T. T., 2006:*Will Perturbing Soil Moisture Improve Warm-Season Ensemble Forecasts? A Proof of Concept. Mon. Wea. Rev., 134,***3174–3189**.

[14] Sutton, C. J., Hamill, T. M.and Warner, T. T., 2004:*Impacts of perturbed soil moisture conditions on short-range ensemble variability, 16th NWP/20th W& F Conference, Seattle, American Meteorological Society.*

[15] Wang, Y., Kann, A., Bellus, M., Pailleux, J., and Wittmann, C., 2010:*A strategy for perturbing surface conditions in LAMEPS, AtmosSciLett, 11,***108–113**.

Ensemble Prediction System (EPS)-based forecast prepared from perturbations of soil conditions

Andrzej Mazur, Grzegorz Duniec

Department for Numerical Weather Forecasts. Institute of Meteorology and Water Management – National Research Institute. PL-01-673 Warsaw, 61 Podleśna str.

1 Summary

The significance of Ensemble Prediction System (EPS)-based forecasts is now greater than ever. Perturbations of the lower boundary state (i.e. of soil and - the boundary between soil and lower atmosphere) applied to EPS are also believed to play an important role at any resolution. The aim of this study was to develop, test and verify a simple method of preparing an ensemble of forecasts using a perturbation of selected soil parameters. The first phase involved tests of specified group of different model set-ups and pre-selection of parameters to be used in further experiments.

Then, sensitivity tests were carried out to verify the correct selection of ensemble members in a quasi-operational mode. The aim of the tests was to obtain a response whether a small perturbation of soil-related parameter(s) would be considerable efficient to cause significant changes in the forecast and create "proper" ensemble. Two methods of preparing a well-defined ensemble based on the soil parameters perturbation were evaluated for (potential) operational implementation in the COSMO model.

2 Introduction and methods

As a part of COSMO Towards Ensembles at the Km-scale In Our Countries (COTEKINO) priority project of Consortium for Small-scale Modeling (COSMO) at the Institute of Meteorology and Water Management – National Research Institute (IMWM-NRI) a simple method was proposed to produce reasonable number of valid ensemble members, taking into consideration predefined soil-related model parameters. The first phase was based on tentative analysis of the influence on a reference results from various model set-ups (i.e. parameters, numerical schemes, physical parameterizations, etc.) combined with rough changes of these parameters, like the surface-area index or bottom of the last hydrological active soil layer. The analysis provided an answer about "importance" of soil parameters and a possibility to neglect "less significant" ones. Having results of this approach as a first step (see Duniec and Mazur, 2014; Mazur and Duniec, 2014), in the second phase further sensitivity tests were performed. This allowed for detailed selection of various configurations and for assessing methods of perturbation of important soil parameters.

After completion of numerous model runs following conclusions were drawn: (i) climatological layer depth (cz_bot_w_so) had a noteworthy impact on values of water and ice content down to lower boundary of soil model; (ii) surface area index of evaporating fraction (c_soil) had a noteworthy impact on values of relative humidity, air and dew point temperatures at 2m agl. and on the wind speed and direction at 10m agl.; (iii) other parameters had rather insignificant impact on forecast values in comparison with reference ones. Thus, sensitivity tests were set-up with the following numerical schemes applied: (a) a shallow convection parameterization was set as a basic convection scheme, and (b) a 3-order Runge-Kutta advection.

Changes of cz_bot_w_so had a significant impact on water and ice content as well as soil temperature down to 1458 cm, but its impact on the lower atmosphere fields, such as temperature, precipitation, dew point temperature and wind speed was relatively small. Moreover, this parameter, as of an integer type -from 1 to 7 - was not very useful for a preparation of an ensemble. On the other hand, perturbation of c_soil has a significant influence on the air temperature, dew point and humidity at 2 m a.g.l., and wind speed/wind direction at 10 m a.g.l., as well as on surface specific humidity. As a floating-point number it may be equal to any value from its range of variability (ie. from 0 to 2.0). So c_soil is (potentially) a much better candidate for base of an ensemble. Thus, all selected cases were studied in detail regarding changes of c_soil parameter (Mazur and Duniec, 2014).

Representative ensemble members could be prepared using two methods:

- Random set the one value of c-soil, globally, on the whole domain (easier to perform, you need to change the namlists) do not need to change the model code.

- An alternative approach -by modifying the source code may distribute the random values of the c-soil from point to point over the entire model domain.

All of results are described in terms of spatial distribution of forecast “spread” – i.e. the standard deviation against mean value.

3 Results and discussion

As a case study basis, eleven selected terms (dates of the start of forecast) were chosen, covering four season and diversity of synoptic situations. In the following figures results of an application of the point-to-point method mentioned above, as a sample preparation method of an ensemble are presented.

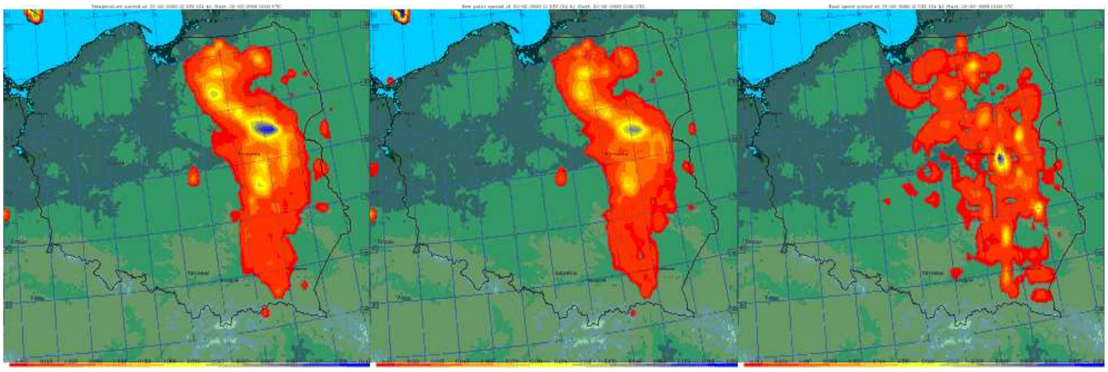

Figure 1: Spread of selected meteorological field over a c_soil based ensemble; winter case (February 22nd, 2009). Left chart - temperature (max spread value - 0.2^oC), middle - dew point temperature (max spread value - 0.2^oC), right - wind speed (max spread value - 0.1 m/s).

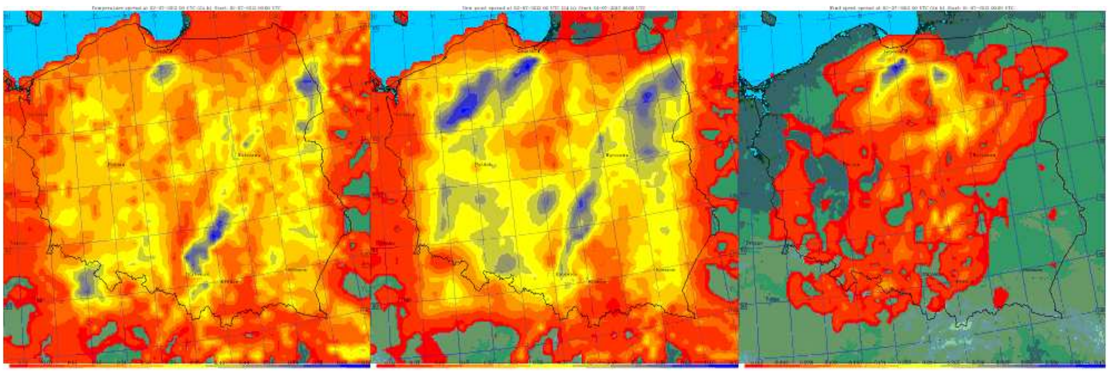

Figure 2: Spread of selected meteorological field over a c_soil based ensemble; summer case (July 1st, 2012). Left chart -temperature (max spread value -0.7^oC),middle - dew point temperature (max spread value - 0.9^oC), right - wind speed (max spread value -1.0 m/s).

In the following figures results of the comparison of ensemble forecasts with measurements at meteorological stations (seashore station Leba, midland station in Warsaw and Poznan, mountain station Zakopane) are shown for selected (winter and summer) cases.

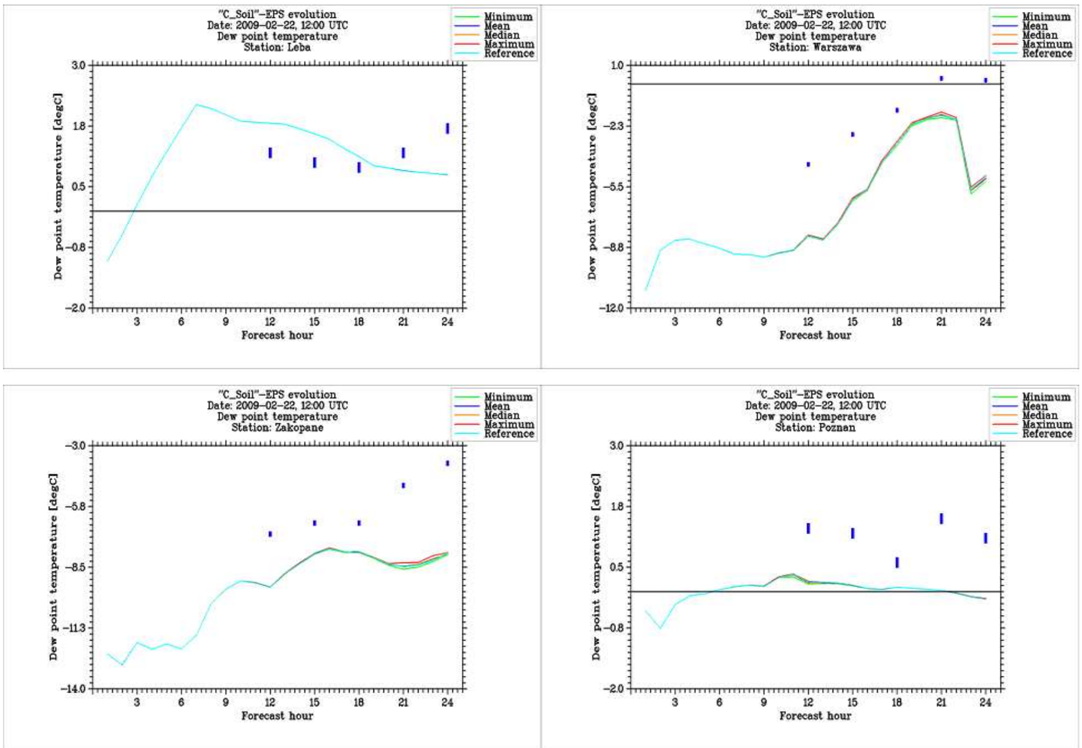

Figure 3: Ensemble forecast with c_soil, for the winter case, February 22^{nd}, 2009. "Spaghetti-plots" against values measured at meteorological stations (vertical bars). Dew point temperature forecast at the following stations:upper left – Leba, upper right – Warsaw, lower left – Poznan , lower right – Zakopane.

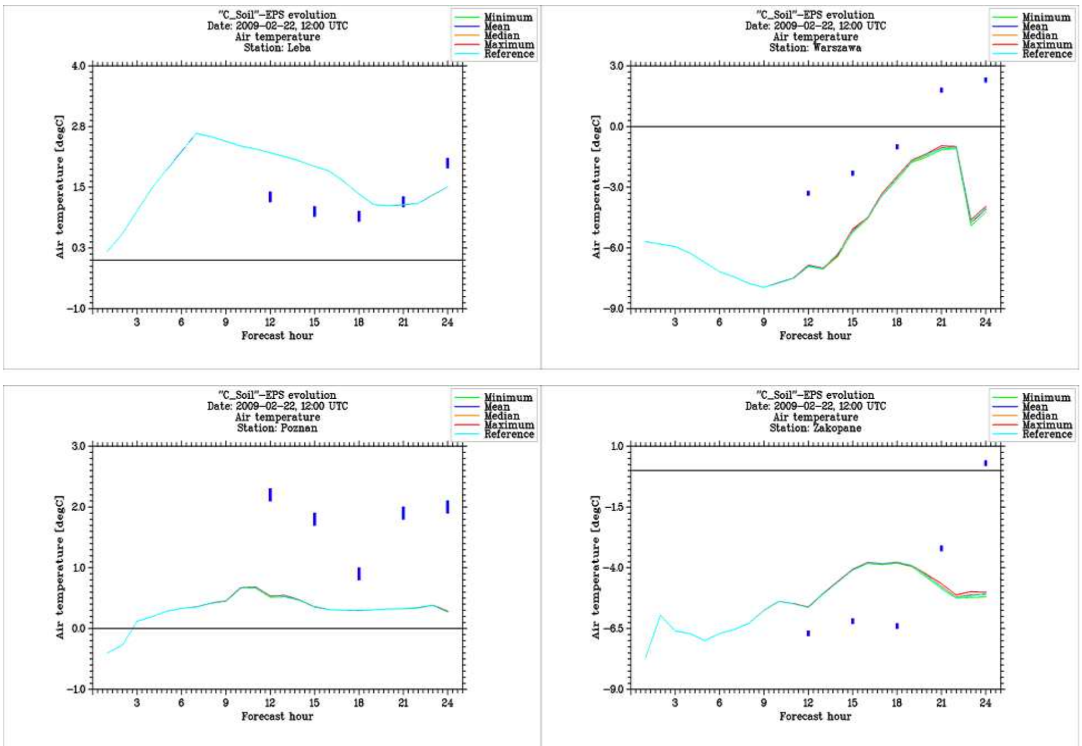

Figure 4: Same case as on Fig.3 but for, air temperature forecast.

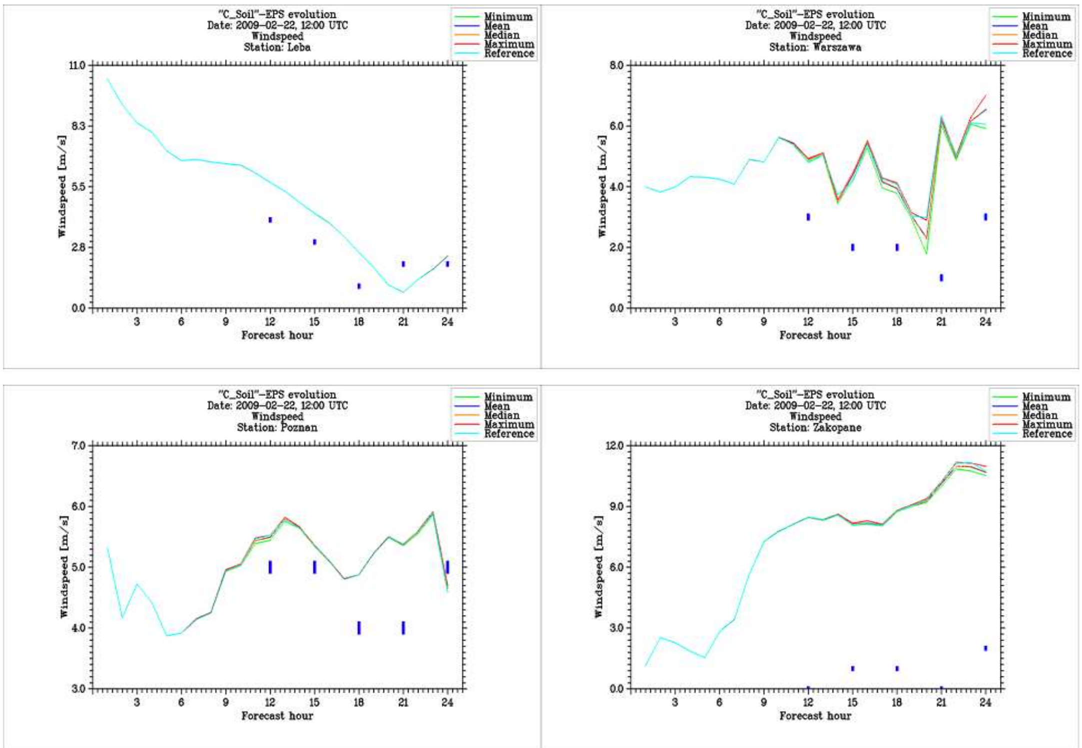

Figure 5: Same case as on Fig.3 but for wind speed forecast.

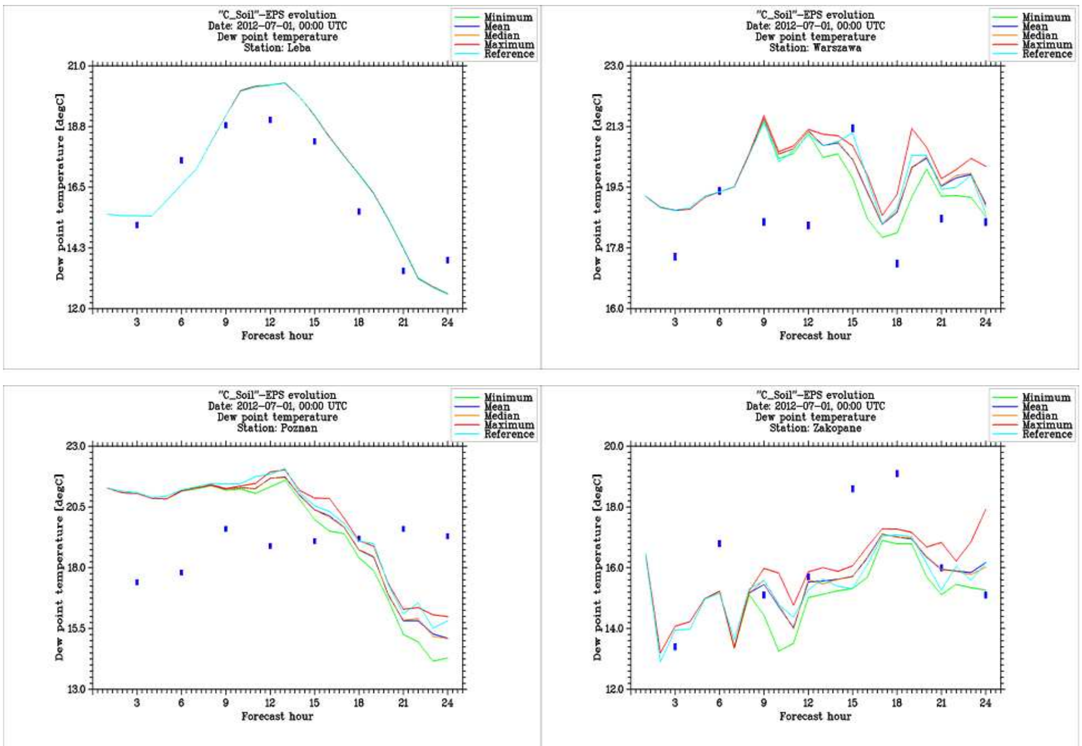

Figure 6: Ensemble forecast with c_soil, summer case, July 1^{st}, 2012. "Spaghetti-plots" against values measured at meteorological stations. Dew point temperature forecast at stations: upper left – Leba, upper right – Warsaw, lower left – Poznan , lower right – Zakopane.

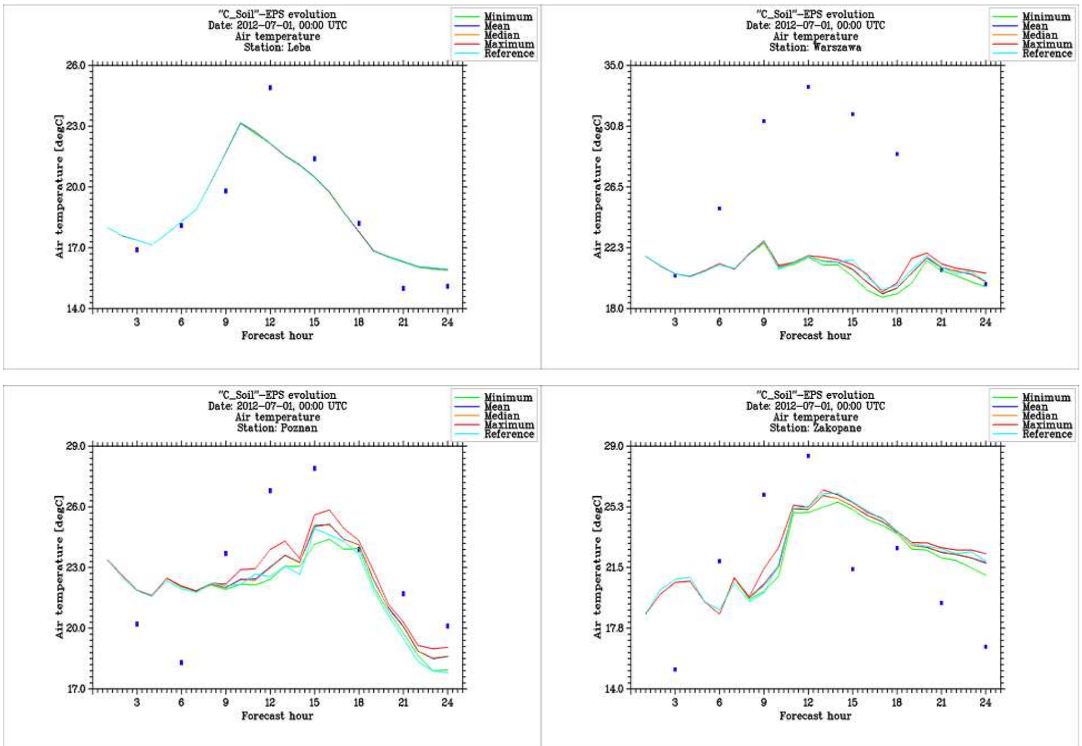

Figure 7: Same case as on Fig.6 but for air temperature forecast.

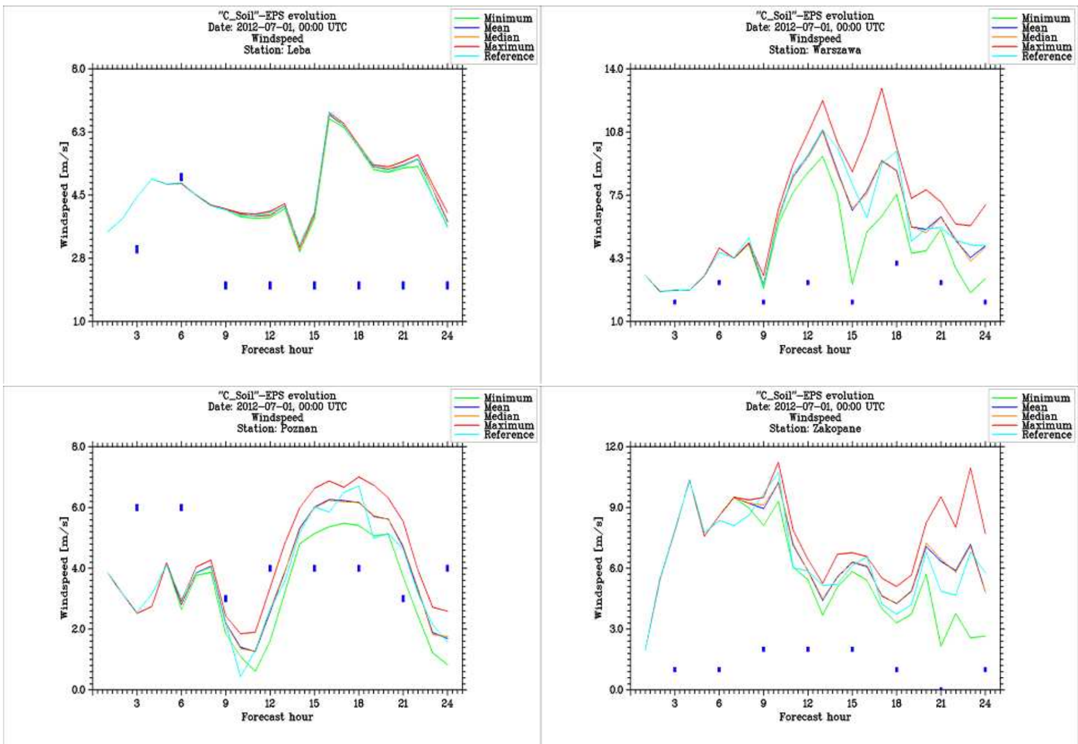

Figure 8: Same case on Fig.6 but for wind speed forecast.

The last part of the study presented here was a combination of changes of soil processes parameterization (Duniec and Mazur 2014) with the preparation of soil-based ensemble forecasts. After replacing the Dickinson equation with the temperature-dependent Darcy equation, similarly to deterministic forecasts, further improvement in forecasts can be seen. Examples of the results are shown in the following figures. Actual values, measured at stations are "closer" to the forecast spread calculated for appropriate hour.

This improvement can be seen to a big extent in forecast of wind speed, especially in central part of Poland, like Warsaw and Poznan, rather than these located at the seashore (Leba) or in mountain regions (Zakopane). This effect is most likely correlated with type or nature of soil in these locations (luvisols in central part of Poland, small land fraction at the sea cost or gravel/pebble settlements in southern Poland).

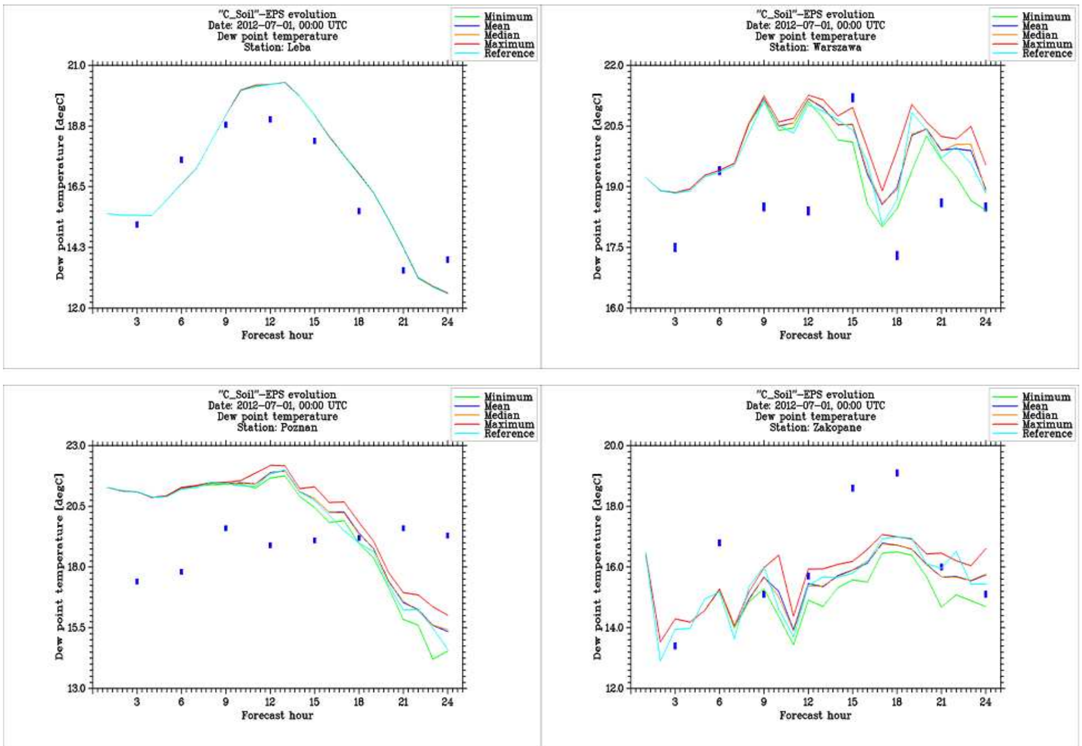

Figure 9: Ensemble forecast with c_soil, summer case, July 1^{st}, 2012, combined with altered soil processes parameterization. "Spaghetti-plots" against values measured at meteorological stations. Dew point temperature forecast at the following sations: upper left – Leba, upper right – Warsaw, lower left – Poznan , lower right – Zakopane.

Last figures show quantitative effect of changes of soil processes parameterization on a forecast quality.

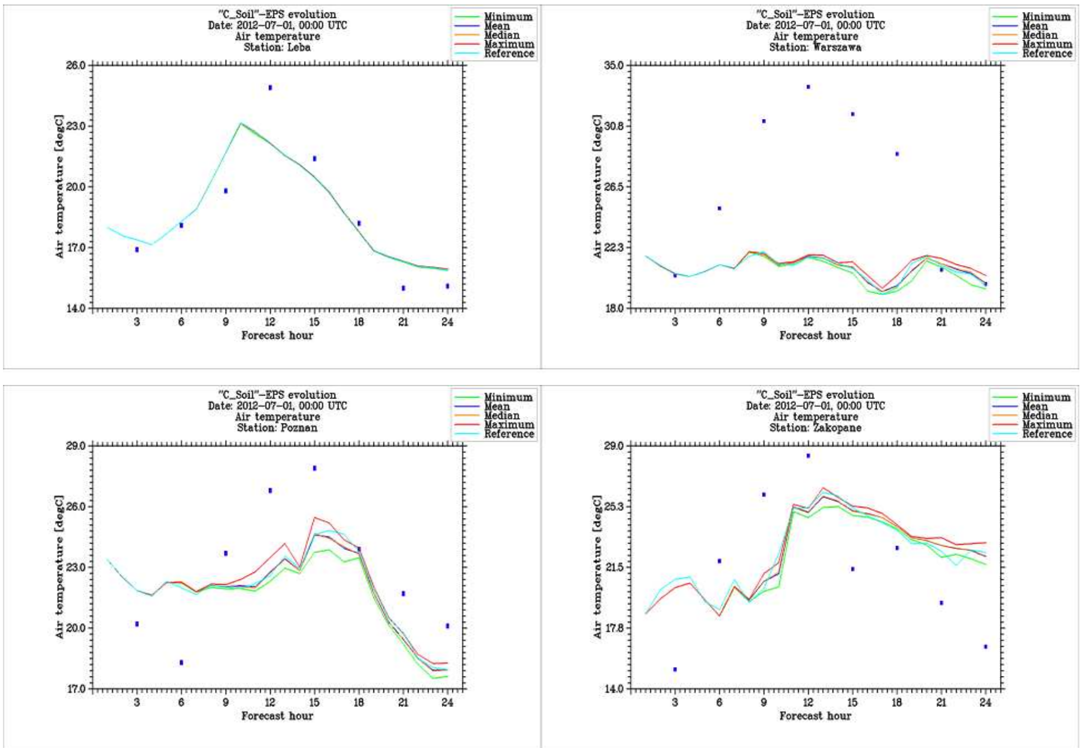

Figure 10: Same case as on Fig.9 for the altered soil processes parameterization, and air temperature forecast.

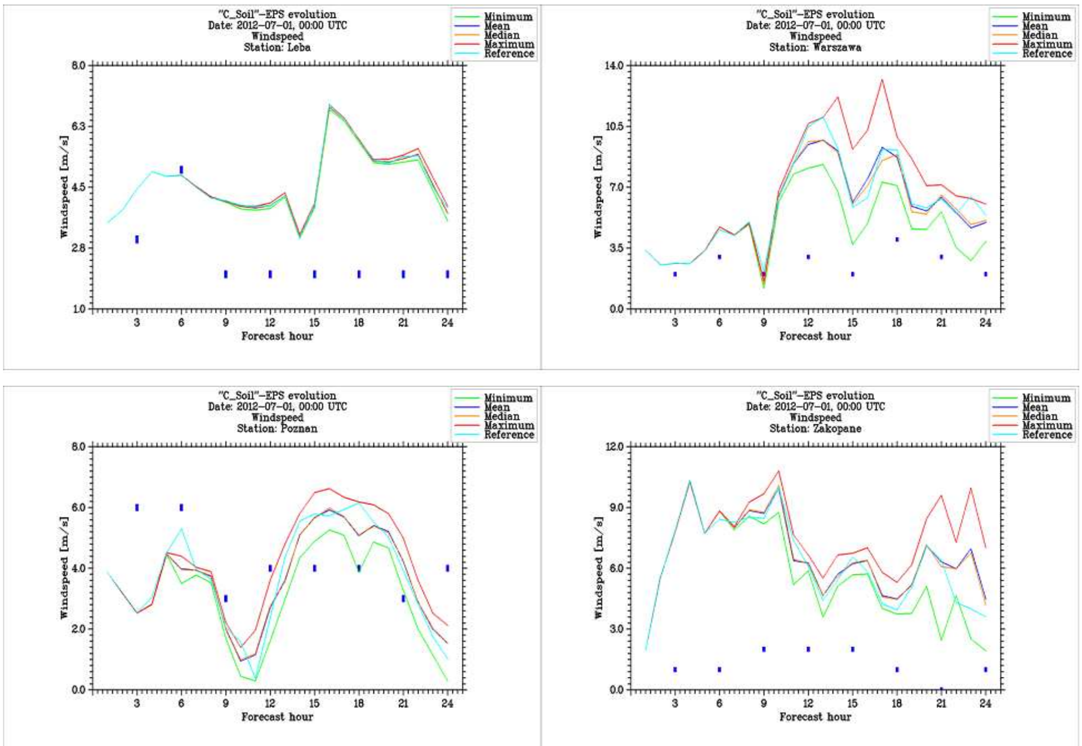

Figure 11: Same case as on Fig.9 for the altered soil processes parameterization and wind speed forecast.

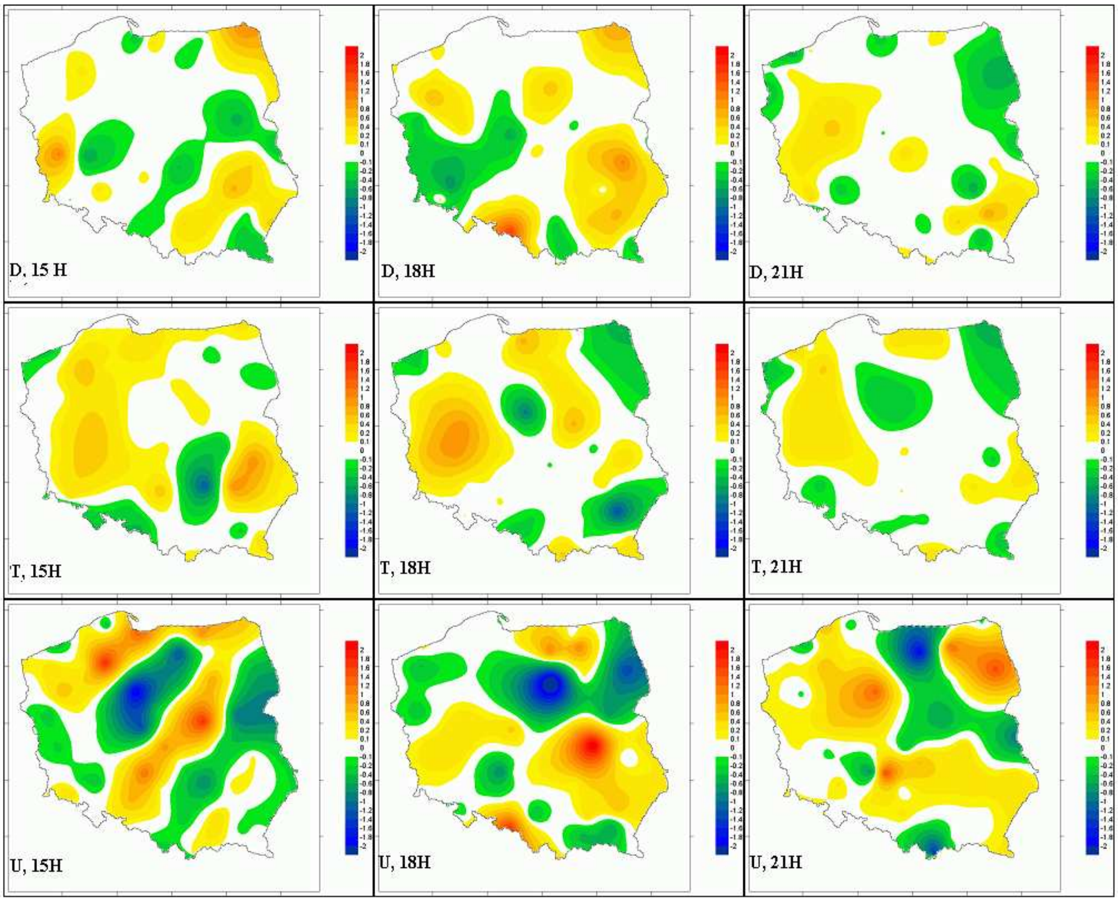

Figure 12: Comparison of “regular” c_soil-based ensemble forecast with the one combined with altered soil processes parameterization. Summer case, July 1st, 2012. Upper row – prediction of dew point temperature for 15th, 18th, and 21st hour of forecast. Middle row - temperature forecast, similarly. Lower row - wind speed forecast, similarly. Areas with “warm” colors represent improvement of forecast, areas with “cold” colors - worsening of forecast (see further explanation in text) due to change of soil processes parameterization.

A comparison of these two types of forecasts was carried out by computation a "distance" of a real value, measured at SYNOP stations, from an interval defined by a forecast's spread, understood as a difference between minimum and maximum values over an ensemble. If the real value was located in the interval, this "distance" was identified as equal to zero. In the figure, areas with "warm" colors (from yellow to red) represent improvement of forecast (i.e., decrease of a "distance" forecast's spread from real values) caused by change of parameterization, whereas areas with "cold" colors (from blue to green) – worsening of forecast.

An overall improvement (spatially computed, mean value of this "distance") for every element shown above was recognized. In case of dew point and air temperature, significant improvement can be especially seen in central and south-eastern part of Poland. In case of wind speed forecasts, the "area of improvement" was moving with forecast hour, in general, from west to east. It should also be stated, however, that this improvement can hardly be seen in a beginning of a forecast(s). It seems that the soil parameterization need some "spin-up" time to have a significant impact on a quality of an ensemble forecast of atmosphere's state.

4 Conclusions

Tests proved that small perturbations of selected parameter(s) were sufficient to induce significant changes in the forecast of the state of atmosphere and to provide qualitative selection of a valid member of an ensemble. However, perturbations have had almost negligible impact in the areas with land fraction much less than one and during the cold season (perhaps due to the specific soil conditions, e.g. frozen ground). A detailed (seasonal/annual) performance analysis is needed for stochastic forecasts. Comparison of ensemble forecasts with observations at meteorological stations showed that, as in the case of deterministic forecasts, introduction of altered soil processes parameterization slightly improved forecasts, mainly in the central/southern part of Poland, rather than closer to the sea or in mountain regions.

References

[1] H. Cloke, A. Weisheimer and F. Pappenberger: Representing uncertainty in land surface hydrology: fully coupled simulations with the ECMWF land surface scheme. *Workshop on Model Uncertainty, 20-24 June 2011, ECMWF, Reading (UK), 2011.*

[2] G. Doms, U. Schattler, A Description of the Nonhydrostatic Regional Model LM, Part I: *Dynamics and Numerics, DWD, 2002.*

[3] G. Doms, J. Forstner, E. Heise, H. – J. Herzog, M. Raschendorfer, T. Reinhardt, B. Ritter, R. Schrodin, J. – P.Schulz, G. Vogel, A Description of the Nonhydrostatic Regional Model LM, Part II:*Physical Parameterization, DWD, 2007.*

[4] U. Schattler, G. Doms, C. Schraff, A Description of the Nonhydrostatic Regional Model LM, Part VII:*User's Guide, DWD, 2009.*

[5] M. Z. Jacobson, Fundamentals of Atmosferic Modeling, *Cambridge University Press, 2000.*

[6] I. B. Rewut, Soil physics (in Polish: Fizyka gleby), *PWRiL, 1980.*

[7] T. T. Warner, Numerical Weather and Climate Prediction, *Cambridge University Press, 2011.*

[8] A. Mazur, G. Duniec: Sensitivity test on the behavior of different COSMO suites to different lower boundary initial conditions. *Presented during COSMO User Seminar, 16-21.03.2014, Offenbach, Germany.*

[9] G. Duniec, A. Mazur: COTEKINO Priority Project – Results of Sensitivity Tests, *COSMO Newsletter No. 14: April 2014*, **106-113**.

[10] A. Mazur, G. Duniec: Soil state perturbations as an input for Ensemble Prediction System (EPS) forecast, Side, Antalya/Turkey, 14-16 October, 2014, Turkey, Erol Ofset Matbaacilik Yayincilik Ambalaj San. Ve Tic.Ld.Sti. Pazar Mah. Necati Efendi Sok. No.41/A, Ilkadim,Sukman, 2014

[11] C. Sutton, T. Hamill, T. Warner, Will perturbing soil moisture improve warm-season ensemble forecasts? A proof of concept. *Mon. Weather Rev. 134, 3174–3189, 2006.*

Impact of high-resolution boundary conditions on the quality of COSMO-LEPS forecasts

Andrea Montani, C. Marsigli, T. Paccagnella

ARPA–SIMC, Bologna, Italy

1 Introduction

The use of Limited-Area-Model Ensemble Prediction Systems (LAMEPS), either in operational or research mode, is getting more and more widespread across Europe. Several activities are taking place in different weather services to assess the usefulness of these systems and their skill in the timely prediction of high-impact weather events at great spatial and time detail. In the framework of the development of European LAMEPS, the ECMWF Research Department performed a number of global-model ENS reruns with two different configurations (further details available under `https://software.ecmwf.int/wiki/display/LAMEPS/LAMEPS+Home`).

The former experiment was run with the operational horizontal resolution of T_L639 (32 km), while the latter one (referred to as exp H) was run at the higher resolution of T_L1279 (16 km). Both ensembles had the following configuration: 20 perturbed forecasts, one control forecast, a forecast range of 144 hours and 62 vertical levels. Model level data were archived 1–hourly until a lead time of 48 h and 3–hourly afterwards. All experiments were initialized twice daily, starting at 00 and 12 UTC.

Data were provided for three two-week periods, selected in such a way to encompass several high-impact weather events occurred over Europe, as summarised in Table 1. The availability of this unique dataset made possible the performance of several tests by the LAMEPS community, with either convection–permitting or convection–parameterised ensemble systems.

Table 1: Selected periods for ECMWF ENS reruns.

period	start	end	no. of days	type of events
1)	24 Oct 2011	7 Nov 2001	15	floods over Italy and France
2)	27 Dec 2011	8 Jan 2012	13	storms over Northern Europe
3)	11 Jun 2012	28 Jun 2012	18	Alpine summer convection
all cases			46	

As for the experimentation with COSMO–LEPS (Montani et al., 2011), the limited-area-model ensemble prediction system operationally run by ARPA-SIMC on behalf of the COSMO Consortium (`http://www.cosmo-model.org`), the attention was focussed on the fields by the high-resolution ENS experiments (exp H), which were used to provide both initial and boundary conditions for limited-area reruns.
The methodology followed to perform the experiments and to assess the skill of the different forecasting systems is described in the next two sections.

2 Methodology

Four different sets of ensembles were compared:

1. **opecleps** ($\Delta x = 7$ km, 40 Model Levels, 16 members), the operational COSMO-LEPS running at the time of the experiments (COSMO model version 4.12), with 16 members selected out of 102 (from 2 successive runs of operational ECMWF ENS) using the cluster-analysis technique described in Montani et al. (2011);
2. **TESTcleps_OldModel** ($\Delta x = 7$ km, 40 Model Levels, 16 members), the test version of COSMO-LEPS nested on high-res ENS (COSMO model version 4.12) and with 16 members selected out of 42 (from 2 successive runs of high-res ENS);

3. **TESTcleps_NewModel** ($\Delta x = 7$ km, 40 Model Levels, 16 members), the same as "TESTcleps_OldModel", but with COSMO model version 4.26, with new microphysics package;
4. **H_ENS** ($\Delta x = 16$ km, 62 Model Levels, 21 members), the high-resolution global ENS, driving both "TESTcleps" systems.

In order to compare the skill of the 4 systems, we considered the probabilistic prediction of total precipitation exceeding a number of thresholds for several forecast ranges, analysing only the performance of the runs starting at 12UTC.

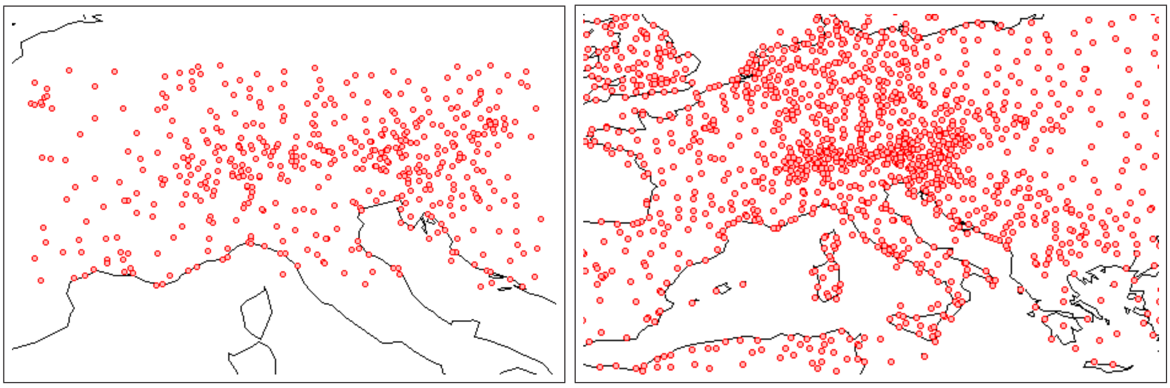

Figure 1: SYNOP stations used for the verification of the ensemble systems: "mapdom" (left panel) and "fulldom" (right panel).

The evaluation of the models' performances was carried out over different verification domains: the former one (referred to as "mapdom") was centred over the Alpine area and covered the area [43-50N, 2-18E]; the latter one (referred to as "fulldom") emcompassed the full COSMO-LEPS domain with the area [35-58N, 10W-30E]. As for observations, it was decided to use the data obtained from the SYNOP reports available on the Global Telecommunication System (GTS). There were approximately 400 (1400) SYNOP reports falling in the "mapdom" ("fulldom") verification domain, as reported in Fig. 1. The comparison of model forecasts against observations was carried out by selecting the model grid-point closest to the observation. The skill of

Table 2: Main features of the verification configuration.

variable:	12-hour cumulated precipitation (18-06, 06-18UTC);
starting time:	12 UTC;
period:	all cases of Table 1;
region:	43-50N, 2-18E (mapdom); 35-58N, 10W-30E (fulldom);
method:	nearest grid–point;
observations:	SYNOP reports, $\sim$ 400 (1400) stations/day for "mapdom" ("fulldom");
fcst ranges:	6-18h, 18–30h, . . . , 114-126h;
thresholds:	1, 5, 10, 15, 25, 50 mm/12h;
scores:	ROC area, BSS, RPSS, OUTL.

the different systems was examined for 6 different precipitation thresholds: 1, 5, 10, 15, 25 and 50 mm/12h. The following probabilistic scores were computed: the Brier Skill Score (BSS), the Ranked Probability Skill Score (RPSS), the Relative Operating Characteristic Curve (ROC) area, the Rank Histograms (RK) and the Percentage of Outliers (OUTL).

For a description of these scores, the reader is referred to Marsigli et al. (2008) and Wilks (1995). The main features of the verification exercise are summarised in Table 2.

3 Results

In this section, the main results of the intercomparison are presented. The forecast accuracy of the 4 systems is measured separately for each of the three periods of Table 2 as well as for the full length of the verification exercise in order to get an overall picture of systems' performances.

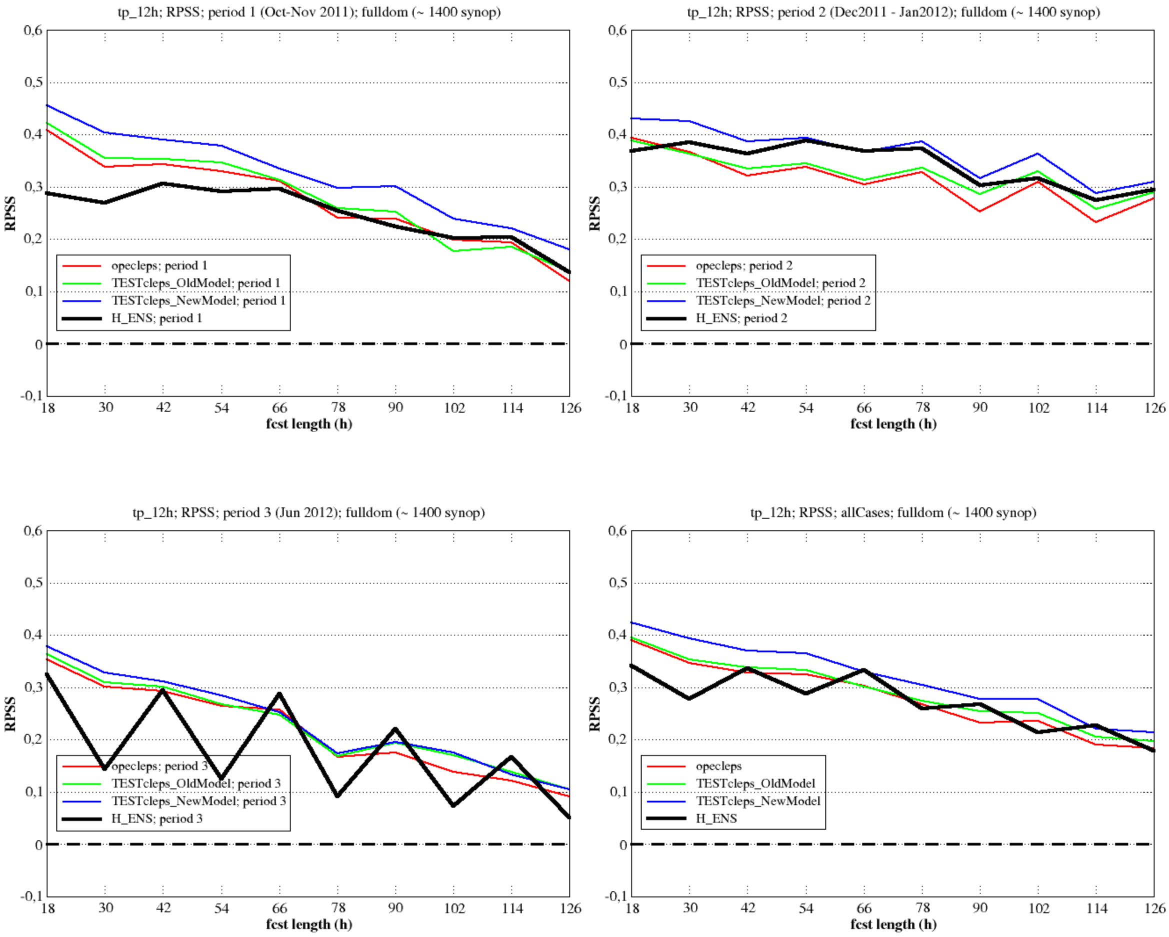

Figure 2: RPSS values for 12-hour cumulated precipitation as a function of the forecast range for period 1 (top-left panel), period 2 (top-right panel), period 3 (bottom-left panel) and all cases (bottom-right panel). The scores are reported over the "fulldom" for the following forecast systems: opecleps (red line), TESTcleps_OldModel (green line), TESTcleps_NewModel (blue line) and H_ENS (thick black line).

As for the "fulldom" area (about 1440 SYNOP reports in the region), the skills of COSMO ensembles and H_ENS are summarised in Fig. 2. The attention is focussed on the probabilistic prediction of 12-hour cumulated precipitation and the values of the RPSS are plotted against the forecast range for each of the three periods of Table 2 and for all cases.

The skill of each individual ensemble system changes from case to case; as an example, the performance of all systems is less accurate for the summer event (period 3, bottom-left panel), which is mainly driven by convection processes over complex terran, with a lower degree of predictability. Nevertheless, some common features can be detected. In the 4 panels, it can be noticed that very similar results are obtained by opecleps and TESTcleps_OldModel (red and green lines, respectively) for almost all forecast ranges.

These two systems differ mainly on the quality of the boundaries, which are provided at higher resolution in the latter configuration. Therefore, it looks as if the benefits of more detailed boundaries are only partly transferred to the skill of the limited-area integrations. A clearer positive impact can be noticed for ranges longer than 78 hours, when TESTcleps_OldModel shows higher scores than opecleps. This is especially true for the verification scores of periods 2 and 3 (top-right and bottom-left panels of Fig. 2, respectively).
Overall speaking, the best results are obtained by the TESTcleps_NewModel configuration (blue line), where COSMO–LEPS benefits of both higher-resolution boundaries by H_ENS and improved model set-up.

The better performance of TESTcleps_NewModel is evident for all ranges and is especially true for short forecast steps. As for the global ensemble H_ENS, it can be noticed that its performance is usually the worst one in the short range, while the system gets more and more valuable for longer ranges. It is also worth pointing out the 12-hour cycle of model performance for period 3 (bottom-left panel). For this case, the skill of the model is higher in the verification interval 18-06 UTC (night-time precipitation), while a worse performance can be seen for day-time precipitation, verifying between 06 and 18 UTC.

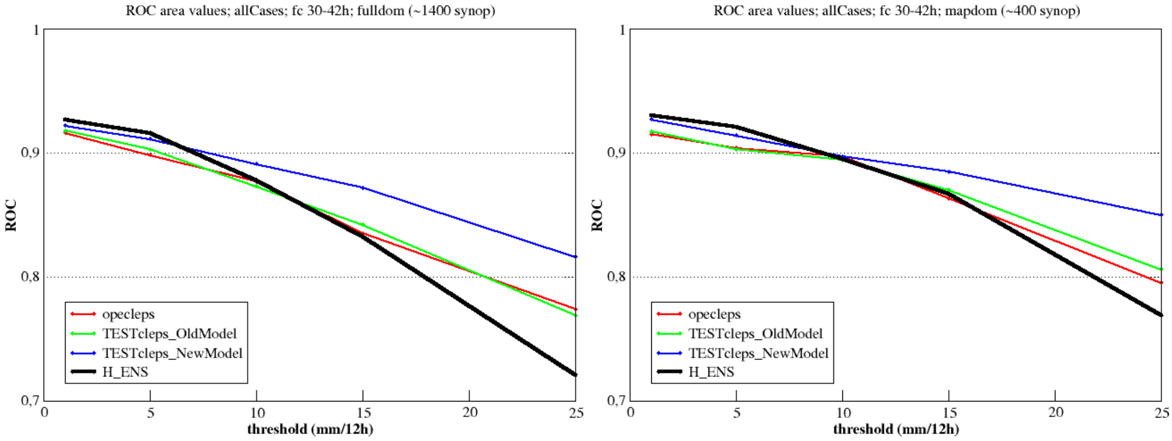

Figure 3: ROC area values for 12-hour cumulated precipitation as a function of threshold value for the forecast range 30-42h. The scores are reported over the "fulldom" (left panel) and "mapdom" (right panel) for all cases and for the following forecast systems: opecleps (red line), TESTcleps_OldModel (green line), TESTcleps_NewModel (blue line) and H_ENS (thick black line).

Similar conclusions can be drawn if the attention is focussed on the skill of the systems in terms of ROC area. Fig. 3 reports the performance of the 4 systems over the forecast interval 30-42h as a function of precipitation intensity. It can be noticed that, on either "fulldom" or "mapdom" (left and right panel, respectively), the highest scores are obtained by TESTcleps_NewModel, with similar performances by opecleps and TESTcleps_OldModel.
As for H_ENS, the performance of the model is satisfactory for low threshold events, while the system shows a performance decay for high-precipitation cases. For all investigated systems, it can also be noticed that higher scores are obtained for the verification in the "mapdom" domain. Also in this case, the performance of all systems is slightly more accurate when verification is performend over the "fulldom" area.

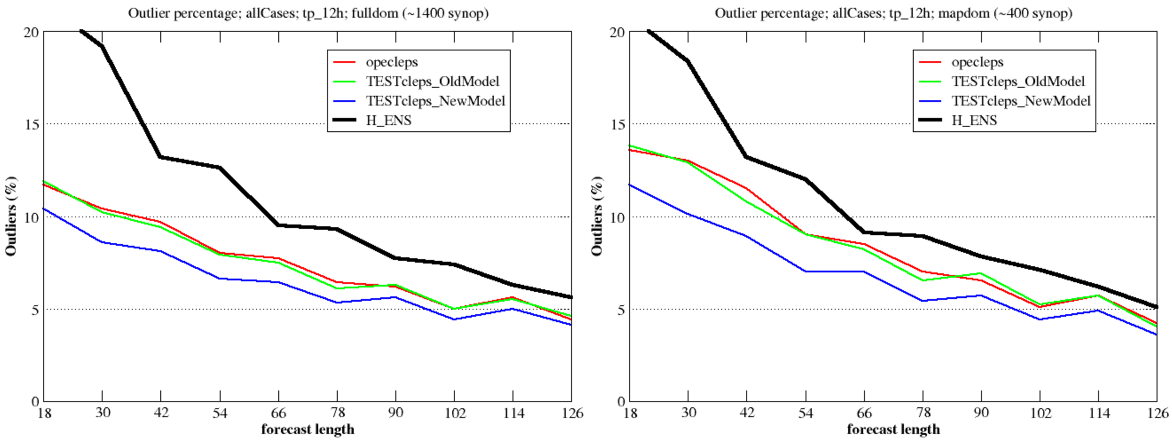

Figure 4: Percentages of Outliers for 12-hour cumulated precipitation as a function of the forecast range. The scores are reported over the"fulldom" (left panel) and "mapdom" (right panel) for all cases and for the following forecast systems: opecleps (red line), TESTcleps_OldModel (green line), TESTcleps_NewModel (blue line) and H_ENS (thick black line).

Finally, the skills of the systems are assessed in terms of Outliers' percentage over the "fulldom" and "mapdom" areas (left and right panels of Fig. 4). Lower values of outliers are found for verification performed in the "fulldom", indicating a better performance of the systems in this region. Despite the larger ensemble size (21 vs 16), the global system H_ENS presents larger amounts of outliers than COSMO runs. This is true for all forecast ranges, but the gap is especially evident in the first 66 hours. As for COSMO systems, the overall higher quality of TESTcleps_NewModel is confirmed. The added value of better boundaries and improved set-up is clearly evident in the short range, while, at longer ranges, the skills of the different COSMO systems converge towards the 5% value of outliers.

4 Conclusions

The main results of the verification exercise carried out in the framework of LAMEPS experimentation can be summarised as follows:

- the impact of using high-resolution boundaries with respect to the operational configuration is limited;
- a clear improvement in limited-area model integrations is obtaibed if, in addition to high resolution boundaries, a newer model version with updated microphysics is used;
- in either cases, the added value with respect to the global ensemble is noticeable, especially in the short range.

As for the future, it is planned to consolidate the verification results, by considering the performance of all system for other variables, considering also the spread/skill performance for the different periods.

References

[1] Marsigli C., Montani A., Paccagnella T., 2008. A spatial verification method applied to the evaluation of high–resolution ensemble forecasts. *Met. Appl.*, **15**, 125–143.

[2] Montani A., Cesari D., Marsigli C., Paccagnella T., 2011. Seven years of activity in the field of mesoscale ensemble forecasting by the COSMO–LEPS system: main achievements and open challenges. *Tellus*, **63A**, 605-–624. DOI: 10.1111/j.1600-0870.2010.00499.x

[3] Wilks, D.S., 1995. Statistical Methods in the Atmospheric Sciences. Academic Press, New York, 467.

Performance of the COSMO-based ensemble systems during Sochi-2014 pre-Olympics

Andrea Montani[1], D. Alferov[2], E. Astakhova[2], C. Marsigli[1], T. Paccagnella[1]

[1]*ARPA–SIMC, Bologna, Italy*
[2]*Hydrometcenter of Russia, Moscow, Russia*

1 Introduction

A few month ago, the Winter Olympics and Paralympic Games took place in Sochi, Russia, from 7 to 23 February 2014 and from 7 to 16 March 2014. In the framework of these events, WMO WWRP initiated a dedicated blended Forecast Demonstration/Research and Development Project (FDP/RDP). **FROST-2014** (**F**orecast and **R**esearch in the **O**lympic **S**ochi **T**estbed; `http://frost2014.meteoinfo.ru/`) aimed at advancing the understanding of nowcasting and short-range prediction processes over complex terrain, since the region of Sochi is characterized by a complex topography, with the Caucasus mountains in the vicinity of the Black Sea (Kiktev, 2011), as shown in Fig. 1, where the main features of the Olympic venues are presented.

Figure 1: Main features of the Olympic venues for Sochi–2014.

Several activities were performed by the COSMO consortium (`http://www.cosmo-model.org`) to support NWP aspects of the FROST-2014 project. In the framework of probabilistic forecasting, the following actions were undertaken:

(1) FDP part: relocation of COSMO-LEPS (Montani et al., 2011) over the Sochi area, generating a new system named COSMO-S14-EPS ("S14" stands for Sochi2014);

(2) RDP part: development of a convective-scale ensemble system for the Sochi area, referred to as COSMO-Ru2-EPS ("Ru2" stands for Russian 2.2 km; Montani et al., 2014).

As for (1), COSMO-S14-EPS, the convection-parameterized ensemble prediction system based on COSMO model and targeted for the Sochi-area, was set-up, implemented and maintained throughtout the full pre-Olympic and Olympic periods. In addition to providing probabilistic guidance for the prediction of high-impact weather over the Olympic mountainous areas up to day 3, COSMO-S14-EPS also provided initial and boundary conditions for activity (2), linked to the generation of the convective-permitting ensemble, COSMO-Ru2-EPS, which ran on an experimental basis during the pre-Olympics season and on a quasi-operational basis during the Olympics.

2 Methodology and implementation

As previously mentioned, COSMO-S14-EPS is a relocation of COSMO-LEPS over the area interested by the Olympic competitions and COSMO-Ru2-EPS is a pure dynamical downscaling of COSMO-S14-EPS over a small domain centred on the Olympic venues. The main features of implmentation for both systems are described in Montani et al. (2014) and summarised in Table 1.

Table 1: Main characteristics of COSMO-S14-EPS and COSMO-Ru2-EPS.

	COSMO-S14-EPS	COSMO-Ru2-EPS
Horizontal resolution	7 km	2.2 km
Vertical resolution	40 ML	50 ML
Forecast length	72h	48h
Ensemble size	10	10
Initial time	00/12 UTC	00/12 UTC
Convection	Parameterized	Resolved
Running at	ECMWF	Roshydromet
ICs and BCs	from selected ECMWF-EPS members	from COSMO-S14-EPS members
Model perturbations	Physical parameterizations	

COSMO-S14-EPS was implemented on ECMWF super–computers in November 2011 and ran on a regular basis from 19 December 2011 to 30 April 2014 thanks to the billing units provided by the ECMWF Special Project SPCOFROST.
COSMO-S14-EPS forecasts were used to generate a set of standard probabilistic products, including probability of surpassing a threshold, ensemble mean and ensemble standard-deviation for several surface and upper-air variables. In addition to this, the individual forecast members for a specially defined sub-area were also transferred to the Hydrometcenter of Russia (Roshydromet) where the epsgrams for predetermined points (mainly, locations of outdoor and indoor competitions) were prepared. All these products, delivered in real time to Roshydromet, were used by the Sochi forecasters via the FROST-2014 Web-site (`http://frost2014.meteoinfo.ru/forecast/goomap` and `http://frost2014.meteoinfo.ru/forecast/arpa-new/`).
Apart from the ensemble products, COSMO-S14-EPS provided both initial and hourly-boundary conditions (up to t+48h) to Roshydromet for the experimentation with the convection-resolving ensemble COSMO-Ru2-EPS, which ran between January and February 2013 as well as from November 2013 to April 2014 and whose main features are also summarized in Table 1. Figure 2 provides a synthetic overview of the forecasting chain involving COSMO-S14-EPS and COSMO-Ru2-EPS during the Olympic Games.

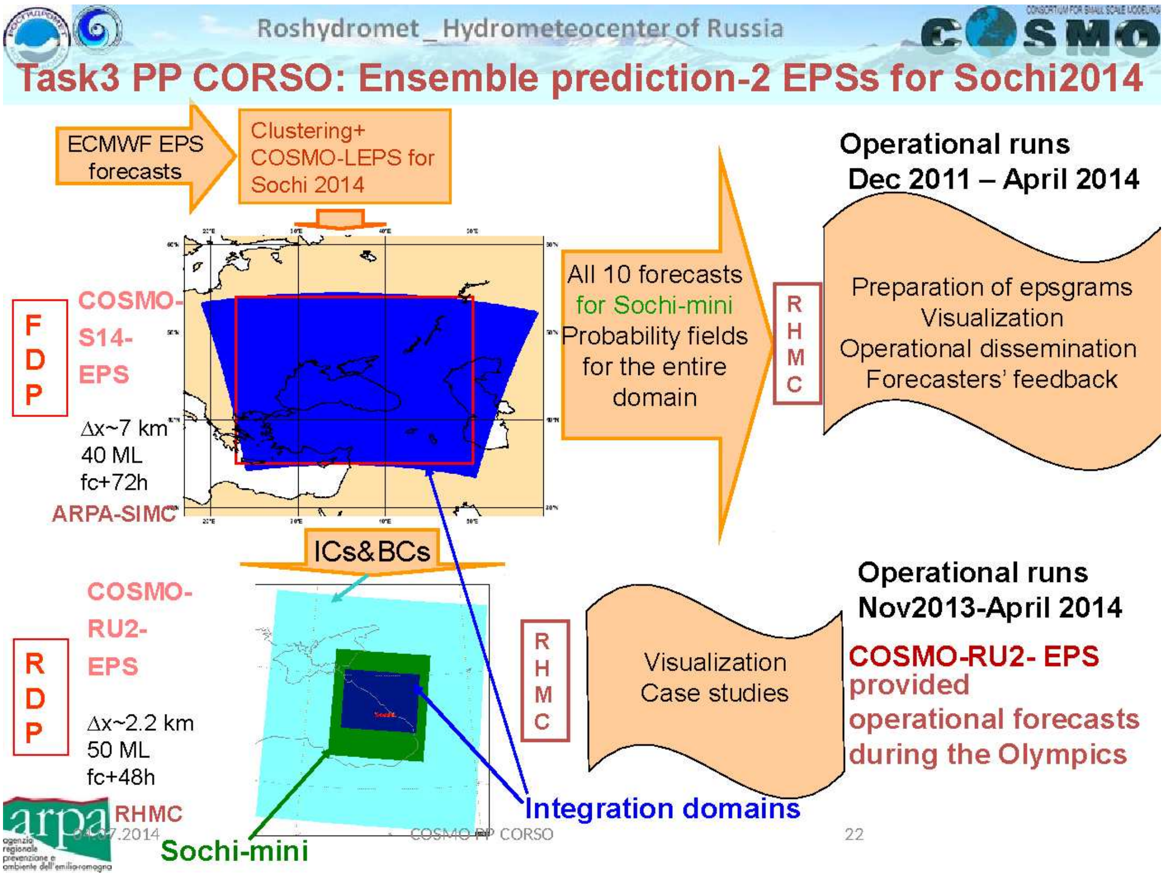

Figure 2: Illustration of the forecasting chain used during winter Olympic 2014.

In the next section, we present some preliminary results relative to the intercomparison between COSMO-S14-EPS and COSMO-Ru2-EPS in terms of 2-metre temperature relative to the pre-Olympics season. The investigation aims at highlighting the added value of enhanced horizontal resolution in the probabilisitc prediction of surface fields.

3 Verification results

In this section, the preliminary results of a verification exercise are presented; the skills of COSMO-S14-EPS and COSMO-Ru2-EPS are assessed over the period January-February 2013. For both systems, we considered the probabilistic prediction of 2-metre temperature exceeding a number of thresholds for several forecast ranges. As for observations, it was decided to use the data obtained from the SYNOP reports available on the Global Telecommunication System (GTS) as well as from a number of non-GTS local stations.

This enabled the possibility to assess the performance of the systems over a relatively dense observation dataset (69 stations), since the verification domain was restriced to an area centred over the Olympic venue (42.5-45N, 37.5-41.5E). As for the comparison of model forecasts against observations, we selected the grid–point closest (in 3D) to the observation.

The performance of both systems was examined for 4 different thresholds: -5, 0, +5 and +10 ^oC. Verification was performed using COSMO software VERSUS. The following probabilistic scores were computed: the Brier Skill Score (BSS) and the Relative Operating Characteristic (ROC) area. For a description of these scores, the reader is referred to Wilks (1995). The main features of the verification exercise are also summarised in Table 2.

The skill of the two systems in terms of probabilistic prediction of 2-metre temperature is summarised in Fig. 3, where the values of the ROC area are plotted against the forecast range for 4 different weather events: temperature below -5^oC (top-left), above 0^oC (top-right), above +5^oC (bottom-left) and above +10^oC (bottom-right). It can be noticed that the ROC area values are well above 0.8 for three out of the four thresholds, indicating that both COSMO-S14-EPS and COSMO-Ru2-EPS manage to discriminate these events. The performance of the two systems is quite similar, with a slight predominance of COSMO-Ru2-EPS which has higher scores for most of the thresholds/forecast ranges. Worse scores are obtained by both systems for the highest threshold

Table 2: Main features of the verification configuration.

variable:	2-metre temperature;
starting time:	12 UTC;
period:	from 1 January to 28 February 2013;
region:	42.5–45 N, 37.5–41.5 E;
method:	nearest 3D optimised grid–point;
observations:	SYNOP reports + local stations (69 in total);
fcst ranges:	from fc+3h to fc+72h every 3h;
thresholds:	-5, 0, +5, +10 ^{o}C;
scores:	ROC area, BSS.

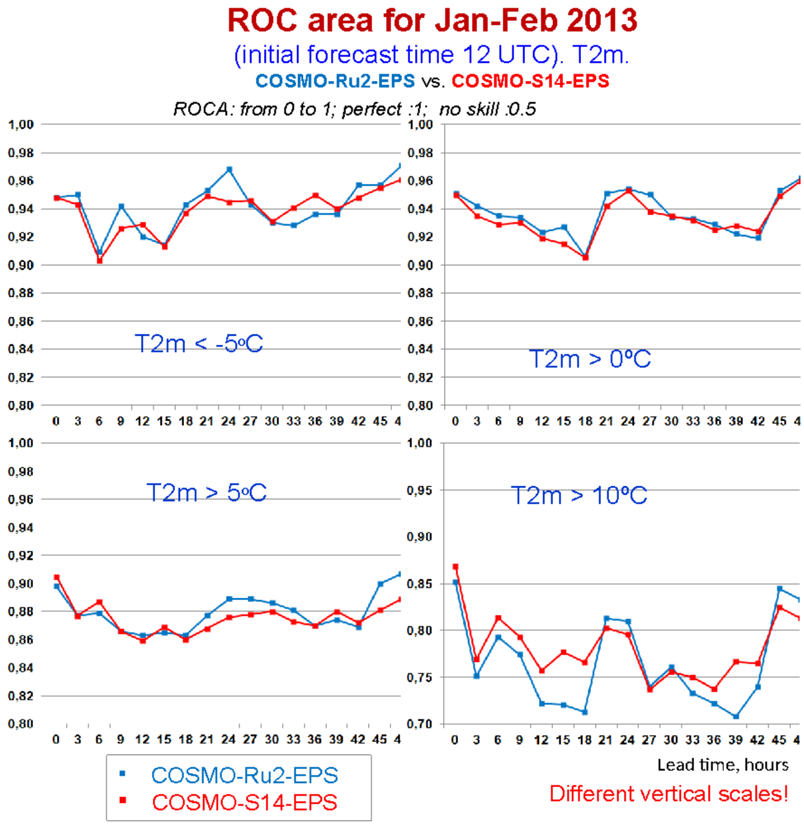

Figure 3: ROC area values as a function of forecast range for four different weather events: 2-metre temperature below -5^{o}C (top-left panel), above 0^{o}C (top right), above +5^{o}C (bottom left) and above +10^{o}C (bottom-right with different vertical scales). The scores are calculated over the period January-February 2013. Red (blue) lines refer to COSMO-S14-EPS (COSMO-Ru2-EPS).

(bottom-right panel), where COSMO-S14-EPS outperforms COSMO-Ru2-EPS. It is worth pointing out that this is the rarest event with few observations; therefore, the statistical significance of this result needs to be confirmed by a more detailed investigation over a longer verification period.

Similar results are obtained when the attention is focussed on the Brier Skill Score (BSS), shown in Fig. 4. Also with this score, the satisfactory performance of both systems is confirmed: the BSS is always positive for COSMO-S14-EPS and COSMO-Ru2-EPS, indicating an added value of both systems with respect to climatology as regards the probabilistic prediction of 2-metre temperature for the thresholds of Table 2. Similarly to Fig. 3, it can be noticed that COSMO-Ru2-EPS usually outperforms the lower-resolution ensemble, although the difference is not very marked. As for the +10^{o}C threshold (bottom-right panel of Fig. 4), the skill of the

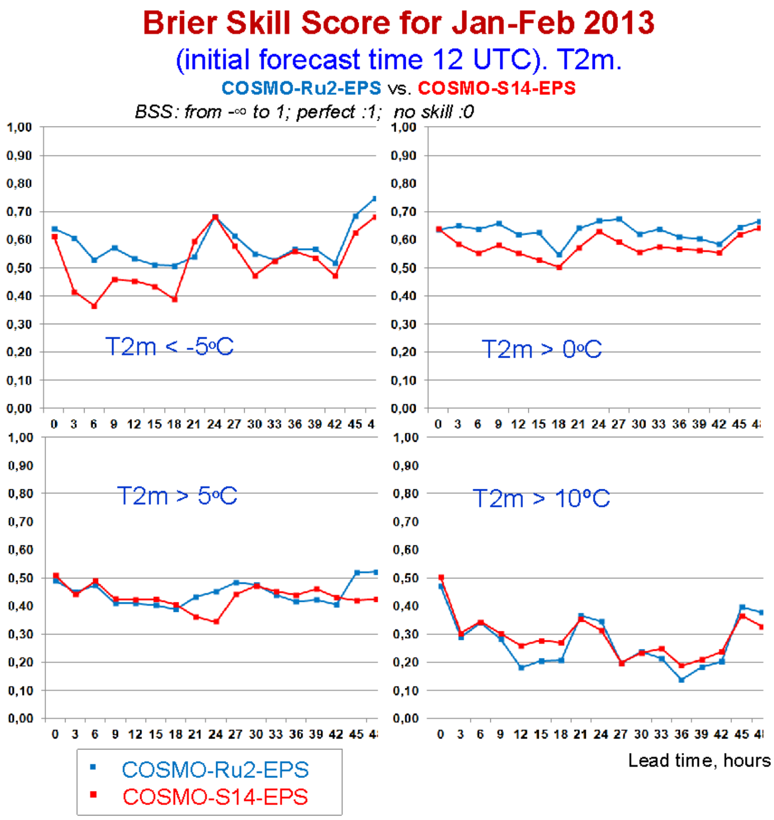

Figure 4: The same as Fig. 3 but for the Brier Skill Score. The vertical scale is the same in all panels.

two ensembles is almost identical, with slightly higher scores for COSMO-S14-EPS.

4 Summary and Outlook

The main results of the ensemble prediction system experimentation within FROST-2014 can be summarized as follows:

- two limited-area ensemble prediction systems, based on COSMO-model and referred to as COSMO-S14-EPS (convection-parameterised) and *COSMO-Ru2-EPS* (convection-permitting), were implemented and run on an operational/*quasi–operational* basis during the pre-Olympic and Olympic seasons;
- a preliminary verificationn exercise was undertaken by assessing the probabilistic skill of both systems in terms of 2-metre temperature during the pre-Olympic season (January-February 2013) over a region centred around Sochi;
- both COSMO-S14-EPS and COSMO-Ru2-EPS turned out to have an overall good performance with ability to discriminate different weather events;
- the added value of the higher resolution in COSMO-Ru2-EPS was confirmed by the better probabilistic scores obtained by this system.

As for the future, it is planned to consolidate the verification results, by considering the performance of both system for other variables (in particular, precipitation) and over a longer verification period which includes the Olympic season.

References

[1] Kiktev D., 2011. Forecast and Research: the Olympic Sochi Testbed(FROST-2014). Concept paper. Available at http://frost2014.meteoinfo.ru

[2] Aligo, E. A., Gallus, W. A. and Segal, M., 2007: Summer Rainfall Forecast Spread in an Ensemble Initialized with Different Soil Moisture Analyses. *Wea. Forecasting*, 22, **299-314**.

[3] Kiktev D., 2011. Forecast and Research: the Olympic Sochi Testbed (FROST-2014). Concept paper. Available at http://frost2014.meteoinfo.ru

[4] Montani A., Cesari D., Marsigli C., Paccagnella T., 2011. Seven years of activity in the field of mesoscale ensemble forecasting by the COSMO-LEPS system: main achievements and open challenges. *Tellus*, **63A**, 605-–624. DOI: 10.1111/j.1600-0870.2010.00499.x

[5] Montani A., Marsigli C., Paccagnella T., 2013. Development of a COSMO-based limited-area ensemble system for the 2014 Winter Olympic Games.*Cosmo Newsletter No. 13*, 93-99. Available at http://www.cosmo-model.org

[6] Montani A., Alferov D., Astakhova E., Marsigli C., Paccagnella T., 2014.Ensemble forecasting for Sochi-2014 Olympics: the COSMO-based ensemble prediction systems. *Cosmo Newsletter No. 14*, 88-94. Available at http://www.cosmo-model.org

[7] Wilks, D.S., 1995. Statistical Methods in the Atmospheric Sciences. Academic Press, New York, 467.

List of COSMO Newsletters and Technical Reports

(available for download from the COSMO Website: `www.cosmo-model.org`)

COSMO Newsletters

No. 1: February 2001.

No. 2: February 2002.

No. 3: February 2003.

No. 4: February 2004.

No. 5: April 2005.

No. 6: July 2006; Proceedings from the COSMO General Meeting 2005.

No. 7: May 2008; Proceedings from the COSMO General Meeting 2006.

No. 8: August 2008; Proceedings from the COSMO General Meeting 2007.

No. 9: December 2008; Proceedings from the COSMO General Meeting 2008.

No.10: January 2010; Proceedings from the COSMO General Meeting 2009.

No.11: February 2011; Proceedings from the COSMO General Meeting 2010.

No.12: March 2012; Proceedings from the COSMO General Meeting 2011.

No.13: April 2013; Proceedings from the COSMO General Meeting 2012.

No.14: April 2014; Proceedings from the COSMO General Meeting 2013.

No.15: July 2014; Proceedings from the COSMO General Meeting 2014.

COSMO Technical Reports

No. 1: Dmitrii Mironov and Matthias Raschendorfer (2001):
Evaluation of Empirical Parameters of the New LM Surface-Layer Parameterization Scheme. Results from Numerical Experiments Including the Soil Moisture Analysis.

No. 2: Reinhold Schrodin and Erdmann Heise (2001):
The Multi-Layer Version of the DWD Soil Model TERRA_LM.

No. 3: Günther Doms (2001):
A Scheme for Monotonic Numerical Diffusion in the LM.

No. 4: Hans-Joachim Herzog, Ursula Schubert, Gerd Vogel, Adelheid Fiedler and Roswitha Kirchner (2002):
LLM — the High-Resolving Nonhydrostatic Simulation Model in the DWD-Project LITFASS.
Part I: Modelling Technique and Simulation Method.

No. 5: Jean-Marie Bettems (2002):
EUCOS Impact Study Using the Limited-Area Non-Hydrostatic NWP Model in Operational Use at MeteoSwiss.

No. 6: Heinz-Werner Bitzer and Jürgen Steppeler (2004):
Description of the Z-Coordinate Dynamical Core of LM.

No. 7: Hans-Joachim Herzog, Almut Gassmann (2005):
Lorenz- and Charney-Phillips vertical grid experimentation using a compressible nonhydrostatic toy-model relevant to the fast-mode part of the 'Lokal-Modell'

No. 8: Chiara Marsigli, Andrea Montani, Tiziana Paccagnella, Davide Sacchetti, André Walser, Marco Arpagaus, Thomas Schumann (2005):
Evaluation of the Performance of the COSMO-LEPS System

No. 9: Erdmann Heise, Bodo Ritter, Reinhold Schrodin (2006):
Operational Implementation of the Multilayer Soil Model

No. 10: M.D. Tsyrulnikov (2007):
Is the particle filtering approach appropriate for meso-scale data assimilation?

No. 11: Dmitrii V. Mironov (2008):
Parameterization of Lakes in Numerical Weather Prediction. Description of a Lake Model.

No. 12: Adriano Raspanti (2009):
Final report on priority project VERSUS (VERification System Unified Survey).

No. 13: Chiara Mirsigli (2009):
Final report on priority project SREPS (Short Range Ensemble Prediction System).

No. 14: Michael Baldauf (2009):
COSMO Priority Project "Further Developments of the Runge-Kutta Time Integration Scheme" (RK); Final Report.

No. 15: Silke Dierer (2009):
COSMO Priority Project "Further Developments of the Runge-Kutta Time Integration Scheme" (RK); Final Report.

No. 16: Pierre Eckert (2009):
COSMO Priority Project "INTERP"; Final Report.

No. 17: D. Leuenberger, M. Stoll, A. Roches (2010):
Description of some convective indices, implemented in the COSMO model.

No. 18: Daniel Leuenberger (2010):
Statistical Analysis of high-resolution COSMO Ensemble forecasts, in view of Data Assimilation.

No. 19: A. Montani, D. Cesari, C. Marsigli, T. Paccagnella (2010):
Seven years of activity in the field of mesoscale ensemble forecasting by the COSMO-LEPS system: main achievements and open challenges.

No. 20: A. Roches, O. Fuhrer (2012):
Tracer module in the COSMO model.

No. 21: M. Baldauf (2013):
A new fast-waves solver for the Runge-Kutta dynamical core.

No. 22: C. Marsigli, T. Diomede, A. Montani, T. Paccagnella, P. Louka, F. Gofa, A. Corigliano (2013):
The CONSENS Priority Project.

No. 23: M. Baldauf, O. Fuhrer, M. J. Kurowski, G. de Morsier, M. Muellner, Z. P. Piotrowski, B. Rosa, P. L. Vitagliano, D. Wojcik, M. Ziemianski (2013):
The COSMO Priority Project 'Conservative Dynamical Core' Final Report.

No. 24: A. K. Miltenberger, A. Roches, S. Pfahl, H. Wernli (2014):
Online Trajectory Module in COSMO: A short user guide.

No. 25: P. Khain, I. Carmona, A. Voudouri, E. Avgoustoglou, J.-M. Bettems, F. Grazzini (2015):
The Proof of the Parameters Calibration Method: CALMO Progress Report.

No. 26: D. Mironov, E. Machulskaya, B. Szintai, M. Raschendorfer, V. Perov, M. Chumakov, E. Avgoustoglou (2015):
The COSMO Priority Project 'UTCS' Final Report.